A Comparison of Turbulent Flow Predictions for Rectangular Ducts Using Five Vorticity Source Models

by

Ziliang Zhou

A thesis
presented to the University of Manitoba
in partial fulfillment of the
requirements for the degree of
Master of Science
in
Department of Mechanical Engineering

Winnipeg, Manitoba

(c) Ziliang Zhou, 1985

A COMPARISON OF TURBULENT FLOW PREDICTIONS FOR RECTANGULAR DUCTS USING FIVE VORTICITY SOURCE MODELS

BY

ZILIANG ZHOU

A thesis submitted to the Faculty of Graduate Studies of
the University of Manitoba in partial fulfillment of the requirements
of the degree of

MASTER OF SCIENCE

© 1985

Permission has been granted to the LIBRARY OF THE UNIVERSITY OF MANITOBA to lend or sell copies of this thesis. to the NATIONAL LIBRARY OF CANADA to microfilm this thesis and to lend or sell copies of the film, and UNIVERSITY MICROFILMS to publish an abstract of this thesis.

The author reserves other publication rights, and neither the thesis nor extensive extracts from it may be printed or otherwise reproduced without the author's written permission.

ACKNOWLEDGEMENTS

I would like to express my sincere gratitude and appreciation to Dr. A. C. Trupp(Thesis supervisor), Mechanical Engineering Department, for his precious guidance, encouragement and sincere help.

Thanks are also due to Professor Hsu and Professor Schilling for their help during the study.

The financial support provided by teaching and research assistantships with the Department of Mechanical Engineering during the course of this work is gratefully acknowledged.

ABSTRACT

The fully developed turbulent flow and heat transfer characteristics in rectangular ducts has been investigated numerically. The prediction employed the $k-\epsilon$ two-equation model and the general elliptic finite difference procedure of Gosman et al(1969). For the vorticity source term, five different algebraic models have been used. They are:

1. LY model by Launder & Ying(1972). This model assumes that the Reynolds stress $\overline{v^2}-\overline{w^2}$ can be determined by the local gradients in the mean axial velocity distribution.

2. Seale's model by Seale(1982). This model claims that the vorticity source term can be determined mainly by the duct geometry.

3. NR model by Naot & Rodi(1982). This model assumes that the Reynolds stress $\overline{v^2}-\overline{w^2}$ might be determined by the gradients of both the main flow and the secondary velocities.

4. k model by the present author. This model assumes that the Reynolds stress $\overline{v^2}-\overline{w^2}$ can be determined in terms of the gradients of the turbulent kinetic energy k.

5. ϵ model by the present author. This model assumes that the Reynolds stress $\overline{v^2}-\overline{w^2}$ can be determined in terms of the gradients of the energy dissipation rate ϵ.

The results obtained by using each of the five models were found to compare fairly well with the available experimental data. Overall,the present work compares the results of five different vorticity source models for the prediction of secondary flow in ducts having more than one cell of secondary flow in each symmetric part.

The comparison suggests that whereas all five models performed reasonably well, on an over-all basis, Seale's model is slightly prefered over the others in predicting the flow characteristics in duct of complicated cross-section.

NOMENCLATURE

a_ϕ , b_ϕ	Finite difference equations coefficients
A, B	Universal law of the wall constants
C_1, C_2, C_μ, C_D	Turbulence model constants
C_i' i=1,5	Vorticity source model constants
c_p	Constant pressure specific heat
D_h	Equivalent hydraulic diameter
f	Friction factor, $f=8\bar{\tau}/(\rho\bar{U}_b^2)$
k	Mean turbulent kinetic energy, $(\overline{u}^2+\overline{v}^2+\overline{w}^2)^{\frac{1}{2}}/2$
k^+	$k/(\bar{u}^*)^2$
k_c	coefficient of heat conductivity
l	Turbulence mixing length
$\dot{m}$	Mass flow rate
Nu	Nusselt number, $Nu=\bar{\dot{q}}''D_h/(k_c(\bar{T}_w-\bar{T}_b))$
$\overline{P}$	Pressure
Pr	Prandtl number

Pr_t	Turbulent Prandtl number
$\dot{q}''$	local heat flux at the wall
Re	Reynolds number based on $\bar{U}_b$ and D_h
S	Source term
$\bar{T}$	Temperature
u*	Local friction velocity
$\bar{u}$*	Average friction velocity
U	Instantaneous axial velocity
$\bar{U}$	Axial mean velocity
$\bar{U}_b$	Average mean velocity(bulk velocity)
$\bar{V}$sec	Resultant of $\bar{V}$ and $\bar{W}$, $(\bar{V}^2+\bar{W}^2)^{\frac{1}{2}}$
u, v, w	Fluctuating components of the velocities in the x,y,z direction respectively
V, W	Instantaneous velocities in the lateral and bi-normal directions
$\bar{V}$, $\bar{W}$	Lateral and bi-normal mean velocities(secondary velocity)
x	Axial coordinate
y, z	Lateral and bi-normal coordinate
a	Thermal diffusivity

ϵ	Dissipation rate of turbulence kinetic energy
κ	Von-Karman constant
λ	Aspect ratio of rectangular duct
ξ	Convergence criterion
μ	Laminar dynamic viscosity
μ_t	Eddy viscosity
υ	Kinematic viscosity, μ/ρ
υ_t	μ_t/ρ
ρ	Fluid density
σ_κ , σ_ϵ	Turbulence model constants
τ	Local wall shear stress
$\bar{\tau}$	Mean wall shear stress
ϕ	Parameter in the general elliptic equation
Ψ	Stream function
ω	Axial vorticity

Subscripts

b	Bulk
c	Duct centerline

h	Hydraulic
i,j	Finite difference indices
max	Maximum
–	overbar designates time-averaging

Superscript

+	Non dimensionalized

CONTENTS

TABLES

FIGURES

I

INTRODUCTION

The design and development of compact heat exchangers, including those in nuclear reactor cores, depends as much on knowledge of the local mean flow characteristics as on the overall flow and heat transfer. There is an urgent need for detailed predictions of turbulent flow and heat transfer in straight passages of non-circular cross-section. Such predictions would enable designs of compact heat exchangers and the many other non-circular passages to be made directly on the basis of the fluid flow and thermal performence required, and thus enabling optimum use of the available space.

Over the past 15 years a number of turbulence models and numerical procedures have been developed. The most widely used procedure has been based on the $k-\epsilon$ turbulence model for the effective viscosity, together with a general elliptic finite difference scheme by Gosman et al[1]. By this method, the vorticity source modelling becomes a key ingredient in a successful and versatile computation.

Yadava[2] applied the $k-\epsilon$ model to a square duct and predicted the fully developed turbulent flow characteristics using three different vorticity source models. His study was purposely confined to a simple geometry consisting of only one flow cell in each symmetric part. The results showed that the LY, Seale's and k correlation models are all suitable for the prediction of flow characteristics in a square duct. Overall, the three models performed more or less equally well.

In the present work, the applicability of the various vorticity source models to predict the flow characteristics in ducts of more complicated cross-section is explored. The study shows that LY and Seale's models are suitable for the prediction in rectangular ducts. However, the k correlation model failed to achieve a converged solution and had to be abandoned. The NR model was also tested to predict the rectangular flow and satisfactory results were obtained. In addition to the existing vorticity source models, the present author noticed the similarity of the distributions of U,k and ϵ and developed another two vorticity source models in terms of the k and ϵ distributions respectively. The five vorticity source models were used successfully to predict the flow and heat transfer characteristics in rectangular ducts with aspect ratios of 1:1, 2:1, 2.5:1, 3:1 and 4:1.

II

LITERATURE REVIEW

GENERAL

Fully developed turbulent flow in straight non-circular passages is considerably more complex than in circular tubes due to the presence of turbulence-driven secondary flow in the passage cross-plane. These flows cause the main flow to spiral through the passage and although they are relatively weak compared with the main flow, they have a significant influence on the local mean-flow distributions of interest, chiefly the wall shear stress and axial velocity.

Passages of non-circular cross-section are often encountered in engineering practice. Examples are flows in heat exchangers, ventilation and air-conditioning systems, nuclear reactors,turbomachinery, open channels, canals and rivers. The flow in such ducts is accompanied by secondary motions in the plane perpendicular to the streamwise direction. By transporting high-momentum fluid towards the corners, it causes a bulging of the velocity contours towards the corners. In open channel flows, this secondary motion moves fluid with relatively low streamwise momentum towards the centre portion of the channel and causes the observed depression of the velocity maximum below the surface.

Furthermore, the secondary motion produces an increase of the wall shear stress towards corners, an effect which is of great importance for sediment-transport and erosion problems. Similarly, the heat transfer at duct walls is influenced significantly by the secondary motions.

For these reasons it is important to understand and be able to accurately predict secondary-flow phenomena and any attempt to deal with the turbulent flows in ducts or passages of non-circular cross-section must pay special attention to the simulation of this secondary flow motion.

EXPERIMENTS

In his experimental work of turbulent flow in straight ducts of square cross-section, Nikuradse[3] found that the contours of axial mean velocity(isovels) bulged outwards near the corners. This is quite different from pipe flow. Prandtl[4] suggested that these were the result of secondary flows toward the corners which to satisfy continuity required a return flow at the mid-point of the walls. This secondary flow was termed as Prandtl's second kind of secondary motion.

Quantification of these secondary flows was not reported until Hoagland[5] devised a hot-wire technique, which was subsequently employed, with improved accuracy, by Brundrett & Baines[6], Gessner[7], Gessner & Jones[8] and Launder & Ying[9]. Principally, Hoagland studied the flows in rectangular ducts with aspect ratios of 1:1, 2:1, 3:1. He used the hot-wire anemometer and pitot tube instrumentation to measure the mean primary(axial) velocities. The secondary velocities were determined from observation of flow direction using a very sensitive hot wire system developed by himself. In the experiment, he noticed that the secondary flows were found to behave in the manner originally suggested by Prandtl. They were about the same magnitude in all three ducts. Maximum secondary velocities of approximately 1 to 1.5 percent of the axial centerline velocity were found to occur near the wall in the corner region where large wall shear stress gradients were observed. The secondary flows, by convecting axial momentum, were seen to have a significant effect on the primary flow distribution, particularly by causing the wall shear stress to be nearly uniform around the duct periphery except for the corner region.

Leutheusser[10] reported the turbulent mean flow distributions in smooth rectangular ducts of aspect ratios of 1:1 and 3:1 over a range of Reynolds number between 10^4 and 10^5. He concluded from the experiment that the distribution of the axial mean velocity rendered nondimensional by division with the velocity at the center of the cross-section,exhibited a distinct trend toward greater uniformity with increasing Reynolds number. The distribution of the wall stress, normalized with the average wall shear stress, also tended toward greater uniformity with increasing Reynolds number. Contrary to conditions prevailing in circular pipes and two-dimensional channels, static pressures in the interior of the conduits were found to be higher than those at the periphery. Friction coefficients for rectangular conduits appeared to be smaller than those for circular pipes.

Although Prandtl[11] gave some explanation of the origins of the secondary motion, it was not until the work of Brundrett & Baines[6] that a fairly complete description was provided. They showed that it was gradients in Reynolds stresses in the plane of the cross-section that give rise to a source of streamwise vorticity. Their work included hot-wire measurements of all six components of the Reynolds stress. From these data they deduced that, in rectangular-sectioned ducts, it was predominantly the normal-stress gradients which generated the velocities in the plane of the cross-section. They showed that the basic pattern of secondary flow is independent of Reynolds number, but that with increasing values of Reynolds number the flows penetrate further into the corners and approach closer to the walls.

Gessner & Jones[8] used an X-array hot-wire probe which enabled the Reynolds stresses to be measured more accurately. They derived a momentum equation for the velocity component along a secondary-flow streamline and measured the terms in this equation at points located on this streamline as well as the normal gradients by moving the hot-wire normal to the streamline at each point. This way, the individual terms in the momentum equation could be measured quite accurately. Brundrett and Baines, like Hoagland, established that at any point in the duct the Reynolds number does not affect the ratio of primary to secondary velocity. Gessner & Jones' measurements indicated, however, that the secondary motion diminished substantially relative to the axial velocity as the Reynolds number was increased. They found that the greatest skewness of local wall shear-stress vectors occurs in the immediate vicinity of corners. For the rectangular channels the skewness on the longer wall is greater than the skewness on the shorter wall at points equidistant from the corner. They concluded that in planes normal to the axial-flow direction, opposing forces are exerted by (1) the Reynolds stresses and (2) static-pressure gradients. Small differences in magnitude of these forces cause secondary flow.

Launder & Ying[9] used two square ducts(one duct smooth and the other rough) for their experiment. They found that the secondary velocities normalized with average friction velocity is sensibly independent of whether the duct is rough or smooth. They have argued that the effect of Reynolds number on the secondary motion can be reduced if not eliminated by normalizing the secondary velocities with the friction velocity rather than with the bulk velocity.

In addition to square and rectangular ducts, experimental work has been done in ducts with many other cross-section shapes. Such measurements have been reported by Lyall[12] in two-square interconnected sub-channels, Kacker[13] in a circular duct containing two small rods, Rowe[14] in ducts containing rods arranged in a square array, Kjellstrom[15] and Trupp & Azad[16] in triangular-array rod bundles, Carajilescov & Todreas[17] in a duct simulating an interior sub-channel of a triangular array, Rehme[18] in a single row of rods between two flat walls, Aly, Trupp & Gerrard[19] in an equilateral triangular duct, Seale[20] in a simulated rod bundle, and Hooper & Rehme[21] in closely-spaced rod arrays.

Other than the fully developed turbulent flow, several experimental results have been reported on the developing flows in square and rectangular ducts. Experimenters included Ahmed & Brundrett[22], Po[23], Melling & Whitelaw[24] and Lund[25]. Most of these experiments were conducted in ducts of square cross-section.

PREDICTION

Closed form analytical solutions of turbulent flow are still not possible due to the closure problems. However, various attempts have been made by several investigators in order to predict the flow numerically and achieve reasonable agreement with the available experimental data.

For the numerical prediction of turbulent flow in non-circular ducts, two questions always arised: (1) What kind of turbulence model should be used, (2) What kind of numerical scheme should be choosen.

Turbulence Models

In order to obtain closure of the Reynolds equation, many kinds of turbulence models have been developed in the last half century. Depending upon the number of turbulence parameters used as the dependent variables in the differential transport equations, Reynolds[26] classified turbulence models as follows:

1. Zero-equation models---models using only the pde for the mean velocity field, and no turbulence pde's.

2. One-equation models---models involving an additional pde relating to the turbulence velocity scale.

3. Two-equation models---models incorporating an additional pde related to a turbulence length scale.

4. Stress-equation models---models involving pde's for all components of the turbulent stress tensor.

5. Large-eddy simulations---computations of the three-dimensional time-dependent large-eddy structure and a low-level model for the small-scale turbulence.

The first recognisable turbulence model, the mixing-length model proposed by Prandtl[27], is a zero-equation model. Its central presumptions were: that time-averaged shear stresses and time-averaged velocity gradients are related by formulae of the same type as prevail for laminar fluids; that the "effective viscosity" entering these formulae is proportional to the product of local density, a local turbulence-length scale, and a local velocity of random motion; and that this random velocity is proportional to the length scale multiplied by a local gradient of velocity.

Following Prandtl's model, several other models appeared, including the Von Karman[28] mixing length model and the Van Driest[29] modified mixing length theory.

The one-equation model was initiated by the work of Kolmogorov[30] and Prandtl[31]. Kolmogorov proposed that the random velocity might be taken as the square root of the local kinetic energy k of the fluctuating motion, and that length scale might be equal to this velocity divided by a characteristic frequency ζ. For both k and ζ, he proposed differential equations, purporting to describe how the variations of these quantities were influenced by generation, dissipation, convection and diffusion.

Prandtl made an independent suggestion, a few years later, which contained part of the Kolmogorov hypothesis. He used the same differential equation for determining the k variation; but he retained his assumption that the length scale could be taken as proportional to the distance from a wall.

During the last twenty years, a number of works have sought to provide models of wider applicability by supplying a transport equation from which the length scale may be determined. Here may be mentioned, for example, the work of Harlow & Nakayama[32], Rodi & Spalding[33], Ng & Spalding[34], Spalding[35], and Jones & Launder[36]. Each of these models provides an equation for the turbulent kinetic energy in addition to a scale-determining equation. Closure is thus accomplished through the Prandtl-Kolmogorov formula for the effective turbulent viscosity ν .

$$\nu_t = k^{\frac{1}{2}} l \qquad (2.1)$$

where k denotes the turbulent kinetic energy and l a length scale proportional to that of the energy-containing motions. Since an equation for the turbulence energy is solved, it is clearly not essential for the dependent variable of the second transport equation to be the length scale itself; any variable of the form $k^{a} l^{b}$ would be suitable. Thus Ng & Spalding and Rodi & Spalding have used an equation for the energy-length-scale product while Harlow & Nakayama and Jones & Launder have preferred the energy dissipation rate, which at high turbulence Reynolds numbers may be interpreted as $k^{\frac{3}{2}}/l$.

Recently, the $k-\epsilon$ two-equation model has been favored by many investigators including Launder & Spalding[37], Gosman & Rapley[38][39], Seale[40], Nakayama,Chow & Sharma[41] and Demuren & Rodi[42]. Satisfactory prediction results have been obtained for various kinds of secondary flow problems.

Numerical Scheme

Generally, the ways of applying finite difference method of discretizing the transport equations fall into two groups: the vorticity-based method and the primitive method.

The vorticity-based method has an advantage which is that there is no pressure term appearing in the transport equation. This method is made easily accessible through the book by Gosman, Pun, Runchal, Spalding and Wolfshtein[1]. This method has been applied to solve various two-dimensional problems. The elimination of pressure from the two momentum equations by cross differentiation leads to a vorticity transport equation. This, when combined with the definition of a stream function for steady two-dimensional situations, is the basis of the vorticity-based method. The differential equations from the conservation laws are generalized by one standard elliptic partial differential equation. Using an upwind finite difference method, this differential equation is replaced by the simultaneous algebraic equations which are solved by the iterative method.

By using the $k-\epsilon$ model and the vorticity-based method, a means must be found to express the Reynolds stresses appearing in the source term of the vorticity transport equation. The problem of vorticity source modelling thus arises.

Vorticity Source Models

The first vorticity source model was developed by Launder & Ying[43]. These authors recognized that a model using an isotropic eddy viscosity for calculating the turbulent stresses in the streamwise vorticity equation does not produce any secondary motion at all and that more refined modelling of these stresses is required. Accordingly they derived a model for the stresses v^2-w^2 and vw by simplifying the transport equations for these stresses as given in a model form by Hanjalic & Launder[44]. From these differential equations, algebraic expressions for the above stresses were obtained by neglecting the convection and diffusion terms(assumption of local equilibrium) and by further neglecting all secondary velocity gradients. The primary shear stresses uv and uw were calculated from a standard eddy-viscosity model. At that time, they were still using the k-l one-equation model. The turbulent kinetic energy k appearing in the stress relations was obtained by solving a transport equation for k, and the distribution of the length-scale l was determined from the algebraic geometrical formula of Buleev[45]. This algebraic stress model denoted LY has been used over a fairly wide range of straight duct flows including the square duct by Launder & Ying, the equilateral triangular duct by Aly,Trupp & Gerrard[19] and triangular array rod bundle by Trupp & Aly[46].

Based on the work of Alshamani[47][48], Seale[40] tackled complex geometries and came up with an algebraic vorticity source model, which is calculated directly and without iteration. He illustrated that the model could reproduce secondary velocities in square and triangular cross-section ducts, and in a duct consisting of two interconnected subchannels. This model is hereafter called the Seale's model.

Yadava[2] introduced another model, k correlation model, in which the vorticity source term is calculated based upon the relationships between turbulent intensities as proposed by Alshamani[48]. Together with LY model and Seale's model, three models were tested in the square duct. Detail comparison of the characteristics of these three models has been given in his thesis.

Primitive Method

The primitive method has been developed successfully by the work of Patankar & Spalding[49][50], Patankar[51], Spalding[52]. One of the advantages of the primitive method is that it can be used for three-dimensional problems.

Using the complete six Reynolds stress model proposed by Gessner & Emery[53] and the curvilinear mesh system, Gosman

& Rapley[38][39] obtained a number of results of secondary flow in ducts of different geometries including equilateral triangular duct, square duct, rectangular duct, elliptical duct and different tube assemblies.

Nakayama et al[41] employed the extended LY model(the complete six Reynolds stress model from Gessner & Emery[53]) to predict the secondary flow in square, rectangular and trapezoidal ducts. Detailed local structures of turbulence were discussed.

Naot & Rodi[54] and Demuren & Rodi[42] noticed the importance of the secondary velocity gradients in the Reynolds equation and proposed a new algebraic stress model which might be called the NR model. For this model, satisfactory results were obtained in the square duct and in a partially rough rectangular channel.

It seems at the present time, that the $k-\epsilon$ equation and LY model have been used successfully accompanied by both the primitive method and the vorticity-based method. From the viewpoint of the mathematic treatment, fully developed turbulent flow is a two-dimensional problem in nature. For this reason, the $k-\epsilon$ two-equation model and Gosman et al[1] vorticity-based method have been used by the present author to predict the secondary flow in rectangular duct with five different vorticity source models.

III

GOVERNING EQUATIONS

In this chapter, the governing equations for the fully developed turbulent flow in a rectangular duct are presented. Due to the duct configuration, the Cartesian coordinate system is employed. The symmetrical property of the duct requires only one fourth part of the cross-section of the duct to be considered. The governing equations include the Reynolds equations, vorticity and stream function equations, k & ϵ equations and the temperature equation. These equations describe the fully developed, steady and incompressible turbulent flow of a constant property fluid with negligible body force.

CONTINUITY AND REYNOLDS EQUATIONS

The conservation-of-mass principle states that, in a steady-flow process, the net rate of flow of mass into any control volume is zero. The continuity equation reads:

$$\frac{\delta \overline{V}}{\delta y} + \frac{\delta \overline{W}}{\delta z} = 0 \qquad (3.1)$$

and

$$\frac{\delta u}{\delta x} + \frac{\delta v}{\delta y} + \frac{\delta w}{\delta z} = 0 \qquad (3.1\text{-A})$$

The equations of motion for the turbulent flows can be derived from the Navier-Stokes equations.

Using the tensor notation, the Navier-Stokes equation is:

$$\rho \frac{Du_j}{Dt} = \frac{\partial}{\partial t}(\rho u_j) + \frac{\partial}{\partial x_i}(\rho u_i u_j) = \frac{\partial \tau_{ij}}{\partial x_i} + \rho \overline{F}_j \qquad (3.2)$$

while the Reynolds equation is:

$$\rho \frac{Du_j}{Dt} = -\frac{\partial \overline{P}}{\partial x_j} + \frac{\partial}{\partial x_i}\left(\mu \frac{\partial u_j}{\partial x_i} - \rho \overline{u_i' u_j'}\right) + \rho \overline{F}_j \qquad (3.3)$$

For our case, the Reynolds equations for the three directions are:

$$\rho\left(\overline{V}\frac{\partial \overline{U}}{\partial y} + \overline{W}\frac{\partial \overline{U}}{\partial z}\right) = -\frac{\partial \overline{P}}{\partial x} + \mu\left(\frac{\partial^2 \overline{U}}{\partial y^2} + \frac{\partial^2 \overline{U}}{\partial z^2}\right) - \rho\left(\frac{\partial \overline{uv}}{\partial y} + \frac{\partial \overline{wu}}{\partial z}\right) \qquad (3.4)$$

$$\rho\left(\overline{V}\frac{\partial \overline{V}}{\partial y} + \overline{W}\frac{\partial \overline{V}}{\partial z}\right) = -\frac{\partial \overline{P}}{\partial y} + \mu\left(\frac{\partial^2 \overline{V}}{\partial y^2} + \frac{\partial^2 \overline{V}}{\partial z^2}\right) - \rho\left(\frac{\partial \overline{v^2}}{\partial y} + \frac{\partial \overline{vw}}{\partial z}\right) \qquad (3.5)$$

$$\rho\left(\overline{V}\frac{\partial \overline{W}}{\partial y} + \overline{W}\frac{\partial \overline{W}}{\partial z}\right) = -\frac{\partial \overline{P}}{\partial z} + \mu\left(\frac{\partial^2 \overline{W}}{\partial y^2} + \frac{\partial^2 \overline{W}}{\partial z^2}\right) - \rho\left(\frac{\partial \overline{vw}}{\partial y} + \frac{\partial \overline{w^2}}{\partial z}\right) \qquad (3.6)$$

In the above expressions, the over-bar designates time-averaged quantities.

If equations (3.4), (3.5) and (3.6) are differentiated with respect to x, it is easy to show that the magnitude of $\partial \overline{P}/\partial x$ is constant over the cross-section of the flow.

The roles of the various terms in the axial momentum equation (3.4) are more easily understood if the equation is rearranged in the following form:

$$-\frac{1}{\rho}\frac{\delta \overline{P}}{\delta x}=\left[\frac{\delta \overline{uv}}{\delta y}+\frac{\delta \overline{wu}}{\delta z}\right]-\upsilon\left[\frac{\delta^2 \overline{U}}{\delta y^2}+\frac{\delta^2 \overline{U}}{\delta z^2}\right]+\overline{V}\frac{\delta \overline{U}}{\delta y}+\overline{W}\frac{\delta \overline{U}}{\delta z} \qquad (3.7)$$

(Source) (Diffusion)(Convection)

The convection terms indicate the change in the axial momentum of a fluid particle due to the convection by secondary velocities. These terms are absent in a flow through circular conduit. The diffusion terms represent the change in the axial momentum due to viscous effects and Reynolds shear stresses. The source terms, represents the change in the axial momentum due to the axial pressure gradient.

AXIAL VORTICITY AND STREAM FUNCTION EQUATIONS

The following definition for the stream function (Ψ) and axial vorticity (ω) forms the basis for the calculation procedure:

$$\rho\overline{V}=\delta\Psi/\delta z \qquad (3.8)$$

$$\rho\overline{W}=-\delta\Psi/\delta y \qquad (3.9)$$

$$\omega=\delta\overline{W}/\delta y-\delta\overline{V}/\delta z \qquad (3.10)$$

The pressure gradients in equations (3.5) and (3.6) may be eliminated by the cross-differentiation. By making use of the continuity equation(3.1) as well as the definition of ω, the transport equation for the axial vorticity may be written as:

$$\underbrace{\overline{V}\frac{\delta\omega}{\delta y}+\overline{W}\frac{\delta\omega}{\delta z}}_{(1)}=\underbrace{\frac{\delta^2}{\delta y\delta z}(\overline{v^2}-\overline{w^2})}_{(2)}-\underbrace{\left(\frac{\delta^2\overline{vw}}{\delta y^2}-\frac{\delta^2\overline{vw}}{\delta z^2}\right)}_{(3)}+\underbrace{\upsilon\left(\frac{\delta^2\omega}{\delta y^2}+\frac{\delta^2\omega}{\delta z^2}\right)}_{(4)} \qquad (3.11)$$

This equation as well as the expression for ω include only velocities and gradients in the y and z directions and obviously exists only if the secondary velocities exist and vice versa.

The terms (1) represent the convection of the streamwise vorticity by the mean motion. The terms (2) and (3) express the influence of the turbulent stresses on the production or destruction of streamwise vorticity, and (4) the damping by viscosity.

Substitution of equations (3.8) and (3.9) into (3.10) results in the stream function equation:

$$\frac{\delta}{\delta y}\left(\frac{\delta\Psi}{\delta y}\right)+\frac{\delta}{\delta z}\left(\frac{\delta\Psi}{\delta z}\right)+\rho\omega=0 \qquad (3.12)$$

THE $k-\varepsilon$ EQUATIONS

For the axial momentum equation(3.7), it can be seen that the quantities $\overline{uv}$ and $\overline{uw}$ have to be specified. These shear stress components lie in planes parallel to the direction of the primary velocity and therefore, the conventional turbulent-viscosity concept serves well enough for their simulation. These shear stress components are approximated as:

$$\overline{uv} = -\frac{1}{\rho}\mu_t\frac{\delta\overline{U}}{\delta y} \qquad (3.13)$$

$$\overline{wu} = -\frac{1}{\rho}\mu_t\frac{\delta\overline{U}}{\delta z} \qquad (3.14)$$

where μ is the isotropic turbulent (eddy) viscosity and is given by the Prandtl-Kolmogorov formula:

$$\mu_t = C_\mu \rho k^2/\epsilon \qquad (3.15)$$

where k and ϵ are determined by the corresponding transport equations which read:

$$\rho[\overline{V}\frac{\delta k}{\delta y}+\overline{W}\frac{\delta k}{\delta z}]-\frac{\delta}{\delta y}[(\mu+\frac{\mu_t}{\sigma_k})\frac{\delta k}{\delta y}]-\frac{\delta}{\delta z}[(\mu+\frac{\mu_t}{\sigma_k})\frac{\delta k}{\delta z}]$$

$$-\mu_t[(\frac{\delta\overline{U}}{\delta y})^2+(\frac{\delta\overline{U}}{\delta z})^2]+\rho\epsilon = 0 \qquad (3.16)$$

$$\rho[\overline{V}\frac{\delta\epsilon}{\delta y}+\overline{W}\frac{\delta\epsilon}{\delta z}]-\frac{\delta}{\delta y}[(\mu+\frac{\mu_t}{\sigma_\epsilon})\frac{\delta\epsilon}{\delta y}]-\frac{\delta}{\delta z}[(\mu+\frac{\mu_t}{\sigma_\epsilon})\frac{\delta\epsilon}{\delta z}]$$

$$-C_1\frac{\mu_t\epsilon}{k}[(\frac{\delta\overline{U}}{\delta y})^2+(\frac{\delta\overline{U}}{\delta z})^2]+C_2\rho\frac{\epsilon^2}{k}= 0 \qquad (3.17)$$

The equations above represent the high-Reynolds number $k-\epsilon$ turbulence model which are used in the present prediction. The various model constants are determined by reference to the experimental data. The effects of the various terms in equations (3.16) and (3.17) on k and ϵ are parallel to those terms in equation(3.7) on axial velocity. The convection terms in equations (3.4),(3.11),(3.16) and (3.17) may be expressed in terms of stream functions(Ψ) in the following forms:

$$\frac{\delta}{\delta y}\left(\bar{U}\frac{\delta\Psi}{\delta z}\right)-\frac{\delta}{\delta z}\left(\bar{U}\frac{\delta\Psi}{\delta y}\right)-\left[\frac{\delta}{\delta y}(\mu+\mu_t)\frac{\delta\bar{U}}{\delta y}\right]-\left[\frac{\delta}{\delta z}(\mu+\mu_t)\frac{\delta\bar{U}}{\delta z}\right]+\frac{\delta\bar{P}}{\delta x}=0 \qquad (3.18)$$

$$\frac{\delta}{\delta y}\left(\omega\frac{\delta\Psi}{\delta z}\right)-\frac{\delta}{\delta z}\left(\omega\frac{\delta\Psi}{\delta y}\right)-\frac{\delta}{\delta y}\left[\frac{\delta}{\delta y}(\mu\omega)\right]-\frac{\delta}{\delta z}\left[\frac{\delta}{\delta z}(\mu\omega)\right]$$

$$-\rho\frac{\delta^2(\overline{v^2}-\overline{w^2})}{\delta y\delta z}+\rho\left(\frac{\delta^2\overline{vw}}{\delta y^2}-\frac{\delta^2\overline{vw}}{\delta z^2}\right)=0 \qquad (3.19)$$

$$\frac{\delta}{\delta y}\left(k\frac{\delta\Psi}{\delta z}\right)-\frac{\delta}{\delta z}\left(k\frac{\delta\Psi}{\delta y}\right)-\left[\frac{\delta}{\delta y}\left(\mu+\frac{\mu_t}{\sigma_k}\right)\frac{\delta k}{\delta y}\right]-\left[\frac{\delta}{\delta z}\left(\mu+\frac{\mu_t}{\sigma_k}\right)\frac{\delta k}{\delta z}\right]$$

$$-\mu_t\left[\left(\frac{\delta\bar{U}}{\delta y}\right)^2+\left(\frac{\delta\bar{U}}{\delta z}\right)^2\right]+\rho\epsilon=0 \qquad (3.20)$$

$$\frac{\delta}{\delta y}\left(\epsilon\frac{\delta\Psi}{\delta z}\right)-\frac{\delta}{\delta z}\left(\epsilon\frac{\delta\Psi}{\delta y}\right)-\left[\frac{\delta}{\delta y}\left(\mu+\frac{\mu_t}{\sigma_\epsilon}\right)\frac{\delta\epsilon}{\delta y}\right]-\left[\frac{\delta}{\delta z}\left(\mu+\frac{\mu_t}{\sigma_\epsilon}\right)\frac{\delta\epsilon}{\delta z}\right]$$

$$-C_1\frac{\mu_t\epsilon}{k}\left[\left(\frac{\delta\bar{U}}{\delta y}\right)^2+\left(\frac{\delta\bar{U}}{\delta z}\right)^2\right]+C_2\rho\frac{\epsilon^2}{k}=0 \qquad (3.21)$$

TEMPERATURE EQUATION

The temperature equation can be derived from the energy conservation equation and is expressed as:

$$\frac{\delta}{\delta y}\left(\overline{T}\frac{\delta\Psi}{\delta z}\right)-\frac{\delta}{\delta z}\left(\overline{T}\frac{\delta\Psi}{\delta y}\right)-\left[\frac{\delta}{\delta y}\left(\frac{\mu}{Pr}+\frac{\mu_t}{Pr_t}\right)\frac{\delta\overline{T}}{\delta y}\right]-\left[\frac{\delta}{\delta z}\left(\frac{\mu}{Pr}+\frac{\mu_t}{Pr_t}\right)\frac{\delta\overline{T}}{\delta z}\right]+\rho\overline{U}\frac{\delta\overline{T}}{\delta x}=0 \quad (3.22)$$

Pr_t is the turbulent Prandtl number and is assigned its usual value of 0.09. The laminar Prandtl number Pr is given the value of 0.7(for air).

BOUNDARY CONDITIONS

The domain and the coordinate are shown in Fig.1. The aspect ratio λ is defined as

$$\lambda=H1/H2 \quad (3.22\text{-}1)$$

where H1 and H2 are the half width and height respectively.

(1) Stream Function(Ψ)

With reference to Fig.1, since no net mass is transfered across the four boundaries(i.e. two solid wall and two symmetrical lines), the stream function is constant along these boundaries. This constant was conveniently set to be zero.

(2) Axial Vorticity(ω)

The vorticity boundary condition at the symmetric lines can be derived from its definition.

At y=0 in Fig.1, from the symmetric property we know that $\partial\overline{W}/\partial y=0$. Along y=0, $\overline{V}$ is zero which results in $\partial\overline{V}/\partial z=0$. Since $\omega=\partial\overline{W}/\partial y-\partial\overline{V}/\partial z$, thus $\omega=0$ at y=0. The same conclusion can be obtained at z=0. Therefore, the vorticity is zero at the two symmetry line boundaries. Near the wall, it was assumed that the vorticity varies linearly with the normal distance from the wall.

(3) $\overline{U}, k, \epsilon$ and $\overline{T}$

Along the symmetry lines, the symmetry demands gradients of $\overline{U}$, k, ϵ and $\overline{T}$ to be zero. Mathematically, it is given as:

For y=0, $0 \leqslant z \leqslant H2$:

$$\frac{\partial\overline{U}}{\partial y}=\frac{\partial k}{\partial y}=\frac{\partial \epsilon}{\partial y}=\frac{\partial\overline{T}}{\partial y}=0 \tag{3.23}$$

For z=0, $0 \leqslant y \leqslant H1$:

$$\frac{\partial\overline{U}}{\partial z}=\frac{\partial k}{\partial z}=\frac{\partial \epsilon}{\partial z}=\frac{\partial\overline{T}}{\partial z}=0 \tag{3.24}$$

It is assumed that the universal law of the wall holds good in secondary flow problems and can be used to represent accurately the velocity profile in the region close to the wall. Therefore, a boundary condition was imposed on the nodes next to the wall. However care was taken in designing the grid such that these first string of nodes are located beyond the viscous sublayer for the Reynolds number involved. The boundary condition is expressed as:

$$\overline{U}=u^*[A\ln(\frac{\rho u^*|z_n-z_p|}{\mu})+B] \qquad (3.25)$$

where u* represents the local friction velocity and A and B are constants. The suffix p denotes the wall node whereas n and m stands for the node next to the wall and the node twice removed from the wall respectively, in the direction normal to the wall.

The local wall friction velocity u* is given by:

$$u^*=\sqrt{\tau/\rho} \qquad (3.26)$$

where the local wall shear stress τ is calculated from the turbulence field data at the second string of nodes(m) in the fluid as follows:

$$\tau=\rho C_\mu^{1/4} k_m^{1/2} \overline{U}_m/[A\ln(\frac{\rho u^*|z_m-z_p|}{\mu})+B] \qquad (3.27)$$

By reference to the properties of the "constant-stress" wall region, the boundary conditions for the turbulent kinetic energy (k) and its dissipation rate (ϵ) were prescribed. They were also imposed at the first string of nodes(n), adjacent to the wall and given by the conventional form:

$$k_n=u^{*2}/C_\mu^{1/2} \qquad (3.28)$$

$$\epsilon_n=u^{*3}/(\kappa z_n) \qquad (3.29)$$

where κ is the universal Von-Karman constant and z_n is the distance normal to the wall.

For the temperature equation, it is assumed that the average circumferential surface flux is uniform along the duct and, at any station, the circumferential wall temperature is constant. The boundary condition on $\overline{T}$ is again the appropriate 'universal' semi-logarithmic law:

$$\overline{T}_n = \overline{T}_w + \frac{\dot{q}''}{\rho c_p u^*}\left[\frac{\overline{U}}{u^*} + P^*\right] \qquad (3.30)$$

where the P-function has the form:

$$P^* = 9.24\left[\left(\frac{Pr}{Pr_t}\right)^{\frac{3}{4}} - 1\right] \qquad (3.31)$$

IV

VORTICITY SOURCE MODELLING

For the axial vorticity equation, its complete closure requires the specification of gradients of the difference in Reynolds normal stresses $\overline{v^2}-\overline{w^2}$ as well as Reynolds shear stress $\overline{vw}$ in the axial vorticity source term.

A number of investigators have shown that the shear stress terms are negligibly small compared with the normal stress terms, e.g. the measurements of Brundrett and Baines[6] in a square duct, and those of Aly et al[19] in a triangular duct. Trupp and Aly[46] found that the normal stress vorticity production predominated everywhere in the subchannels of triangular array rod bundle. Vorticity production, therefore, was considered to be solely due to the inbalance in the normal stresses, i.e. $\overline{v^2}-\overline{w^2}$.

In the present work, five models have been prescribed to determine the vorticity production.

THE LY MODEL

Launder and Ying [43] proposed the first vorticity source model as:

$$(\overline{v^2}-\overline{w^2})=C_1'\frac{k}{\epsilon}[\overline{uv}\frac{\partial\overline{U}}{\partial y}-\overline{wu}\frac{\partial\overline{U}}{\partial z}] \qquad (4.1)$$

which relates the vorticity-generating Reynolds stresses to axial gradients of the mean velocity.

Substituting equation (3.13) and (3.14) into equation (4.1) gives:

$$(\overline{v^2}-\overline{w^2})=C_1'\mu_t\frac{k}{\rho\epsilon}[(\frac{\partial\overline{U}}{\partial z})^2-(\frac{\partial\overline{U}}{\partial y})^2] \qquad (4.2)$$

This model, with extended form by Gessner & Emery[53], has been widely used to predict sucessfully the secondary flow in ducts of various kinds of cross-section. However, the constant C_1' has a wide range of values among different investigators, e.g. Launder & Ying[43] used $C_1'=0.0185$, Gessner & Po[55] used $C_1'=0.101$ and Aly, Trupp & Gerrard[19] used $C_1'=0.011$. In the present case, different values of C_1' were chosen for each of the different aspect ratio for the rectangular ducts. Detail will be discussed in chapter 6.

THE SEALE'S MODEL

Alshamani[48] examined the axial, normal and tangential turbulence intensity measurements carried out by several investigators and observed a similarity in the distribution of these turbulence intensities. He concluded that any two components of turbulence intensity are very nearly linearly related. Based on the data of Sandborn[56], Laufer[57][58], Lawn[59][60], Clark[61][62] and Comte-Bellot[63], Alshamani proposed correlations among turbulent shear stress, turbulent kinetic energy and axial turbulence intensity. According to these correlations, Yadava[2] introduced an expression for Reynolds normal stress in terms of turbulent kinetic energy as follows:

$$(\overline{v^2}-\overline{w^2})=u^{*2}(0.2708-0.1245k^{+}-0.0286k^{+2}) \qquad (4.3)$$

Using this Turbulent Properties Correlations Model, Yadava predicted successfully the secondary flow in a square duct where one octant contains only one flow cell.

However, when this model was applied by the present author to rectangular ducts which involves multiple flow cells in each quadrant, there was no convergent solution for any aspect ratio. When using this model to generate secondary flows in his SRB duct, Seale[40] experienced results that were not satisfactory, the secondary velocities were about three times larger than those measured and produced distortions to the predicted contours of axial velocity and turbulence kinetic energy which did not agree with those observed in the measurements. He noted that the vorticity source is extraordinarily sensitive to the exact distribution of k^+; the predicted distribution did not have the necessary accuracy to allow correct secondary velocities to be generated. Hence this model was abandoned.

Seale[40] used Alshamani's correlations and made some modifications on the differentiation of Reynolds stresses and proposed another vorticity source model:

$$\rho \frac{\partial^2}{\partial y \partial z}(\overline{v^2}-\overline{w^2})=8C_2'\rho u^{*2}k_{c,+}/[(\hat{Y}max)mY_P Y_L Y_N \frac{\partial \hat{Y}}{\partial z}] \quad (4.4)$$

where

$$\begin{aligned} &Y_P=1-\hat{Y}/\hat{Y}max, \quad Y_m=1-2.4Y_P^2, \quad Y_L=1-y/\hat{Y}max \\ &Y_N=[2+Y_m+(4-Y_m)Y_L^2]-[(1-Y_L^2)(4-Y_m)] \\ &k_{c,+}=1, \ m=2.4 \end{aligned} \quad (4.5)$$

y: normal distance from wall
$\hat{Y}$: normal distance from wall to surface of no-shear
$\hat{Y}max$: maximum value of $\hat{Y}$

Y_L is a normalized distance from the wall and varies from 1 at the wall to Y_P at the surface of no shear. The surface of no shear is assumed to be coincident with the position of the maximum axial velocity on the normal from the wall.

One of the special characteristics of this model is that it does not need the precise calculation of Reynolds stress and is calculated directly and without iteration.

The $\hat{Y}$ line is defined as the straight line of corner bisector as shown in Fig.35. Like the LY model, it was also found necessary to vary C_2' depending on the aspect ratio.Further details are provided later.

THE NR MODEL

Launder, Reece & Rodi[64] proposed a Reynolds-stress-equation model which accounts for near-wall effects on the turbulent fluctuations by a special wall-proximity correction to the pressure-strain model. Naot & Rodi[54] simplified this model to an algebraic-stress model, which is called NR model, and applied it to calculate the secondary motion in developed duct and open-channel flows. It was also used by Demuren & Rodi[42] to calculate the secondary flow in a square duct and a partially rough rectangular channel. Similar to LY, NR neglected the convection and diffusion terms in the Reynolds stress equation(assumption of local equilibrium) and calculated the primary stresses with the standard eddy-viscosity model. However, the terms involving secondary velocity gradients in the modelled transport equation for $\overline{v^2}$,$\overline{w^2}$ and $\overline{vw}$ were not neglected but approximated by products of an isotropic eddy viscosity and the corresponding secondary velocity gradients. The NR model is expressed as:

$$\overline{v^2} = \frac{\dfrac{2k}{c\epsilon}\left[\dfrac{\epsilon}{3}(\alpha+\beta+c-1)+\beta\overline{uv}\dfrac{\partial\overline{U}}{\partial y}-\overline{vw}\left\{(1-\alpha)\dfrac{\partial\overline{V}}{\partial z}-\beta\dfrac{\partial\overline{W}}{\partial y}\right\}-\gamma k\dfrac{\partial\overline{V}}{\partial y}\right]}{1+\dfrac{2k}{C_1\epsilon}(1-\alpha-\beta)\dfrac{\partial\overline{V}}{\partial y}} \tag{4.6}$$

$$\overline{w^2} = \frac{\frac{2k}{c\epsilon}\left[\frac{\epsilon}{3}(\alpha+\beta+c-1)+\beta\overline{wu}\frac{\delta\overline{U}}{\delta z}-\overline{vw}\left\{(1-\alpha)\frac{\delta\overline{W}}{\delta y}-\beta\frac{\delta\overline{V}}{\delta z}\right\}-\gamma k\frac{\delta\overline{W}}{\delta z}\right]}{1+\frac{2k}{C_1\epsilon}(1-\alpha-\beta)\frac{\delta\overline{W}}{\delta z}} \tag{4.7}$$

where

$$\frac{k}{c\epsilon}\left[\overline{vw}\left\{(1-\alpha)\frac{\delta\overline{V}}{\delta z}-\beta\frac{\delta\overline{W}}{\delta y}\right\}+\gamma k\frac{\delta\overline{V}}{\delta y}\right]=\upsilon_t\frac{\delta\overline{V}}{\delta y} \tag{4.8}$$

$$\frac{k}{c\epsilon}\left[\overline{vw}\left\{(1-\alpha)\frac{\delta\overline{W}}{\delta y}-\beta\frac{\delta\overline{V}}{\delta z}\right\}+\gamma k\frac{\delta\overline{W}}{\delta z}\right]=\upsilon_t\frac{\delta\overline{W}}{\delta z} \tag{4.9}$$

The α, β and c are given by

$$\begin{aligned} &\alpha=0.7636-0.06f \\ &\beta=0.1091+0.06f \\ &c=1.5-0.5f \\ &f=L/\langle y\rangle, \text{ with } 1/\langle y\rangle=0.5\int_0^{2\pi} d\phi/s, \quad L=C_\mu^{3/4}k^{3/2}/(\kappa\epsilon) \end{aligned} \tag{4.10}$$

The NR model is expressed as:

$$\overline{v^2}-\overline{w^2}=C_3'\left\{\frac{\frac{2k}{c\epsilon}\left[\frac{\epsilon}{3}(\alpha+\beta+c-1)-\beta\upsilon_t\left(\frac{\delta\overline{V}}{\delta y}\right)^2\right]-2\upsilon_t\frac{\delta\overline{V}}{\delta y}}{1+\frac{2k}{c\epsilon}(1-\alpha-\beta)\frac{\delta\overline{V}}{\delta y}} - \frac{\frac{2k}{c\epsilon}\left[\frac{\epsilon}{3}(\alpha+\beta+c-1)-\beta\upsilon_t\left(\frac{\delta\overline{W}}{\delta z}\right)^2\right]-2\upsilon_t\frac{\delta\overline{W}}{\delta z}}{1+\frac{2k}{c\epsilon}(1-\alpha-\beta)\frac{\delta\overline{W}}{\delta z}}\right\} \tag{4.11}$$

THE κ MODEL

This model, as well as the following ϵ model, is proposed by the present author according to the numerical experience.

From the viewpoint of governing equation, boundary condition and the distribution of k and $\overline{U}$, they are very similar to each other. LY model links the Reynolds stresses to the gradients of the axial velocity, as follows:

$$\overline{v^2}-\overline{w^2}=C_1'\mu_t\frac{k}{\rho\epsilon}\left[\left(\frac{\delta\overline{U}}{\delta z}\right)^2-\left(\frac{\delta\overline{U}}{\delta y}\right)^2\right] \qquad (4.12)$$

Similarly, the Reynolds stresses might be determined by the gradients of k. Parallel to the LY model, the k model was proposed as:

$$\overline{v^2}-\overline{w^2}=C_4'\frac{\mu_t}{\rho\epsilon}\left[\left(\frac{\delta k}{\delta z}\right)^2-\left(\frac{\delta k}{\delta y}\right)^2\right] \qquad (4.13)$$

This model was used to predict the secondary flows in rectangular ducts of aspect ratios of 1:1, 2:1, 2.5:1, 3:1, 4:1, and it achieved reasonable results compared to the experimental data. Details will be provided later.

This model is proposed based on the numerical experience. Presently, there is no theoretical background or explicit experimental evidence. However, in order to rationalize this model, a proposal is made in the following paragraph.

As is well known in laminar flow, the shear stress is determined by the gradient of velocity as:

$$\tau_{yx} = \mu \frac{\delta \overline{U}}{\delta y} \tag{4.14}$$

where μ is the fluid viscosity.

In turbulent flow, a similar equation is:

$$\tau_{yx}^{t} = \mu_t \frac{\delta \overline{U}}{\delta y} \tag{4.15}$$

but with

$$\mu_t = C_\mu \rho k^2/\epsilon \tag{4.16}$$

for the k-ϵ two-equation model.

All these equations state that the shear stress is determined by the gradient of axial velocity. In turbulent flow, we have another variable to describe the characteristic of turbulence. It is the turbulent kinetic energy k.

If we consider that the shear stress could be determined by the gradient of k, a proposal is made as:

$$\tau_{yx}^{t} = C' \mu_t \frac{1}{\sqrt{k}} \frac{\delta k}{\delta y} \tag{4.17}$$

where μ_t is the same as (4.16). C' is a constant.

From LY model:

$$\overline{v^2} - \overline{w^2} = C_1' \frac{k}{\epsilon} [\overline{uv} \frac{\delta \overline{U}}{\delta y} - \overline{wu} \frac{\delta \overline{U}}{\delta z}] \tag{4.18}$$

Substituting (3.13) and (3.14) into (4.18):

$$\overline{v^2} - \overline{w^2} = C_1' \frac{k\rho}{\epsilon \mu_t} [-\overline{uv}^2 + \overline{wu}^2] \tag{4.19}$$

From (4.17) we see:

$$\overline{uv}=C'\frac{\upsilon_t}{\sqrt{k}}\frac{\partial k}{\partial y} \tag{4.20}$$

$$\overline{wu}=C'\frac{\upsilon_t}{\sqrt{k}}\frac{\partial k}{\partial z} \tag{4.21}$$

Substituting (4.20) and (4.21) into (4.19):

$$\overline{v^2}-\overline{w^2}=C_4'\frac{\mu_t}{\rho\epsilon}\left[\left(\frac{\partial k}{\partial z}\right)^2-\left(\frac{\partial k}{\partial y}\right)^2\right] \tag{4.22}$$

which is the same as (4.13).

Now we see that if we accept the proposal(4.17), based on the LY model, we can easily get the k model. We need only one proposal to get this model and there is no conflict to the existing theory about the definition of μ_t. C_4' is determined based on the results to suit the best overall agreement between predicted and experimental results.

Equation (4.17) is only a proposal and needs experimental evidence and a theoretical background. It is the work for further research.

THE ϵ MODEL

This model is based on the idea that the Reynolds stresses could be determined by the gradient of energy dissipation rate ϵ and is very similar to the k model. The corresponding proposal is

$$\tau_{yx}^{+} = C'' \mu_t \frac{\overline{U}\delta\epsilon}{\epsilon\delta y} \tag{4.23}$$

where μ_t is the same as(4.16), $\overline{U}$ the axial velocity, ϵ is the energy dissipation rate and C" is the constant.

From LY model

$$\overline{v^2}-\overline{w^2}=C_1' \frac{k\rho}{\epsilon\mu_t}[-\overline{uv}^2+\overline{wu}^2] \tag{4.24}$$

From (4.23)

$$\overline{uv}=C'' \frac{\upsilon_t}{\epsilon} \frac{\overline{U}\delta\epsilon}{\delta y} \tag{4.25}$$

$$\overline{wu}=C'' \frac{\upsilon_t}{\epsilon} \frac{\overline{U}\delta\epsilon}{\delta z} \tag{4.26}$$

Substituting (4.25) and (4.26) into (4.24):

$$\overline{v^2}-\overline{w^2}=C_5' \frac{\overline{U}^2\mu_t k}{\rho\epsilon^3}[(\frac{\delta\epsilon}{\delta z})^2-(\frac{\delta\epsilon}{\delta y})^2] \tag{4.27}$$

which is the ϵ model.

Successful prediction results have been obtained by this ϵ model for the secondary flow in different aspect ratios of rectangular ducts.

Now we have five vorticity source models. Generally speaking, the LY, k, ϵ models are more fundamental. The Seale's model need the definition of the $\hat{y}$ line which varys with the different duct geometries. The NR model also needs some definition of L,etc. Detailed results and comparisons are given in chapter 6.

SUMMARY OF EQUATIONS

Transport Equations

(1) Axial Velocity Equation:

$$\frac{\delta}{\delta y}\left(\bar{U}\frac{\delta\Psi}{\delta z}\right)-\frac{\delta}{\delta z}\left(\bar{U}\frac{\delta\Psi}{\delta y}\right)-\left[\frac{\delta}{\delta y}(\mu+\mu_t)\frac{\delta\bar{U}}{\delta y}\right]-\left[\frac{\delta}{\delta z}(\mu+\mu_t)\frac{\delta\bar{U}}{\delta z}\right]+\frac{\delta\bar{P}}{\delta x}=0 \quad (4.28)$$

(2) Axial Vorticity Equation:

$$\frac{\delta}{\delta y}\left(\omega\frac{\delta\Psi}{\delta z}\right)-\frac{\delta}{\delta z}\left(\omega\frac{\delta\Psi}{\delta y}\right)-\frac{\delta}{\delta y}\left[\frac{\delta}{\delta y}(\mu\omega)\right]-\frac{\delta}{\delta z}\left[\frac{\delta}{\delta z}(\mu\omega)\right]$$

$$-\rho\frac{\delta^2(\overline{v^2}-\overline{w^2})}{\delta y\delta z}=0 \quad (4.29)$$

(3) Stream Function Equation:

$$\frac{\delta}{\delta y}\left(\frac{\delta\Psi}{\delta y}\right)+\frac{\delta}{\delta z}\left(\frac{\delta\Psi}{\delta z}\right)+\rho\omega=0 \quad (4.30)$$

(4) Turbulent Kinetic Energy Equation:

$$\frac{\delta}{\delta y}\left(k\frac{\delta\Psi}{\delta z}\right)-\frac{\delta}{\delta z}\left(k\frac{\delta\Psi}{\delta y}\right)-\left[\frac{\delta}{\delta y}\left(\mu+\frac{\mu_t}{\sigma_k}\right)\frac{\delta k}{\delta y}\right]-\left[\frac{\delta}{\delta z}\left(\mu+\frac{\mu_t}{\sigma_k}\right)\frac{\delta k}{\delta z}\right]$$

$$-\mu_t\left[\left(\frac{\delta\bar{U}}{\delta y}\right)^2+\left(\frac{\delta\bar{U}}{\delta z}\right)^2\right]+\rho\epsilon=0 \quad (4.31)$$

(5) Turbulent Energy Dissipation Rate Equation:

$$\frac{\delta}{\delta y}\left(\epsilon\frac{\delta\Psi}{\delta z}\right)-\frac{\delta}{\delta z}\left(\epsilon\frac{\delta\Psi}{\delta y}\right)-\left[\frac{\delta}{\delta y}\left(\mu+\frac{\mu_t}{\sigma_\epsilon}\right)\frac{\delta\epsilon}{\delta y}\right]-\left[\frac{\delta}{\delta z}\left(\mu+\frac{\mu_t}{\sigma_\epsilon}\right)\frac{\delta\epsilon}{\delta z}\right]$$

$$-C_1\frac{\mu_t\,\epsilon}{k}\left[\left(\frac{\delta\bar{U}}{\delta y}\right)^2+\left(\frac{\delta\bar{U}}{\delta z}\right)^2\right]+C_2\rho\frac{\epsilon^2}{k}=0 \tag{4.32}$$

(6) Temperature Equation:

$$\frac{\delta}{\delta y}\left(\bar{T}\frac{\delta\Psi}{\delta z}\right)-\frac{\delta}{\delta z}\left(\bar{T}\frac{\delta\Psi}{\delta y}\right)-\left[\frac{\delta}{\delta y}\left(\frac{\mu}{Pr}+\frac{\mu_t}{Pr_t}\right)\frac{\delta\bar{T}}{\delta y}\right]-\left[\frac{\delta}{\delta z}\left(\frac{\mu}{Pr}+\frac{\mu_t}{Pr_t}\right)\frac{\delta\bar{T}}{\delta z}\right]+\rho\bar{U}\frac{\delta\bar{T}}{\delta x}=0 \tag{4.33}$$

Algebraic Equations

(1) Vorticity Source Modelling

(1.1) LY Model

$$(\overline{v^2}-\overline{w^2})=C_1'\mu_t\frac{k}{\rho\epsilon}\left[\left(\frac{\delta\bar{U}}{\delta z}\right)^2-\left(\frac{\delta\bar{U}}{\delta y}\right)^2\right] \tag{4.34}$$

(1.2) Seale's Model

$$\rho\frac{\delta^2}{\delta y\delta z}(\overline{v^2}-\overline{w^2})=8C_2'\rho u^{*2}k_{c,t}\Big/\left[(\hat{Y}max)mY_P\,Y_L\,Y_N\frac{\delta\hat{Y}}{\delta z}\right] \tag{4.35}$$

where

$$\begin{aligned}&Y_P=1-\hat{Y}/\hat{Y}max,\quad Y_m=1-2.4Y_P^2,\quad Y_L=1-y/\hat{Y}max\\&Y_N=[2+Y_m+(4-Y_m)Y_L^2]-[(1-Y_L^2)(4-Y_m)]\\&k_{c,t}=1,\ m=2.4\end{aligned} \tag{4.35-A}$$

y: normal distance from wall
$\hat{Y}$: normal distance from wall to surface of no-shear
$\hat{Y}$max: maximum value of $\hat{Y}$

(1.3) NR Model

$$\overline{v^2}-\overline{w^2}=C_3'\left\{\frac{\frac{2k}{c\epsilon}\left[\frac{\epsilon}{3}(\alpha+\beta+c-1)-\beta\upsilon_t\left(\frac{\partial\overline{V}}{\partial y}\right)^2\right]-2\upsilon_t\frac{\partial\overline{V}}{\partial y}}{1+\frac{2k}{c\epsilon}(1-\alpha-\beta)\frac{\partial\overline{V}}{\partial y}}\right.$$

$$\left.-\frac{\frac{2k}{c\epsilon}\left[\frac{\epsilon}{3}(\alpha+\beta+c-1)-\beta\upsilon_t\left(\frac{\partial\overline{W}}{\partial z}\right)^2\right]-2\upsilon_t\frac{\partial\overline{W}}{\partial z}}{1+\frac{2k}{c\epsilon}(1-\alpha-\beta)\frac{\partial\overline{W}}{\partial z}}\right\} \tag{4.36}$$

(1.4) k Model

$$\overline{v^2}-\overline{w^2}=C_4'\frac{\mu_t}{\rho\epsilon}\left[\left(\frac{\partial k}{\partial z}\right)^2-\left(\frac{\partial k}{\partial y}\right)^2\right] \tag{4.37}$$

(1.5) ϵ model

$$\overline{v^2}-\overline{w^2}=C_5'\frac{\overline{U}^2\mu_t\,k}{\rho\epsilon^3}\left[\left(\frac{\partial\epsilon}{\partial z}\right)^2-\left(\frac{\partial\epsilon}{\partial y}\right)^2\right] \tag{4.38}$$

(2) Turbulent Viscosity

$$\mu_t=C_\mu\,\rho k^2/\epsilon \tag{4.39}$$

(3) Source Term for Axial Velocity Equation

$$\frac{\partial\overline{P}}{\partial x}=-4\overline{\tau}/D_h \tag{4.40}$$

(4) Source Term for Temperature Equation

$$\frac{\partial\overline{T}}{\partial x}=(\text{Wetted perimeter})\frac{\dot{q}''}{\dot{m}c_p} \tag{4.41}$$

(5) Friction Factor

$$f=8\overline{\tau}/(\rho\overline{U}_b^2) \tag{4.42}$$

Boundary Conditions

(1) Symmetry lines

$$\Psi=\omega=0 \tag{4.43}$$

$$\frac{\delta \overline{U}}{\delta y}=\frac{\delta k}{\delta y}=\frac{\delta \epsilon}{\delta y}=\frac{\delta \overline{T}}{\delta y}=0 \quad \text{for } y=0, \quad 0\leqslant z\leqslant H2 \tag{4.44}$$

$$\frac{\delta \overline{U}}{\delta z}=\frac{\delta k}{\delta z}=\frac{\delta \epsilon}{\delta z}=\frac{\delta \overline{T}}{\delta z}=0 \quad \text{for } z=0, \quad 0\leqslant y\leqslant H1 \tag{4.45}$$

(2) Walls

$$\Psi=0 \tag{4.46}$$

$$\omega_p=\omega_n+\frac{z_p-z_n}{z_n-z_m}(\omega_n-\omega_m) \tag{4.47}$$

$$\overline{U}_n=u^*[A\ln(\frac{\rho u^*|z_n-z_p|}{\mu})+B] \tag{4.48}$$

$$k_n=u^{*2}/C\mu \tag{4.49}$$

$$\epsilon_n=u^{*3}/(\kappa z_n) \tag{4.50}$$

where $u^*=\sqrt{\tau/\rho}$ (4.51)

$$\overline{T}_n=\overline{T}_w+\frac{\dot{q}''}{\rho c_p u^*}[\frac{\overline{U}}{u^*}+P^*] \tag{4.52}$$

where

$$P^*=9.24[(\frac{Pr}{Pr_t})^{\frac{3}{4}}-1] \tag{4.53}$$

All the governing equations are summerized in table 2.

V

NUMERICAL SCHEME

INTRODUCTION

As stated early, an upwind finite difference scheme of Gosman et al (1969) has been used for the prediction. This procedure starts with a standard elliptic partial differential equation as follows:

$$a_{\phi}\left[\frac{\partial}{\partial y}\left(\phi\frac{\partial\Psi}{\partial z}\right)-\frac{\partial}{\partial z}\left(\phi\frac{\partial\Psi}{\partial y}\right)\right]-\left[\frac{\partial}{\partial y}\left(b_{\phi,y}\frac{\partial\phi}{\partial y}\right)+\frac{\partial}{\partial z}\left(b_{\phi,z}\frac{\partial\phi}{\partial z}\right)\right]+S_{\phi}=0 \qquad (5.1)$$

The representative symbols in this equation are identified for each equation from (4.28) to (4.33) in table 2.

FINITE DIFFERENCE EQUATION

For the purpose of the derivation of the finite difference equation, a Cartesian coordinate grid network has been employed over the field of interest. Fig.2 displays a part of such a grid; there is shown a typical node P, and the four surrounding nodes N, S, E and W. The finite difference equation will eventually be expressed primarily in terms of the values of the variables at these nodes, and to a less extent in terms of the values on the nodes labelled NE, NW, SE and SW.

The integration of the differential equation will be performed over the area enclosed by the small rectangle, shown by the dotted lines, which encloses the point P. The sides of this rectangle are supposed to lie midway between the neighbouring grid lines.

The double integration over the domain shown in Fig.2 yields:

$$a_\phi \int_{z,s}^{n} \int_{y,w}^{e} \left[\frac{\delta}{\delta y}\left(\phi \frac{\delta\Psi}{\delta z}\right) - \frac{\delta}{\delta z}\left(\phi \frac{\delta\Psi}{\delta y}\right)\right] dydz$$

(Convection terms = I_c)

$$-\int_{z,s}^{n} \int_{y,w}^{e} \left[\frac{\delta}{\delta y}\left(b_{\phi,y} \frac{\delta\phi}{\delta y}\right) + \frac{\delta}{\delta z}\left(b_{\phi,z} \frac{\delta\phi}{\delta z}\right)\right] dydz$$

(Diffusion terms = I_d)

$$= -\int_{z,s}^{n} \int_{y,w}^{e} S_\phi \, dydz \qquad (5.2)$$

(Source terms = I_S)

Equation (5.2) can also be written as:

$$I_c - I_d + I_S = 0 \qquad (5.3)$$

The integrals for each term appearing in equation (5.2) are evaluated individually in the following subsections.

<u>Convection Terms</u>

From (5.2)

$$I_c = a_\phi \left\{ \int_{z,s}^{n} \left[\phi_e \left(\frac{\delta\Psi}{\delta z}\right)_e - \phi_w \left(\frac{\delta\Psi}{\delta z}\right)_w\right] dz - \int_{y,w}^{e} \left[\phi_n \left(\frac{\delta\Psi}{\delta y}\right)_n - \phi_s \left(\frac{\delta\Psi}{\delta y}\right)_s\right] dy \right\} \qquad (5.4)$$

which can be expressed as:

$$I_c = I_{c_1} + I_{c2} + I_{c3} + I_{c4} \tag{5.5}$$

where

$$I_{c_1} = a_\phi \int_{z,s}^{n} \phi_e \left(\frac{\delta\Psi}{\delta z}\right)_e dz \tag{5.6}$$

and so on.

If ϕ and Ψ are well-behaved functions, then there exists an average value of which we denote by such that:

$$\overline{\phi_e} = \frac{\int_{z,s}^{n} \phi_e (\delta\Psi/\delta z)_e \, dz}{\int_{z,s}^{n} (\delta\Psi/\delta z)_e \, dz} = \frac{I_{c_1}}{a_\phi (\Psi_{ne} - \Psi_{se})} \tag{5.7}$$

where the subscripts ne and se refer to the relevant corners of the rectangle shown in Fig. 2. It follows that we may re-write equation (5.6) as:

$$I_{c_1} = a_\phi \overline{\phi_e} (\Psi_{ne} - \Psi_{se}) \tag{5.8}$$

Our next task is to express in terms of values of the variables at the nodes of the grid; and to do this, we make three assumptions.

(1) The function ϕ is uniform within each rectangle and has the value of node P.

(2) The value of the stream function at a particular corner of the rectangle is equal to the average of the values on the four neighbouring nodes.

(3) The average value of the function ϕ takes the value possessed by the fluid upstream of the specific face under consideration, i.e. the "Upwind Technique".

Applying the upwind difference technique, I_{c1} can be written as:

$$I_{c1} = a_\phi \{ \phi_P [\frac{(\Psi_{ne} - \Psi_{se}) - |\Psi_{ne} - \Psi_{se}|}{2}] + \phi_E [\frac{(\Psi_{ne} - \Psi_{se}) + |\Psi_{ne} - \Psi_{se}|}{2}] \} \qquad (5.9)$$

whereas assumption (2) can be mathematically expressed as:

$$\Psi_{ne} = [\Psi_{NE} + \Psi_N + \Psi_P + \Psi_E]/4 \qquad (5.10)$$

and

$$\Psi_{se} = [\Psi_{SE} + \Psi_S + \Psi_P + \Psi_E]/4 \qquad (5.11)$$

The other terms of equation (5.5), i.e. can be obtained by a similar treatment for each of them.

Assembling and rearrangment of various terms produces the following expression:

$$I_C = A_E(\phi_P - \phi_E) + A_W(\phi_P - \phi_W) + A_N(\phi_P - \phi_N) + A_S(\phi_P - \phi_S) \qquad (5.12)$$

where the coefficients A are:

$$\begin{aligned}
A_E &= \{[\Psi_{SE} + \Psi_S - \Psi_{NE} - \Psi_N] + |\Psi_{SE} + \Psi_S - \Psi_{NE} - \Psi_N|\} a_\phi/8 \\
A_W &= \{[\Psi_{NW} + \Psi_N - \Psi_{SW} - \Psi_S] + |\Psi_{NW} + \Psi_N - \Psi_{SW} - \Psi_S|\} a_\phi/8 \\
A_N &= \{[\Psi_{NE} + \Psi_E - \Psi_{NW} - \Psi_W] + |\Psi_{NE} + \Psi_E - \Psi_{NW} - \Psi_W|\} a_\phi/8 \\
A_S &= \{[\Psi_{SW} + \Psi_W - \Psi_{SE} - \Psi_E] + |\Psi_{SW} + \Psi_W - \Psi_{SE} - \Psi_E|\} a_\phi/8
\end{aligned} \qquad (5.13)$$

Diffusion Terms

Similar to the convection terms, the integration of diffusion terms of equation (5.2) yields:

$$I_d = \int_{z,s}^{n} [(b_{\phi,y})_e(\delta\phi/\delta y)_e - (b_{\phi,y})_w(\delta\phi/\delta y)_w]dz + \int_{y,w}^{e} [(b_{\phi,z})_n(\delta\phi/\delta z)_n - (b_{\phi,z})_s(\delta\phi/\delta z)_s]dy \tag{5.14}$$

which can be expressed as:

$$I_d = I_{d1} + I_{d2} + I_{d3} + I_{d4} \tag{5.15}$$

where

$$I_{d1} = \int_{z,s}^{n} [(b_{\phi,y})_e(\delta\phi/\delta y)_e]dz \tag{5.16}$$

and so on.

If the quantities vary linearly then the following assumptions can be made in the domain under consideration:

$$\begin{aligned}(b_{\phi,y})_e &= [(b_{\phi,y})_E + (b_{\phi,y})_P]/2\\ (\delta\phi/\delta y)_e &= (\phi_E - \phi_P)/(y_E - y_P)\\ z_n - z_s &= (z_N - z_S)/2\end{aligned} \tag{5.17}$$

With these assumptions, equation (5.16) can be integrated to give:

$$I_{d1} = [(b_{\phi,y})_E + (b_{\phi,y})_P](\phi_E - \phi_P)(Z_N - Z_S)/[4(y_E - y_P)] \tag{5.18}$$

The other terms can be evaluated in a similar way. Assembling and rearranging gives:

$$I_d = B_E(\phi_E - \phi_P) + B_W(\phi_W - \phi_P) + B_N(\phi_N - \phi_P) + B_S(\phi_S - \phi_P) \tag{5.19}$$

where

$$B_E = [(b_{\phi,y})_E + (b_{\phi,y})_P](z_N - z_S)/[4(y_E - y_P)]$$

$$B_W=[(b_{\phi,y})_w+(b_{\phi,y})_P](z_N-z_S)/[4(y_P-y_W)]$$
$$B_N=[(b_{\phi,z})_N+(b_{\phi,z})_P](y_E-y_W)/[4(z_N-z_P)] \tag{5.20}$$
$$B_S=[(b_{\phi,z})_S+(b_{\phi,z})_P](y_E-y_W)/[4(z_P-z_S)]$$

<u>Source Term</u>

For the source term

$$I_S=\int_{z,s}^{n}\int_{y,w}^{e} S_\phi\, dydz \tag{5.21}$$

We assume that S is uniform over the area of integration and takes on the value at point P. Therefore, the integration of equation (5.21) finally gives:

$$I_S=S_{\phi,P}(y_e-y_w)(z_n-z_s) \tag{5.22}$$

Since y and z are the space-average value as given in assumption, equation (5.22) takes the form:

$$I_S=S_{\phi,P}Vp \tag{5.23}$$

where

$$Vp=(y_E-y_W)(z_N-z_S)/4 \tag{5.24}$$

<u>The Complete Finite Difference Equation</u>

Assembling and rearranging convection, diffusion and source terms gives:

$$A_E(\phi_P-\phi_E)+A_W(\phi_P-\phi_W)+A_N(\phi_P-\phi_N)+A_S(\phi_P-\phi_S)$$
$$-[B_E(\phi_E-\phi_P)+B_W(\phi_W-\phi_P)+B_N(\phi_N-\phi_P)+B_S(\phi_S-\phi_P)]+S_{\phi,P}Vp=0 \tag{5.25}$$

which ultimately yields the successive-substitution formula as:

$$\phi_P = C_E\,\phi_E + C_W\,\phi_W + C_N\,\phi_N + C_S\,\phi_S + Q \tag{5.26}$$

where

$$\begin{aligned} C_E &= (A_E + B_E)/\Sigma AB \\ C_W &= (A_W + B_W)/\Sigma AB \\ C_N &= (A_N + B_N)/\Sigma AB \\ C_S &= (A_S + B_S)/\Sigma AB \\ Q &= -S_{\phi,P}\,Vp/\Sigma AB \end{aligned} \tag{5.27}$$

$$\Sigma AB = A_E + A_W + A_N + A_S + B_E + B_W + B_N + B_S$$

The A are identified by equations (5.13) and (5.20).

STABILITY ANALYSIS

The stability conditions for the convergence of an iterative solution to equation (5.26) have been stipulated in Said's work([69], pp.69-72). The convergence of an iterative solution to equation(5.26) may be achieved if the following stability conditions are satisfied: (1) the sum of the moduli of the C's must be less than or equal to unity at every node of the grid; (2) this sum must be less than unity on at least one grid node; and (3) the C's and d must not vary too greatly from one cycle of iteration to another. The modified k, ϵ and T source term for stability is given as:

$$k_P = \frac{C_E k_E + C_W k_W + C_N k_N + C_S k_S + \mu_{t,P} \frac{Vp}{\Sigma AB} [(\frac{\delta \bar{U}}{\delta y})^2 + (\frac{\delta \bar{U}}{\delta z})^2]}{\frac{1}{\Sigma AB}[\Sigma AB + \frac{\rho \epsilon_P Vp}{kp}]} \quad (5.28)$$

$$\epsilon_P = \frac{C_E \epsilon_E + C_W \epsilon_W + C_N \epsilon_N + C_S \epsilon_S + C_1 \mu_{t,P} [(\frac{\delta \bar{U}}{\delta y})^2 + (\frac{\delta \bar{U}}{\delta z})^2][\frac{Vp}{\Sigma AB} \frac{\epsilon_P}{k_P}]}{\frac{1}{\Sigma AB}[\Sigma AB + C_2 \rho (\frac{\epsilon_P}{k_P}) Vp]} \quad (5.29)$$

$$\bar{T} = \frac{C_E \bar{T}_E + C_W \bar{T}_W + C_N \bar{T}_N + C_S \bar{T}_S}{[\Sigma AB + \rho \bar{U}_P Vp (\delta \bar{T}/\delta x)/\bar{T}p]/\Sigma AB} \quad (5.30)$$

ITERATIVE TECHNIQUE

The iterative technique includes the Gauss-Seidel iteration with provision for under-relaxation for ω, Ψ, k and ϵ. Because we use the point iteration method, i.e. the grid is systematically scanned node by node and row by row, there is a problem of the scanning direction. For the rectangular duct, there are two walls and two symmetrical lines. It has been found advantageous that the stream function be scanned from the walls to the symmetrical lines while the other variables be scanned from the symmetrical lines to the walls.

CONVERGENCE CRITERION

The convergence criterion was chosen such that the maximum fractional change of any parameter ϕ in the field from one cycle of iteration to the next should not exceed a prescribed value. This was of the form:

$$\left| \frac{(\phi_{ij}^{T} - \phi_{ij}^{T-1})}{\phi_{i,j}^{T}} \right|_{max} \leqslant \xi \tag{5.31}$$

where ξ was taken as 0.001 for all the ϕ variables.

INITIAL CONDITIONS

The initial values of ω and Ψ were assumed to be zero everywhere. $\bar{U}$, k and ϵ were initially assumed to have the distributions with secondary flow suppressed. This means that the program was run for k, ϵ and $\bar{U}$ first in order to obtain the distributions for these three variables, and then these field values were used as the initial conditions for k, ϵ and $\bar{U}$.

GRID SPACING

A non-uniform grid system has been employed. The one-fourth part of the field close to the wall is spaced non-uniformly in which the grid size increase gradually moving away from the wall. The increasing factor is 1.3. The remaining field is spaced uniformlly. The versatile program is designed that it is very easy to change the increasing factor, aspect ratios of rectangular duct and the grid numbers. For most calculations, 13 nodes were used for the short side of the rectangular duct according to the numerical experience. By this way, the grid is 13 X 13 for the square duct, 13 X 21 for 2:1 duct, 13 X 25 for 2.5:1 duct, 13 X 29 for 3:1 duct and 13 X 37 for 4:1 duct. Other finer grid numbers has been used and there is not much difference for these different grid systems.

VI

RESULTS AND DISCUSSIONS

GENERAL

The five coupled, non-linear elliptic equations (4.28)-(4.33), together with the auxiliary algebraic equations (4.34)-(4.53) provide a closed set for calculating turbulent flow in straight ducts. The equations have been solved in a quadrant of the channel by means of the general elliptic finite-difference procedure of Gosman et al[1]. The corresponding computer program was written and is provided in Appendix A. Five vorticity source models were employed to predict the flow characteristics in rectangular ducts with aspect ratios of 1:1, 2:1, 2.5:1, 3:1 and 4:1. The Reynolds number was confined to the practical range of 34,000 to 215,000 and converged solutions were obtained for all five models with some underrelaxing on the ω, Ψ, k and ϵ. Detailed calculation cases are explained by Tables 3-7. The results have been compared with the available experimental data of Hoagland[5], Leutheusser[10], Brundrett & Baines[6], Gessner & Jones[8] and Launder & Ying[9]. They are in fairly good agreement in general. In addition, the temperature equation was solved for the case where the average circumferential surface flux is uniform along the duct and the circumferential wall temperature is constant. Results include the overall Nusselt number and the local heat flux along the wall. Detailed results are discussed in the following subsections.

Secondary Velocity

The stream function lines normalized by hydraulic diameter D_h and the center-line axial velocity U_c for rectangular ducts of 5 different aspect ratios,each with 5 different vorticity source models, are shown in Fig.3-Fig.11 where they are compared with the experimental results of Hoagland[5] and Gessner & Jones[8].

For the square duct, Fig.3 shows that the two flow cells in each quadrant,as predicted by each of the five models, are symmetric with the diagonal which verifies the symmetric property of the secondary velocity field.

The predicted results for the square duct are compared with the experimental data of Gessner & Jones[8] and Hoagland[5] in Fig.4 and Fig.5 respectively. The agreement is seen to be fairly good. Overall, the result from Seale's model is closest to the experimental data. For all the other four results, the center point of each flow cell is shifted towards the duct core region and the secondary flow spreads throughout the whole region of the duct. Furthermore, the experimental data indicates that the secondary flow is more concentrated near the corner. However,the normalized Ψ values do agree well with the two experimental results. Among the five models, Seale's result is the best one. The results from the NR and ϵ models are over-estimated near the duct center line. The results by NR, k and ϵ models are all under-estimated near the corner. Only the LY model result penetrates adequately into the corner region.

The flow cells for the other aspect ratios of rectangular duct were shown in Fig.6-Fig.11. For 2:1 and 3:1, the plots were compared with the experimental data from Hoagland. There are no data available so far for the 2.5:1 and 4:1 rectangular ducts.

As shown in Fig.6, the five results are similar to each other. The Ψ values are under-predicted and the center point of each flow cell is away from the duct corner. The secondary flow spreads throughout the whole region. The same phenomenon was observed for the 3:1 duct as shown in Fig.7-8.

For the flow cells of the 2.5:1 and 4:1 rectangular ducts (Fig.9-Fig.11 inclusive), the peak point of the big cell is situated centrally between the long wall and the symmetric line but is closer to the other symmetric line than to the short wall. However, based on the experimental data for other aspect ratios, it is very likely that the peak point should be much closer to the corner. Otherwise, the present predictions show again the phenomenon that the secondary motion spreads throughout duct.

The secondary velocity contours for the square duct are compared with the experimental data of Hoagland[5] in Fig.12-Fig.16 at Re=75,000. The present results are in reasonable agreement with the experimental data. The result from Seale's model is closer to the data than the other models. For all the other four models, the predictions are over-estimated in the core region which was also observed by Yadava[2].

The secondary velocity profiles (normalized by the average friction velocity) for the square duct are also shown in Fig.17 for a high Reynolds number (215,000). Here the predictions are compared with the measurements of Launder & Ying[9]. Among the five models, the agreement between prediction and experimental data by Seale's model is better than the other four models. Near the corner, the results from Seale's, NR, k and ϵ models are slightly under-estimated. However, the result by LY model is over-estimated which is consistent with the fact that the flow cell penetrates more into the corner. Fig.17 shows that the results by NR, k and ϵ are close to each other.

For the 2:1 rectangular duct, the secondary velocity profiles normalized by the duct centre line axial velocity are compared with the experimental data from Gessner & Jones[8]. Fig.18 shows that the predictions are under-estimated near the corner and over-estimated near the core region. This again reflects the fact that the peak point of the large flow cell is shifted towards the core region.

Axial Velocity

Isovels ($\bar{U}/\bar{U}_c$) in a square duct are shown in Fig.19 where the predicted velocity levels are compared with the experimental data of Leutheusser[10]. The results from five vorticity source models display the distortion of the contours towards the corner as a result of secondary motion which moves high momentum fluid near the center outwards along the diagonals. In Fig.19, the contours are also shown for the case with secondary velocity suppressed. In this case, as expected, the bulges in the contours are absent.

The results by the k and ϵ models are very similar to each other. For the predictions by LY, Seale's and NR models, it seems that the velocities are somewhat under-estimated near the corner. The same phenomena have been observed by several investigators including Nakayama[41] and Yadava[2].

The axial velocity distributions, normalized by bulk velocity,are shown in Fig.20 and are seen to be in reasonable agreement with the measurements of Launder & Ying[9]. Among the five results, the LY prediction is better than the others.

Isovels (normalized by the centerline velocity) for the 3:1 rectangular duct are shown in Fig.21 for Re=56,000 and compared with Leutheusser's experimental data. The prediction shows good agreement with the experimental data near the horizontal wall bisector. The discrepancies in other parts reflect significantly on the secondary flow pattern. As mentioned earlier, the predicted secondary stream flows almost parallel to the long wall and makes less distortion of the isovels toward the corner.

The isovels for 2:1,2.5:1 and 4:1 ducts by LY model are shown in Fig.21-A. The isovel distributions for the other four models were similar. The three cases shown in Fig.21-A, together with Fig.19 and Fig.21, illustrate the changing flow pattern in the progression from a square duct towards two infinite parallel plates.

The ratio of the duct center axial velocity to the bulk axial velocity as predicted by the LY model is shown in Fig.21-B. For a given duct, as a function of Reynolds number, the ratio decreases slightly with increasing Reynolds number (as in pipe flow), whereas for a fixed Reynolds number , the ratio decreases with increasing λ.

Turbulent Kinetic Energy

Contours of turbulent kinetic energy k normalized by average friction velocity are compared with the experimental data of Brundrett & Baines[6] in Fig.22 for the square duct. The results show that the contours are distorted by the secondary velocity. Compared with the experimental data, the bulging by the secondary flow is not strong enough. This might be attributable to the weak secondary velocity along the diagonal.

The normalized k contours for the 2:1, 2.5:1, 3:1 and 4:1 ducts as predicted by the LY model are shown in Fig.22-A. Again, the results shown (LY) are fairly typical of the results from the other four models. The contours near the horizontal wall bisector become flatter with increasing λ. In general, the plots show the distortions of the contours by the secondary flow from the duct center to the wall corner.

Wall Shear Stress

The effects of the secondary motions on the wall shear stress are shown in Figs.23 and 24. For the square duct(Fig.23), the calculated solutions are in close agreement with the measurements, displaying substantially the same variation as Leutheusser's measurements[10] with the peak shear stress actually occuring about midway between the corner and the wall bisector. The distributions confirm the tendency of secondary flow to equalize the wall shear stress along the wall.

The predictions of wall shear stress by the five models for the 3:1 rectangular duct are compared with the experimental data of Leutheusser[10] in Fig.24. Although the five predictions are close to each other, they show no dip near the middle of the long half-wall as indicated by the experiment. This is attributable to the secondary flow distribution. Experimental results show that the secondary flow turns in from the wall near the middle of the half-length to cause lower axial momentum there. However, the predictions show that the secondary flow fully fills the whole duct and the large flow cell peak point is closer to the core region. The secondary stream runs almost parallel along the wall. As shown in Fig.24, this does not allow a dip of the wall shear stress distribution.

The average wall shear stress ratios for the various ducts are shown in Fig.24-A where the wall average has been normalized by the overall duct average. Of course, the ratio is unity for $\lambda=1$ because of the symmetry of the square duct. For $\lambda>1$, as shown in Fig.24-A, the average wall shear stress on the long wall is always greater than that on the short wall, and the difference increases gradually with λ.

Friction Factor

Figs.25 and 26 contain measurements and predictions of the friction factor versus Reynolds number characteristics from the five models for the square duct and the 3:1 rectangular duct. As shown in Fig.25, in the lower range of Re, the prediction from the LY model is slightly below the data and the empirical correlation of Blasius;the maximum discrepancy being less than 5%. Compared to Leutheusser's data for the square duct, the results from LY are closest to the measurements and all the other four models are slightly under-estimated.

For the 3:1 rectangular duct(Fig.26), the predictions by the five models are similar to each other. Compared with Leutheusser's experimental data, they are all slightly under-estimated in the lower range of Re and over-estimated at the higher Re.

The friction factor predicted by Seale's model for the ducts of five aspect ratios are shown in Fig.26-A. For a given Re, the friction factor, as expected[70], increases slightly with an increase in λ.

<u>Local Wall Heat Flux and Nusselt Number</u>

The distribution of local wall heat flux in a square duct is very similar to the local wall shear stress and is shown in Fig.27 compared with the data of Brundrett & Burroughs[65]. The prediction and the data are in good agreement and show that the maximum heat transfer rate occurs about midway between the corner and the wall bisector.

According to the work by Patankar & Acharya[66], the Nusselt number values do not change appreciably with the kind of boundary conditions used. It is, therefore, sufficient to compare the present prediction with the available measurements of Novotny et al[67] and Sparrow et al[68]. The predictions and the experimental data shown in Figs.28 to 32 inclusive again compare favorably for each of the five models.

EFFECTS OF SOME FACTORS

Reynolds Numbers

The programs were run over a wide range of Reynolds numbers for different aspect ratios and different vorticity source models. The results show that Reynolds number has no significant influence on the normalized axial velocity distributions, shear stress and turbulent kinetic energy distribuions. The secondary velocity magnitudes, normalized by average friction velocity, decrease only slightly with increasing Reynolds number. Another aspect is that beyond Re=100,000, the program,in many cases,needs more iterations to reach the converged solution.

Under Relaxation

$\bar{U}$ and $\bar{T}$ behave very well in the iteration procedure and need no under-relaxation. However, the k, ϵ, ω and Ψ need some under-relaxation and the factors were chosen as 0.5 in most cases. According to the numerical experiences, the relaxation factors for vorticity and stream function were chosen as 0.75 for the NR model and 0.3 for the ϵ model in order to increase the convergence speed.

Grid System

The LY model was used to predict the secondary flow in a square duct using both the uniform grid and the non-uniform grid. Results show that for the same number of nodes the non-uniform grid converges faster than the uniform grid.

All the other calculations adopted the non-uniform grid as described in chapter 5.

Initial Condition

According to the present author's experiences, the initial condition has an important effect on convergence. For each aspect ratio, the initial conditions for $\bar{U}$, k and ϵ were chosen as the distributions with secondary motion suppressed. The vorticity and stream function were initiated by zero.

Scanning Direction

Numerical experience shows that it is advantageous in regard to convergence,if the scanning direction of the stream function is from the wall boundary to the duct centre. This might be attributable to the Gauss-Seidel iteration method.

For each particular point in the region, there are four neighbour points joining the iteration procedure. At each step, two of these four points have the old values and the other two have the new values. The stream function is the convection coefficient for each variable in the numerical scheme. Scanning from wall to the centre means transfering the wall boundary information to the duct centre as soon as possible.

COMPARISON OF FIVE MODELS

From the above results, certain judgements can be made on the five vorticity source models as follows:

(a) For the square duct, the Seale's result is more accurate than the others compared with the available experimental data. Table 3 to Table 7 show that the Seale's model converges faster than the other models.

(b) The LY,k and ϵ models are based on the local distributions of $\bar{U}$, k & ϵ and therefore are more fundamental.

(c) The NR model uses the gradients of both axial and secondary velocities. Because of the difficulty in calculating the wall damping function, the accuracy and convergence speed are not as good as the other models.

(d) The choice of vorticity source models revolves around the issue as to how to express the Reynolds stress. The LY model uses the local gradient in mean axial velocity distribution. The k and ϵ models use the k and ϵ distributions respectively. The NR model adopts both the axial and secondary velocity gradients. The Seale's model emphasizes the importance of the duct geometry. Each is somewhat different from the others. However, the predictions show that most of the results are similar to each other, although Seale's result is a little superior than the other four models. Accordingly, it seems that the vorticity source model is realy not so important. To show this viewpoint, another numerical experiment was carried out. For vorticity source, only two nodes near the corner were valued by some constants with the same magnitude and the opposite sign, leaving all the other nodes to be zero. A converged solution with two flow cell was obtained and was acceptable as a solution of secondary flow in a rectangular duct when compared with the several experimental data.

SPECIAL TOPICS

Constants of Vorticity Source Models

Although the LY model has been used successfully in straight ducts of different cross-section shapes, the constant C_1' appears with different values among the different investigators as mentioned early. The present predictions show that C_1' varies with the aspect ratio for rectangular ducts. The same phenomenon has been observed for the other four vorticity source models which together is shown in Fig.33.

Principally, the C_1' was determined to suit the best overall agreement between predicted and experimental results. Fig.33 shows that the curves decrease as the aspect ratio λ increases. Since the magnitude of C_1' determines the strength of the secondary flow, the overall trend is as expected, i.e. $C_1' \to 0$ as $\lambda \to \infty$.

Comments on LY, k & ϵ Models

The LY, k & ϵ models assume that the Reynolds stress $\overline{v^2}-\overline{w^2}$ can be determined by the gradients of local $\bar{U}$, k & ϵ respectively. Detailed inspection of the vorticity source distributions by these three models reveals that they all have a maximum value close to the wall and diminish quickly away from the wall. The prediction shows that the vorticity production is concentrated near the wall. Although these three models use different variables, they have some thing in common. The distributions of $\bar{U}$, k & ϵ are very flat in the region close to the duct centre and have a sharp slope close to the wall. Hence the gradients of these three variables are all high near the wall and almost zero in the region close to the duct centre. This characteristic actually represents the vorticity production property.

Defficiencies of the Predictions

The present numerical predictions have provided overall information about the secondary flow in rectangular ducts of different aspect ratio. The results also illustrate the applicability of five vorticity source models for the prediction of secondary flow in ducts having more than one flow cell in each symmetric part. However, the results are not perfect. The shifting of the large flow cell peak point results in certain discrepancies between the predicted and experimental data;notable especially in the wall shear stress distribution of the 3:1 rectangular duct. In order to improve the result, different and finer grid systems, non-homogeneous C_i' distributions and anisotropic eddy viscosity have been tried. There was not much change. Also, by using the wall shear stress distribution of Leutheusser as a boundary condition, the solution was still not satisfactory. After removing the constant τ boundary condition, the result returned to the original solution. All these numerical experiments illustrated indirectly the uniqueness of the present solutions.

Lyall's duct solution

The preceding numerical results have illustrated the applicability of the five vorticity source models to predict the secondary flow in a rectangular duct which consists of two flow cells in each quadrant. In addition to the rectangular duct, the secondary flow in a duct consisting of two interconnected square duct sub-channel was predicted by Seale's model. The predicted results are compared with Lyall's experimental data as shown in Fig.34. The $\hat{Y}$ line is defined in Fig.35. The secondary velocity profiles are in good agreement with the experimental data. A peak secondary flow value of about 3.0% was obtained. The isovels are under-estimated in the small square duct part. This might be attributable to the weak secondary flow from the duct core region to the corner of the small square duct. Overall, the results show the capability of Seale's model to tackle the secondary flow in ducts of complicated cross-section.

VII

CONCLUSIONS AND RECOMMENDATIONS

Five vorticity source models have been used to predict the turbulent flow characteristics in rectangular ducts with aspect ratios of 1:1, 2:1, 2.5:1, 3:1 and 4:1. Overall, the predictions were in fairly good agreement with the available experimental data. The results illustrated the capability of these vorticity source models to predict the secondary flow in ducts of complicated cross-section.

According to the present work, the following conclusions were drawn:

(1) The empirical constants for each of the five vorticity source models vary with the aspect ratio of the rectangular duct.

(2) For the square duct, the predictions are in good agreement with the available experimental data. For the other rectangular ducts, the peak point of the flow cell is shifted to the duct core region and the predictions are not as good as for the square duct. The predictions show that the secondary flow spreads throughout the duct. However, the predicted heat transfer characteristics including the local wall heat flux and Nusselt number are in good agreement with the experimental data.

(3) The five vorticity source models were inspected through their individual performances in predicting the secondary flow in rectangular ducts. The present numerical results suggest that each may be capable of being used to predict the secondary flow in ducts of more complicated geometries.

(4) The Seale's model converges faster than all the other models and is recommended as the first option to tackle the secondary flow problems in duct of more complicted geometries.

For the future work, the following points might be considered:

(1) As an extension of the present work and that of Yadava[2], it is suggested that various vorticity source models be tested for their abilityto predict the secondary flow in duct with each symmetric part containing more than two flow cells. The present work has demonstrated that the Seale's model is capable of predicting the Lyall's duct.

(2) The present work shows that the empirical constants for each of the five vorticity source models vary with the different aspect ratios. Efforts should continue in developing a new vorticity source model in which the constant is truly a universal constant.

(3) In view of the difference of the present predictions from that of Nakayama([41] better wall shear stress prediction) it is suggested that the same problem be reviewed by the primitive variables method.

(4) The k and ϵ models demonstrated the potential of the capability to predict the secondary flow in ducts of arbitrary cross-section. However, it is necessary to find a solid background for these two models both theoretically and experimentally. It is expected that more and more work will be carried out by using these two models in various fields including the secondary flow problems.

REFERENCES

1. Gosman, A.D., Pun, W.M., Runchal, A.K., Spalding, D.B. & Wolfshtein, M. "Heat and Mass Transfer in Recirculating Flows" Academic Press, 1969.

2. Yadava, S.K. "A Comparison of Turbulent Flow Predictions for Square Ducts Using Three Vorticity Source Models" MSc Thesis, University of Manitoba, Manitoba, Canada, 1983.

3. Nikuradse, J. "Untersuchungen uber die Geschwindikeitsverteitung in Turbulenten Stromungen" Ph.D. Thesis Gottingen, 1926. Also VDI Forschungsheft 281, Berlin, 1926.

4. Prandtl, L. "Proc. Second Int. Congr. of Applied Mech." 1926, p.71 et seq Zurich, 1927. (Also Translated as NACA TM-435)

5. Hoagland, L. C. "Fully Developed Turbulent Flow in Straight Rectangular Ducts-Secondary Flow, its Causes and Effect on the Primary Flow" Ph.D. Thesis, MIT, 1960.

6. Brundrett, E. & Baines, W.D. "The Production and Diffusion of Vorticity in Duct Flow" J. Fluid Mech., Vol.19, pp.375-94, 1964.

7. Gessner, F.B. "Turbulence and Mean-flow Characteristics of Fully Developed Flow in Rectangular Channels" Ph.D. Thesis, Purdue University, 1964.

8. Gessner, F.B. & Jones, J.B. "On Some Aspects of Fully Developed Turbulent Flow in Rectangular Channels" J. Fluid Mech., Vol.23, pp.689-713, 1965.

9. Launder, B.E. & Ying, W.M. "Secondary Flows in Ducts of Square Cross-section" J. Fluid Mech., Vol.54, pp.289-95, 1972.

10. Leutheusser, H. J. "Turbulent Flow in Rectangular Ducts" ASCE, J.Hydraulics Division, Vol.89, No.HY3, pp.1-19, 1963.

11. Prandtl, L. "Essentials of Fluid Mechanics" Hafner, New York, 1953.

12. Lyall, H.G. "Measurement of Flow Distribution and Secondary Flow in Ducts Composed of Two Square Interconnected Subchannels" Symposium on Internal Flows, University of Salford, England, Paper No.33, pp.E16-E23, 1971.

13. Kacker, S.C. "Some Aspects of Fully Developed Turbulent Flow in Non-circular Ducts" J. Fluid Mech., Vol.57, pp.583-602, 1973.

14. Rowe, D.S. "Measurements of Turbulent Velocity Intensity and Scale in Rod Bundle Flow Channels" BNWL Rep.1736, UC-80,Battelle,1973.

15. Kjellstrom, B "Studies of Turbulent Flow Parallel to a Rod Bundle of Triangular Array" AB Atomenergi Rep. AE-RV-196,Sweden,1971.

16. Trupp, A.C. & Azad, R.S. "The Structure of Turbulent Flow in Triangular Array Rod Bundles" Nuclear Engineering and Design, Vol.32, No.1, pp.47-84, 1975.

17. Carajilescov, P. & Todreas, N.E. "Experimental and Analytical Study of Axial Turbulent Flows in an Interior Sub-channel of a Bare Rod Bundle" Transac. ASME, J. Heat Transfer, Vol.98, pp.262-8, 1976.

18. Rehme, K. "Experimentelle Untersuchungen der Turbulenten Stromung in einem Wandkanal eines Stabbundles" Kenforschungszentrum,KFK 2441,1977.

19. Aly, A.M.M., Trupp, A.C., Gerrard, A.D. "Measurements and Prediction of Fully Developed Turbulent Flow in an Equilateral Triangular Duct" J. Fluid Mech., Vol.85, pp.57-83, 1978.

20. Seale, W.J. "Measurements and Predictions of Fully Developed Turbulent Flow in a Simulated Rod Bundle" J. Fluid Mech., Vol.123, pp.399-423, 1982.

21. Hooper, J.D. & Rehme, K. "Large Scale Structural Effects in Developed Turbulent Flow Through Closely-spaced Rod Arrays" J. Fluid Mech., Vol.145, pp.305-337, 1984.

22. Ahmed, S. & Brundrett, E. "Turbulent Flow in Non-circular Ducts. Part 1" Int. J. Heat Mass Transfer, Vol.14, pp.365-75, 1971.

23. Po, J.K. "Developing Turbulent Flow in the Entrance Region of a Square Duct" MS Thesis, University of Washington, 1975.

24. Melling, A. & Whitelaw, J.H. "Turbulent Flow in a Rectangular Duct" J. Fluid Mech., Vol.78, pp.289-315, 1976.

25. Lund, E.G. "Mean Flow and Turbulent Characteristics in the Near Corner Region of a Square Duct" MS Thesis, Dept.Mech.Engng., University of Washington, 1977.

26. Reynolds, W.C. "Computation of Turbulent Flows" Ann. Rev. Fluid Mech. 8: 183-208, 1976.

27. Prandtl, L. "Bericht uber Untersuchingen zur ausgebildeten Turbulenz" ZAMM vol.5, pp.136, 1925.

28. Von Karman, Th. "Mechanische Ahnlichkeit und Turbulenz" Proc. 3rd Int. Cong. appl. Mech., Stockholm, Pt.1, pp.85, 1930.

29. Van Driest, E.R. "On Turbulence Flow Near a Wall" J. Aero. Sci., Vol.23, pp.1007, 1956.

30. Kolmogorov, A.N. "Equations of Turbulent Motions of an Incompressible Turbulent Fluid" Izv. Akad. Nauk SSSR Ser Phys. VI No.1-2, pp.56, 1942.

31. Prandtl, L. "Uber ein neues Formelsystem fur die ausgebildete Turbulenz" Nachrichten von der Akad. der Wissenschaft in Gottinggen, 1945.

32. Harlow, F.H. & Nakayama, P.I. "Transport of Turbulence Energy Decay Rate" Los Alamos Sci. Lab. University of California Rep. LA 3854, 1968.

33. Rodi, W. & Spalding, D.B. "A Two-parameter Model of Turbulence and its Application to Free Jets" Warmeund Stoffubertragung, 3, pp.85-95, 1970.

34. Ng, K.H. & Spalding, D.B. "Some Applications of a Model of Turbulence for Boundary Layers Near Walls" Mech.Engng.Dept. Imperial College.Rep. BL/TN/A/14, 1969.

35. Spalding, D.B. "The Prediction of Two-dimensional Steady Turbulent Flows" Mech. Engng. Dept. Rep. Imperial College, EF/TN/A/16, 1970.

36. Jones, W.P. & Launder, B.E. "The Prediction of Laminarization with a 2-Equation Model of Turbulence" Int.J.Heat.Mass Transfer, 15, 301, 1972.

37. Launder, B.E. & Spalding, D.B. "The Numerical Computation of Turbulent Flows" Computer Methods in Applied Mechanics and Engineering, Vol.3, pp.269-89, 1974.

38. Gosman, A.D. & Rapley, C.W. "A Prediction Method for Fully Developed Turbulent Flow Through Non-circular Passages" Numerical Methods in Laminar and turbulent Flows(ed. C.Taylor et al), Pentech, 1978.

39. Gosman, A.D. & Rapley, C.W. "Fully Developed Flow in Passages of Arbitrary Cross-section" in C.Taylor & K.Morgan(eds), Recent Advances in Numerical Methods in Fluids, Pineridge Press, Swansea, UK, 1980.

40. Seale, W.J. "Turbulence Generated Secondary Flows in Ducts of Non-circular Cross-section" J. Mech. Eng. Sci., Vol.24, No.3, pp.119-27, 1982.

41. Nakayama, A, Chow, W.L. & Sharma, D. "Calculation of Fully Developed Turbulent Flows in Ducts of Arbitrary Cross-section" J. Fluid Mech., Vol.128, pp.199-217, 1983.

42. Demuren, A.O. & Rodi, W "Calculation of turbulence-Driven Secondary Motion in Non-circular Ducts" J. Fluid Mech. Vol. 140, pp.189-222, 1984.

43. Launder, B.E. & Ying, W.M. "Prediction of Flow and Heat Transfer in Ducts of Square cross-section" Proc. Instn. Mech. Engrs., Vol.187, pp.455-61, 1973.

44. Hanjalic, K. & Launder, B.E. "A Reynolds Stress Model of Turbulence and Its Application to Thin Shear Flows" J. Fluid Mech., Vol.52, pp.609-38, 1972.

45. Buleev, N.I. "Theoretical Model of the Mechanism of Turbulent Exchange in Fluid Flow" AERE Translation 957, 1963.

46. Trupp, A.C. & Aly, A.M.M. "Predicted Secondary Flows in Triangular Array Rod Bundles" ASME J. Fluid Eng., Vol.101, pp.354-63, 1979.

47. Alshamani, K.M.M. "Correlations Among Turbulent Shear Stress, Turbulent Kinetic Energy and Axial Turbulence Intensity" AIAA J., Vol.16, No.8, 1978.

48. Alshamani, K.M.M. "Relationships between Turbulent Intensities in Turbulent Pipe and Channel Flows" J. Royal Aeronautical Society, London, Vol.83, pp.159-61, 1979.

49. Patankar, S.V. & Spalding, D.B. "Heat and Mass Transfer in Boundary Layers" Intertext Books, London, 1970.

50. Patankar, S.V. & Spalding, D.B. "A Calculation Procedure for Heat, Mass and Momentum Transfer in 3-D Parabolic Flows" Int. J. Heat Mass Transfer 15, 1787-1806, 1972.

51. Patankar, S.V. "Numerical Heat Transfer and Fluid Flow" McGraw-Hill, 1980.

52. Spalding, D.B. "GENMIX: A General Computer Program for Two-dimensional Parabolic Phenomena" Pergamon Press, 1977.

53. Gessner, F.B. & Emery, A.F. "A Reynolds Stress Model for Turbulent Corner Flows, Part 1: Development of the Model" J. Fluids Engng., Vol.98, pp.261-268, 1976.

54. Naot, D. & Rodi, W. "Numerical Simulations of Secondary Currents in Channel Flow" J. Hydraul. Div. ASCE 108(HY8), 948-68, 1982.

55. Gessner, F.B. & Po, J.K. " A Reynolds Stress Model for Turbulent Corner Flows, Part 2: Comparison between Theory and Experiment" J. Fluids Engng., Vol.98, pp.269-277, 1976.

56. Sandborn, V.A. "Experimental Evaluation of Momentum Terms in Turbulent Pipe Flow" NACA TN 3266, 1954.

57. Laufer, J. "Investigation of Turbulent Flow in a Two Dimensional Channel" NACA TN 2123, 1950.

58. Laufer, J. "The Structure of Turbulence in Fully Developed Pipe Flow" NACA TN 2934, 1953.

59. Lawn, C.J. "Application of the Turbulent Energy Equation to Fully Developed Flow in Simple Ducts" Central Electricity Generating Board, RD/B/R/1575, A,B,C, 1970.

60. Lawn, C.J. "The Determination of the Rate of Dissipation in Turbulent Pipe Flow" J. Fluid Mech., Vol.48, pp.477-505, 1971.

61. Clark, J.A. "Study of Incompressible Turbulent Boundary Layers in a Two Dimensional Wind Tunnel" Ph.D. Thesis, Queen's University of Belfast, 1966.

62. Clark, J.A. "A study of Incompressible Turbulent Boundary Layers in Channel Flows" J. Basic Engineering, No.90, pp.455-68, 1968.

63. Comte-Bellot, G. "Turbulent Flow Between two Parallel Walls" Ph.D. Thesis, University of Grenoble, 1963. (Translated into English by P. Bradshaw in Aeronautical Reseach Council ARC 31 609, F.M. 4102, 1969).

64. Launder, B.E., Reece, G.J. & Rodi, W. "Progress in the Development of a Reynolds Stress Turbulence Closure" J. Fluid Mech., Vol.68, pp.537-66, 1975.

65. Brundrett, E. & Burroughs, P.R. "The Temperature Inner Law and Heat Transfer for Turbulent Air Flow in a Vertical Square Duct" Int. J. Heat Mass Transfer, 10, pp.1133, 1967.

66. Patankar, S.V. & Acharya, S. "Development of a Turbulence Model for Rectangular Passages" Transaction of the CSME, Vol.8, No.3, 1984.

67. Novotny, J.L., McComas, S.T., Sparrow, E.M. & Eckert, E.R.G. "Heat Transfer for Turbulent Flow in Rectangular Ducts with Two Heated and Two Unheated Walls" AIChE J., 10, pp.466, 1964.

68. Sparrow, E.M., Lloyd, J.R. & Hixon, C.W. "Experiments on Turbulent Heat Transfer in an Asymmetrically Heated Rectangular Duct" J. Heat Transfer, 88, pp.170, 1966.

69. Said, M.N.A.A. "Predictions and Measurements of Fully Developed Turbulent Flow in Longitudinal Internally Finned Tubes" Ph.D. Thesis, University of Manitoba, Manitoba, Canada, 1981.

70. Hartnett, J.P., Koh, J.C.Y. & McComas, S.T. "A Comparison of Predicted and Measured Friction Factors for Turbulent Flow Through Rectangular Ducts" Transactions of the ASME, J. Heat Transfer Feb. 1962, pp.82.

Appendix A

COMPUTER PROGRAM

A computer program was developed to predict the secondary flow in rectangular duct. The program was designed as capable of predicting the secondary flow in rectangular duct of various kinds of aspect ratios. Five different vorticity source models were included separately. The following is a representation of the input constant values:

Fortran Symbol	Representation
RE	Reynolds number
ROW	Density of Fluid
CMU	C_μ
CE1	C_1
CE2	C_2
SIGMK	σ_k
CAPA	κ
A ,E	Law of the wall constants
SIGMU	σ_μ
ALFAW	Under-relaxation factor for ω

ALFAEP	Under-relaxation factor for Ψ
ALFAK	Under-relaxation factor for k
ALFAE	Under-relaxation factor for ϵ
ALFAU	Under-relaxation factor for $\overline{U}$
IMAX	Maximum number of iteration
IPRINT	Number of iterations between printout of data
IRPRNT	Number of iterations between printout of residuals
ALMD	Convergence criterion for $\overline{U},\Psi,k,\epsilon$
ALMDW	Convergence criterion for ω
AMU	Dynamic viscosity of fluid
CPRIME	C_i'
SIGME	σ_ϵ
S2,M2,N,X1	Numerical grid parameters

FLOW CHART OF THE COMPUTER PROGRAM

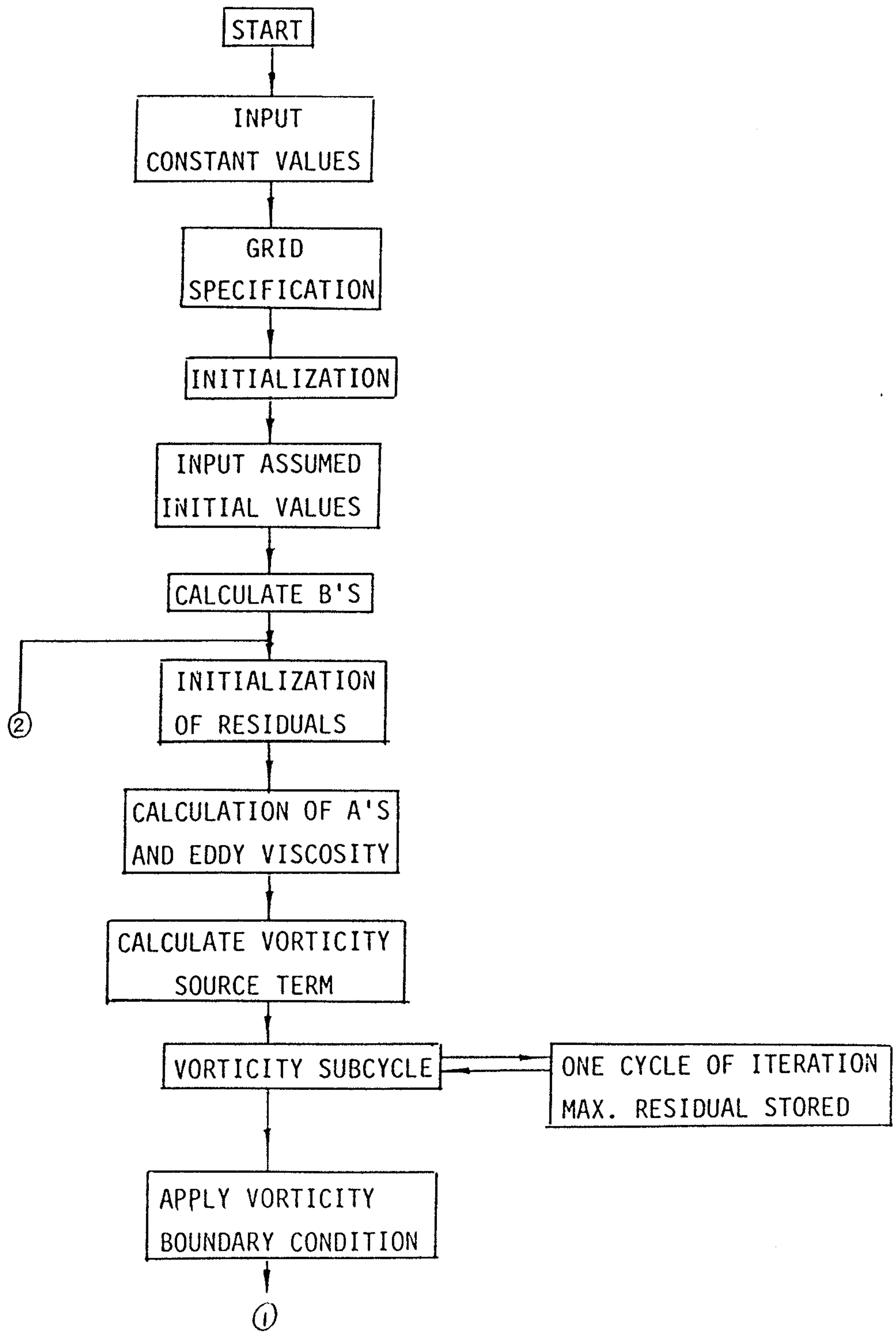

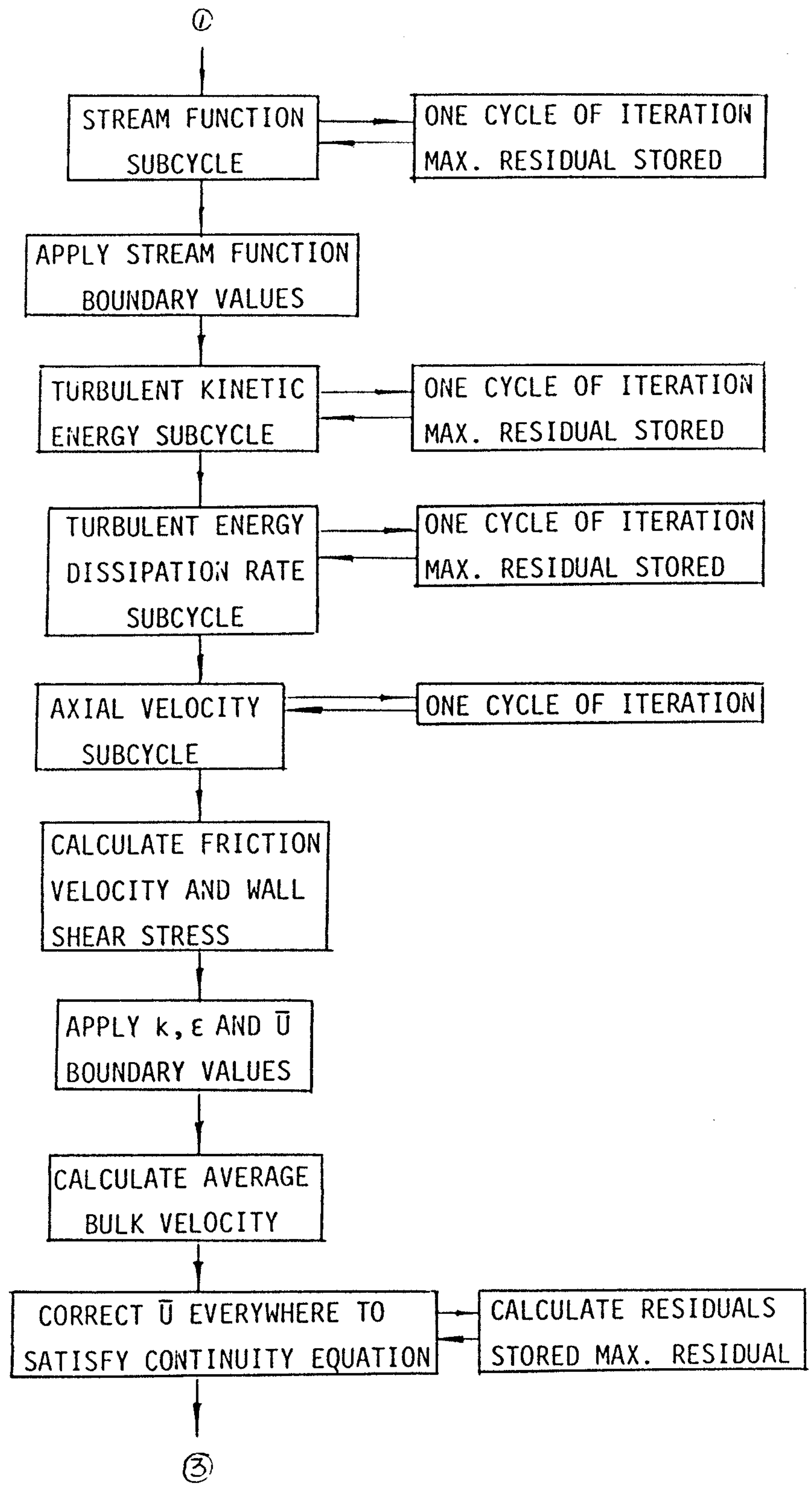
①
STREAM FUNCTION SUBCYCLE
ONE CYCLE OF ITERATION MAX. RESIDUAL STORED
APPLY STREAM FUNCTION BOUNDARY VALUES
TURBULENT KINETIC ENERGY SUBCYCLE
ONE CYCLE OF ITERATION MAX. RESIDUAL STORED
TURBULENT ENERGY DISSIPATION RATE SUBCYCLE
ONE CYCLE OF ITERATION MAX. RESIDUAL STORED
AXIAL VELOCITY SUBCYCLE
ONE CYCLE OF ITERATION
CALCULATE FRICTION VELOCITY AND WALL SHEAR STRESS
APPLY k, ε AND Ū BOUNDARY VALUES
CALCULATE AVERAGE BULK VELOCITY
CORRECT Ū EVERYWHERE TO SATISFY CONTINUITY EQUATION
CALCULATE RESIDUALS STORED MAX. RESIDUAL
③

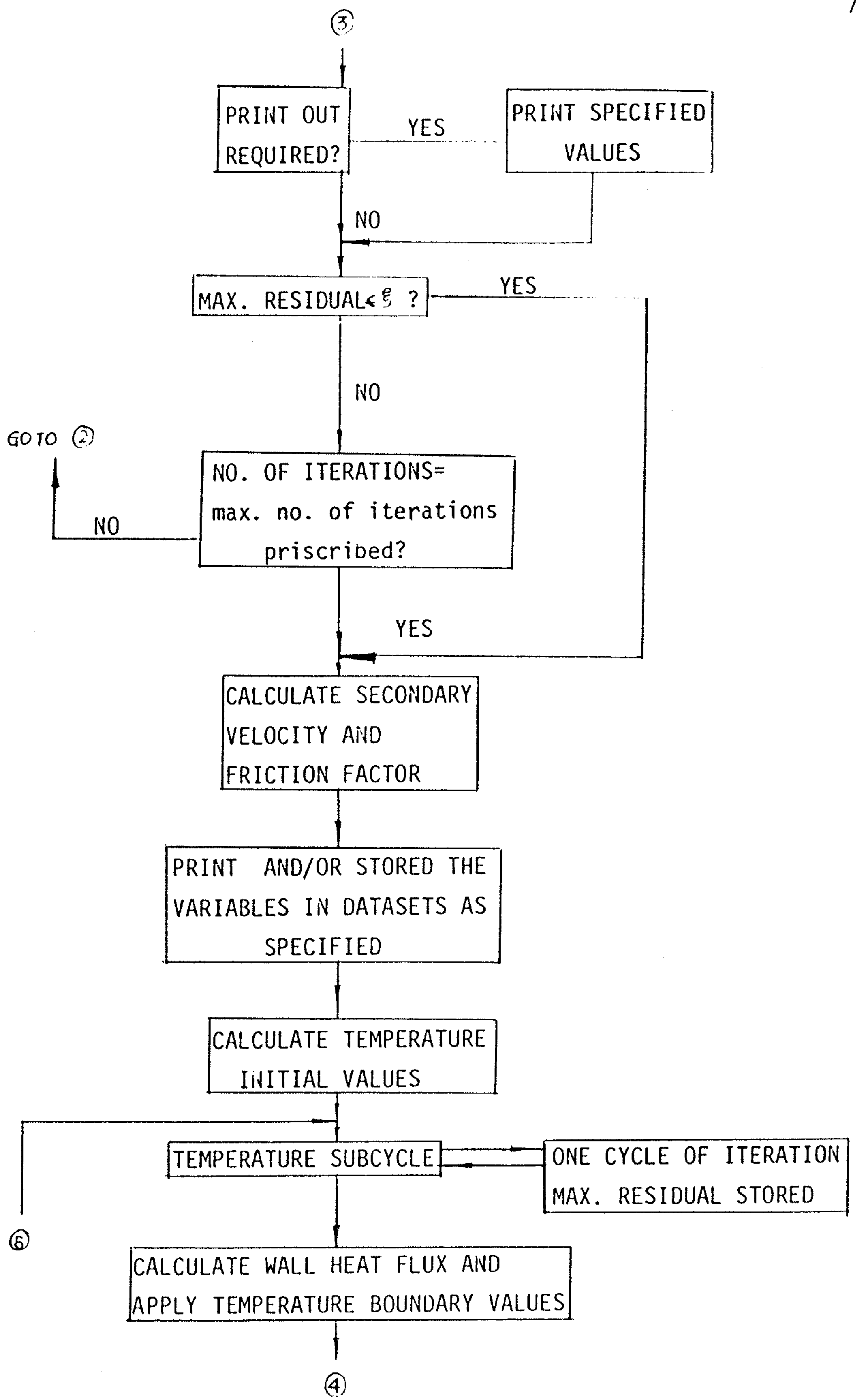

3
PRINT OUT REQUIRED?
YES
PRINT SPECIFIED VALUES
NO
MAX. RESIDUAL< ξ ?
YES
NO
GOTO 2
NO
NO. OF ITERATIONS= max. no. of iterations priscribed?
YES
CALCULATE SECONDARY VELOCITY AND FRICTION FACTOR
PRINT AND/OR STORED THE VARIABLES IN DATASETS AS SPECIFIED
CALCULATE TEMPERATURE INITIAL VALUES
TEMPERATURE SUBCYCLE
ONE CYCLE OF ITERATION MAX. RESIDUAL STORED
6
CALCULATE WALL HEAT FLUX AND APPLY TEMPERATURE BOUNDARY VALUES
4

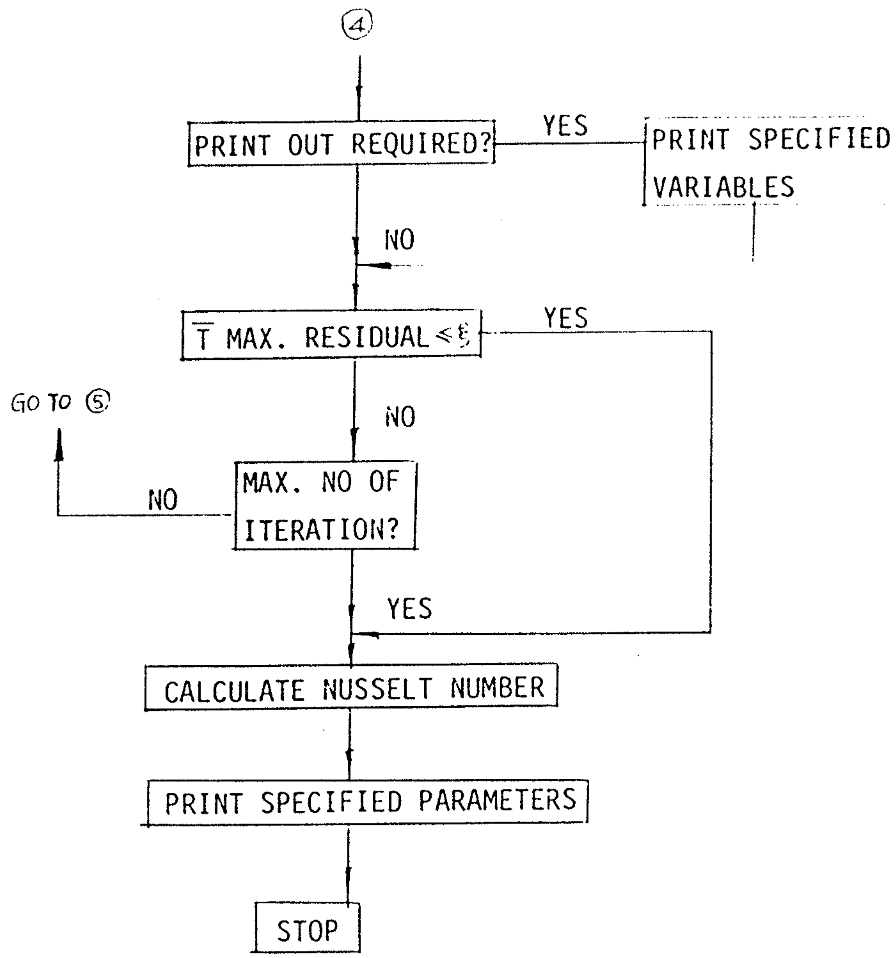
4
PRINT OUT REQUIRED?
YES
PRINT SPECIFIED VARIABLES
NO
$\overline{T}$ MAX. RESIDUAL $\leq \xi$
YES
NO
GO TO 5
NO
MAX. NO OF ITERATION?
YES
CALCULATE NUSSELT NUMBER
PRINT SPECIFIED PARAMETERS
STOP

```
C
      DIMENSION OMEG(41,41),EPS(41,41),TKE(41,41),TED(41,41),U(41,41),
     *V(41,41),W(41,41),AMUT(41,41),AE(41,41),AW(41,41),AN(41,41),AS
     *(41,41),BEF(41,41),BWF(41,41),BNF(41,41),BSF(41,41),VP(41,41)
      DIMENSION DUY(41,41),DUZ(41,41),F1(41,41),F2(41,41),F3(41,41),
     *TOWWW(41),UPP(41),TKEPP(41),TEDPP(41),UOLD(41,41),TT(41),
     *F4(41,41),Y(41),Z(41),TOWW(41),UFW(41),RSWF(41,41),RSE
     *PF(41,41),DA(41,41) ,UFWW(41),YRAT(41,41),YY(41,41),ZZ(41,41)
     *,ZRAT(41,41),VORSOR(41,41),UP(41),TKEP(41),TEDP(41),XR(41,41)
     *,WZ(41),ZW(41),DPD(41,41),YYY(41),ZZZ(41)
     *,ZZL(41,41),WZC(41,41),T(41,41),ZT(41,41),FX(41),FY(41)
C
      DATA RE,ROW/83000.0,1.2047/,CMU,CE1,
     *CE2,SIGMK,CAPA/0.09,1.44,1.92,1.0,.41/,A,E/2.44,5.0/
      DATA SIGMU,ALFAW,ALFAEP,ALFAK,ALFAE,ALFAU/1.0,
     *0.5000,0.5000,0.5000,0.5000,1.0000/,
     *IMAX,IPRINT,IRPRNT,ALMD,ALMDW/5000,500,50,0.001,0.001/
C
      AMU = 0.00001817
      CPRIME=0.00005
      SIGME = 1.167
      ANU = AMU / ROW
C
C     **** GRID SPECIFICATIONS ****
C
      S2=0.0762
      M2=13
      N=3
      X1=1.3
      S1=N*S2
      M1=(4.0*N-1)*(M2-1)/6.0+(M2-1)/2.0+1
      GRSPG1=(S2*3/4)/((M2-1)/2)
      Y(1)=0.0
      Z(1)=0.0
      N1=(M2-1)/2+1
      DO 2091 J=2,N1
      Z(J)=Z(J-1)+GRSPG1
 2091 CONTINUE
      N2=(4*N-1)*(M2-1)/6+1
      DO 2092 I=2,N2
      Y(I)=Y(I-1)+GRSPG1
 2092 CONTINUE
      X2=((X1-1)*S2)/(4.0*(X1**((M2-1)/2)-1))
      TT(1)=X2
      DO 10 I=2,N1
      TT(I)=TT(I-1)*X1
   10 CONTINUE
      N3=N1+1
      DO 79 J=N3,M2
      K=M2+1-J
      Z(J)=Z(J-1)+TT(K)
   79 CONTINUE
      N4=N2+1
      DO 5039 I=N4,M1
      K=M1+1-I
      Y(I)=Y(I-1)+TT(K)
 5039 CONTINUE
      M11=M1-1
      M22=M2-1
      KI=M1-2
      KJ=M2-2

      WRITE(6,*) M1,M2,M11,M22,S1,S2,N,N1,N2,N3,N4,X1,X2,GRSPG1
      WRITE(6,*) TT
      AREA=4.0*S1*S2
      CLWTPR=(S1+S2)*4.0
      DEQ=4.0*AREA/CLWTPR
      UBAV=RE*AMU/(ROW*DEQ)
      PRINT 400, M1,M2,DEQ,RE,UBAV,ROW,AMU,GRSPG1,GRSPG2
      PRINT 401, CMU,CE1,CE2,SIGMK,SIGME,CAPA,CPRIME
      PRINT 485, A,E
      PRINT 439, SIGMU
      PRINT 402, ALFAW,ALFAEP,ALFAK,ALFAE,ALFAU,ALMD,ALMDW
      PRINT 455, AREA,CLWTPR
      WRITE(6,*) IMAX,IPRINT,IRPRNT,M11,M22,KI,KJ,S1,S2,ANU
C
      PRINT 305
      PRINT 432
      WRITE(6,433) (Y(I),I=1,M1)
      PRINT 306
      PRINT 434
      WRITE(6,433) (Z(J),J=1,M2)
C
C     **** INITIALIZATION BY ZERO ****
C
      DO 4 I=1,M1
      DO 4 J=1,M2
      OMEG(I,J) =0.0
      EPS(I,J) = 0.0
      TKE(I,J) = 0.0
      TED(I,J) = 0.0
      U(I,J) =0.0
      V(I,J) = 0.0
      W(I,J) = 0.0
      AMUT(I,J) = 0.0
      VP(I,J) = 0.0
      VORSOR(I,J) = 0.0
      AE(I,J) = 0.0
      AW(I,J) = 0.0
      AN(I,J) = 0.0
      AS(I,J) = 0.0
    4 CONTINUE
C
      READ(10,*) U,TKE,TED,DPDX
      CALL PP(U,M1,M2,1,1.0)
      CALL PP(TKE,M1,M2,2,10.0)
      CALL PP(TED,M1,M2,3,0.1)
      WRITE(6,*) DPDX
C
C     **** COEFFICIENT CALCULATIONS FOR VORTICITY AND STREAM FUNCTION
C     EQUATIONS ****
C
      DO 58 J=2,M22
      DO 58 I=2,M11
      BEF(I,J) = 0.25 * (Z(J+1)-Z(J-1)) / (Y(I+1)-Y(I))
      BWF(I,J) = 0.25 * (Z(J+1)-Z(J-1)) / (Y(I)-Y(I-1))
      BNF(I,J) = 0.25 * (Y(I+1)-Y(I-1)) / (Z(J+1) - Z(J))
      BSF(I,J) = 0.25 * (Y(I+1)-Y(I-1)) / (Z(J) - Z(J-1))
      VP(I,J) = 0.25 * (Y(I+1)-Y(I-1)) * (Z(J+1)-Z(J-1))
   58 CONTINUE
      DO 6031 I=1,M1
      DO 6031 J=1,M2
      YY(I,J)=(Y(I)-Y(I-1))/(Y(I+1)-Y(I))
 6031 CONTINUE
      DO 6032 I=1,M1
      DO 6032 J=1,M2
```

```
 8052 CONTINUE
C
      SUMDA = 0.0
      DO 96 J=2,M2
      DO 96 I=2,M1
      DA(I,J) = (Y(I)-Y(I-1)) * (Z(J)-Z(J-1))
      SUMDA = SUMDA + DA(I,J)
   96 CONTINUE
C
      ROWCMU = ROW * CMU**0.25
      WRITE(6,*) SUMDA,ROWCMU
C
C     **** MAIN LOOP OF ITERATIONS ****
C
      ICOUNT = 0
  900 ICOUNT = ICOUNT + 1
C
C     **** INITIALIZATION OF RESIDUALS ****
C
      RSWM = 0.0
      RSEPM = 0.0
      RSKM = 0.0
      RSEM = 0.0
      RSUM = 0.0
C
      DO 180 I=1,M1
      DO 180 J=1,M2
      F1(I,J) = 0.0
      F2(I,J) = 0.0
      F3(I,J) = 0.0
      F4(I,J) = 0.0
      DUY(I,J) = 0.0
      DUZ(I,J) = 0.0
      RSWF(I,J)=0.0
      RSEPF(I,J)=0.0
      YRAT(I,J)=0.0
      ZRAT(I,J)=0.0
      XR(I,J)=0.0
  180 CONTINUE
C
C
C     **** A'S CALCULATIONS ****
C
C
      DO 31 J=2,M22
      DO 31 I=2,M11
      AE(I,J)=(-EPS(I+1,J-1)-EPS(I,J-1)+EPS(I+1,J+1)+EPS(I,J+1))/8.0
      AW(I,J)=( EPS(I-1,J+1)+EPS(I,J+1)-EPS(I-1,J-1)-EPS(I,J-1))/8.0
      AN(I,J)=( EPS(I+1,J+1)+EPS(I+1,J)-EPS(I-1,J+1)-EPS(I-1,J))/8.0
      AS(I,J)=(-EPS(I-1,J-1)-EPS(I-1,J)+EPS(I+1,J-1)+EPS(I+1,J))/8.0
   31 CONTINUE
C
C
C     **** EDDY VISCOSITY ( MUT ) ****
C
      DO 42 J=1,M2
      DO 42 I=1,M1
      IF(TED(I,J) .EQ. 0.0) GO TO 43
      AMUT(I,J) = CMU * ROW * (TKE(I,J)**2) / TED(I,J)
      GO TO 42
   43 AMUT(I,J) = 0.0
   42 CONTINUE
C
C     **** COEFFICIENT FOR THE VORTICITY SOURCE TERM ****
C     **** DUY AND DUZ ARE TRANSIENT LOCATIONS ****
C
      DO 34 J=2,M22
      DO 34 I=1,M11
      DUZ(I,J)=((U(I,J+1)-U(I,J))*ZZ(I,J)+(U(I,J)-U(I,J-1))/ZZ(I,J))/
     *(Z(J+1)-Z(J-1))
   34 CONTINUE
C
      DO 65 J=1,M22
      DO 65 I=2,M11
      DUY(I,J)=((U(I+1,J)-U(I,J))*YY(I,J)+(U(I,J)-U(I-1,J))/YY(I,J))/
     *(Y(I+1)-Y(I-1))
   65 CONTINUE
C
C     **** DV/DY AND DW/DZ BOUNDARY VALUES ****
C     **** AT THE WALL ( NOTE: DUY AND DUZ=0 AT THE WALL ****
C
C
      DO 14 I=1,M11
      DUZ(I,M2) =-U(I,M22) / (Z(M2) - Z(M22))
   14 CONTINUE
C
      DO 111 J=1,M22
      DUY(M1,J)=-U(M11,J)/(Y(M1)-Y(M11))
  111 CONTINUE
C
C     **** VORTICITY SOURCE TERM CALCULATIONS ****
C     ************** LY MODEL *******************
C
      DO 173 J=1,M2
      DO 173 I=1,M1
      DUYSQ = DUY(I,J)**2
      DUZSQ = DUZ(I,J)**2
      F2(I,J) = (DUYSQ + DUZSQ) / SIGMU
      IF(TED(I,J) .EQ. 0.0) GO TO 178
      FACTOR = CPRIME * AMUT(I,J) * TKE(I,J) / TED(I,J)
      GO TO 179
  178 FACTOR = 0.0
  179 CONTINUE
      F1(I,J) = FACTOR * (DUZSQ - DUYSQ)
      F4(I,J) = FACTOR * DUY(I,J) * DUZ(I,J)
  173 CONTINUE
      DO 126 I=1,M1
      DO 126 J=1,M2
      DUY(I,J) = 0.0
      DUZ(I,J) = 0.0
  126 CONTINUE
C
C
      DO 49 J=2,M22
      DO 49 I=1,M1
      F3(I,J)=((F1(I,J+1)-F1(I,J))*ZZ(I,J)+(F1(I,J)-F1(I,J-1))/ZZ(I,J))
     */(Z(J+1)-Z(J-1))
   49 CONTINUE
      DO 48 J=2,M22
      DO 48 I=2,M11
      DUY(I,J)=((F3(I+1,J)-F3(I,J))*YY(I,J)+(F3(I,J)-F3(I-1,J))/YY(I,J))
     */(Y(I+1)-Y(I-1))
   48 CONTINUE
      DO 55 J=2,M22
      DO 55 I=2,M11
      VORSOR(I,J)=DUY(I,J)
   55 CONTINUE
```

```
C
      DO 56  J=2,M22
      DO 56  I=2,M11
      RSW=0.0
      RSWF(I,J)=0.0
      CE = 2.0 * AMU * BEF(I,J)
      CW = 2.0 * AMU * BWF(I,J)
      CN = 2.0 * AMU * BNF(I,J)
      CS = 2.0 * AMU * BSF(I,J)
      SGMAB = CE + CW + CN + CS
     &+ABS(AE(I,J))+ABS(AW(I,J))+ABS(AN(I,J))+ABS(AS(I,J))
      SOURCE = VP(I,J) * VORSOR(I,J)
      CEE=CE-AE(I,J)+ABS(AE(I,J))
      CWW=CW+AW(I,J)+ABS(AW(I,J))
      CNN=CN+AN(I,J)+ABS(AN(I,J))
      CSS=CS-AS(I,J)+ABS(AS(I,J))
      OMEGA = (CEE* OMEG(I+1,J) + CWW* OMEG(I-1,J) + CNN* OMEG(I,J+1)
     *+ CSS* OMEG(I,J-1) + SOURCE) / SGMAB
C
C     **** CALCULATE RESIDUALS ****
C
      IF(ABS(OMEG(I,J)).GT.ABS(OMEGA)) GOTO 9851
      IF(ABS(OMEGA).LT.0.00001) GOTO 182
      RSW=1-ABS(OMEG(I,J)/OMEGA)
      GOTO 9852
 9851 IF(ABS(OMEG(I,J)).LT.0.001) GOTO 182
      RSW=1-ABS(OMEGA/OMEG(I,J))
 9852 RSWF(I,J) = RSW
      IF(ABS(RSW) .GT. ABS(RSWM)) RSWM=RSW
  182 OMEG(I,J) = ALFAW * OMEGA + (1.0 - ALFAW) * OMEG(I,J)
   56 CONTINUE
C
C     **** THE VORTICITY BOUNDARY VALUE ( AT THE WALL ) ****
C
      SLOPW1=(Z(M2)-Z(M2-1))/(Z(M2-1)-Z(M2-2))
      SLOPW2=(Y(M1)-Y(M1-1))/(Y(M1-1)-Y(M1-2))
      DO 26 I=1,M1
      OMEG(I,M2)= OMEG(I,M22)+SLOPW1* (OMEG(I,M22)-OMEG(I,M2-2))
      RSWF(I,M2)=0.0
   26 CONTINUE
      DO 103 J=1,M2
      OMEG(M1,J)=OMEG(M11,J)+SLOPW2*(OMEG(M11,J)-OMEG(M1-2,J))
      RSWF(M1,J)=0.0
  103 CONTINUE
      DO 9221 I=1,M11
      RSWF(I,1)=0.0
 9221 OMEG(I,1)=0.0
      DO 9222 J=1,M22
      RSWF(1,J)=0.0
 9222 OMEG(1,J)=0.0
C
C     **** STREAM FUNCTION SUBCYCLE ****
C
      DO 62 JJ=2,M22
      DO 62 II=2,M11
      J=M2-JJ+1
      I=M1-II+1
      RSEP=0.0
      RSEPF(I,J)=0.0
      SGMB = 2.0 * (BEF(I,J) + BWF(I,J) + BNF(I,J) + BSF(I,J))
      SOURCE = OMEG(I,J) * VP(I,J) * ROW
C
C     **** HERE C'S = B'S AS A'S ARE ZERO ****
C
      EPSI = (2.0 * (BEF(I,J) * EPS(I+1,J) + BWF(I,J) * EPS(I-1,J) +
     *BNF(I,J) * EPS(I,J+1) + BSF(I,J) * EPS(I,J-1)) + SOURCE) / SGMB
C
C     **** CALCULATE RESIDUALS ****
C
      IF(ABS(EPS(I,J)).GT.ABS(EPSI)) GOTO 9853
      IF(ABS(EPSI).LT.0.000001) GOTO 183
      RSEP=1-ABS(EPS(I,J)/EPSI)
      GOTO 9854
 9853 IF(ABS(EPS(I,J)).LT.0.000001) GOTO 183
      RSEP=1-ABS(EPSI/EPS(I,J))
 9854 RSEPF(I,J) = RSEP
      IF(ABS(RSEP) .GT. ABS(RSEPM)) RSEPM=RSEP
  183 EPS(I,J) = ALFAEP * EPSI + (1.0 - ALFAEP) * EPS(I,J)
   62 CONTINUE
C
  704 CONTINUE
      DO 9223 I=1,M1
      RSEPF(I,1)=0.0
      RSEPF(I,M2)=0.0
      EPS(I,1)=0.0
 9223 EPS(I,M2)=0.0
      DO 9224 J=1,M2
      RSEPF(1,J)=0.0
      RSEPF(M1,J)=0.0
      EPS(1,J)=0.0
 9224 EPS(M1,J)=0.0
C     **** CLEAR LOCATIONS F3 AND F4 ****
C
      DO 69 I=1,M1
      DO 69 J=1,M2
      F3(I,J) = 0.0
      F4(I,J) = 0.0
   69 CONTINUE
C
C     **** COEFFICIENT FOR K EQUATION ****
C
      DO 146 J=2,M22
      DO 146 I=2,M11
      IF(TKE(I,J) .EQ. 0.0) GO TO 146
      F4(I,J) = ROW * VP(I,J) * TED(I,J)/TKE(I,J)
  146 CONTINUE
C
C     **** K SUBCYCLE ****
C
      DO 67  J=2,KJ
      DO 67  I=2,KI
      RSK=0.0
      YRAT(I,J)=0.0
      CE = BEF(I,J) * (2.0 * AMU + (AMUT(I,J) + AMUT(I+1,J))
     */ SIGMK)
      CW = BWF(I,J) * (2.0 * AMU + (AMUT(I,J) + AMUT(I-1,J))
     */ SIGMK)
      CN = BNF(I,J) * (2.0 * AMU + (AMUT(I,J) + AMUT(I,J+1))
     */ SIGMK)
      CS = BSF(I,J) * (2.0 * AMU + (AMUT(I,J) + AMUT(I,J-1))
     */ SIGMK)
      SGMABK = CE + CW + CN + CS
     *+ABS(AE(I,J))+ABS(AW(I,J))+ABS(AN(I,J))+ABS(AS(I,J))
      CEE=CE-AE(I,J)+ABS(AE(I,J))
      CWW=CW+AW(I,J)+ABS(AW(I,J))
      CNN=CN+AN(I,J)+ABS(AN(I,J))
      CSS=CS-AS(I,J)+ABS(AS(I,J))
```

```
      **TKE(I,J-1) + AMUT(I,J) *
C
C     **** CALCULATE RESIDUALS ****
C
      IF(TKE(I,J).GT.TKEY) GOTO 9861
      IF(TKEY.LT.0.000001) GOTO 184
      RSK=1-TKE(I,J)/TKEY
      GOTO 9862
 9861 IF(TKE(I,J).LT.0.00001) GOTO 184
      RSK=1-TKEY/TKE(I,J)
 9862 YRAT(I,J)=RSK
      IF(ABS(RSK) .GT. ABS(RSKM)) RSKM=RSK
  184 TKE(I,J) = ALFAK * TKEY + (1.0 - ALFAK) * TKE(I,J)
   67 CONTINUE
C
C     **** DISSIPATION SOURCE TERM STORED IN LOCATION F3 ****
C
      DO 71 J=2,M22
      DO 71 I=2,M11
      F3(I,J) = CE1 * CMU * TKE(I,J) * F2(I,J) * VP(I,J) * ROW
   71 CONTINUE
C
C     **** DISSIPATION SUBCYCLE ****
C
      DO 73  J=2,KJ
      DO 73  I=2,KI
      RSE=0.0
      ZRAT(I,J)=0.0
      CE = BEF(I,J) * (2.0 * AMU + (AMUT(I,J) + AMUT(I+1,J))
     */ SIGME)
      CW = BWF(I,J) * (2.0 * AMU + (AMUT(I,J) + AMUT(I-1,J))
     */ SIGME)
      CN = BNF(I,J) * (2.0 * AMU + (AMUT(I,J) + AMUT(I,J+1))
     */ SIGME)
      CS = BSF(I,J) * (2.0 * AMU + (AMUT(I,J) + AMUT(I,J-1))
     */ SIGME)
      SGMABE = CE + CW + CN + CS
     &+ABS(AE(I,J))+ABS(AW(I,J))+ABS(AN(I,J))+ABS(AS(I,J))
      CEE=CE-AE(I,J)+ABS(AE(I,J))
      CWW=CW+AW(I,J)+ABS(AW(I,J))
      CNN=CN+AN(I,J)+ABS(AN(I,J))
      CSS=CS-AS(I,J)+ABS(AS(I,J))
      TEDN = (CEE* TED(I+1,J) + CWW* TED(I-1,J) + CNN* TED(I,J+1) + CSS
     ** TED(I,J-1) + F3(I,J))/(SGMABE+CE2*F4(I,J))
C
      IF(TEDN .LT. 0.0) WRITE(6,*) ICOUNT,I,J,CE,CW,CN,CS
C
C     **** CALCULATE RESIDUALS ****
C
      IF(TED(I,J).GT.TEDN) GOTO 9863
      IF(TEDN.LT.0.000001) GOTO 185
      RSE=1-TED(I,J)/TEDN
      GOTO 9864
 9863 IF(TED(I,J).LT.0.000001) GOTO 185
      RSE=1-TEDN/TED(I,J)
 9864 ZRAT(I,J)=RSE
      IF(ABS(RSE) .GT. ABS(RSEM)) RSEM=RSE
  185 TED(I,J) = ALFAE * TEDN + (1.0 - ALFAE) * TED(I,J)
   73 CONTINUE
C
C     **** AXIAL VELOCITY (U) SUBCYCLE ****
C
      DO 74  J=2,KJ
      DO 74  I=2,KI
      CE = BEF(I,J) * (2.0 * AMU + (AMUT(I,J) + AMUT(I+1,J))
     */ SIGMU)
      CW = BWF(I,J) * (2.0 * AMU + (AMUT(I,J) + AMUT(I-1,J))
     */ SIGMU)
      CN = BNF(I,J) * (2.0 * AMU + (AMUT(I,J) + AMUT(I,J+1))
     */ SIGMU)
      CS = BSF(I,J) * (2.0 * AMU + (AMUT(I,J) + AMUT(I,J-1))
     */ SIGMU)
      SGMABU = CE + CW + CN + CS
     &+ABS(AE(I,J))+ABS(AW(I,J))+ABS(AN(I,J))+ABS(AS(I,J))
      CEE=CE-AE(I,J)+ABS(AE(I,J))
      CWW=CW+AW(I,J)+ABS(AW(I,J))
      CNN=CN+AN(I,J)+ABS(AN(I,J))
      CSS=CS-AS(I,J)+ABS(AS(I,J))
      U(I,J) = (CEE* U(I+1,J) + CWW* U(I-1,J) + CNN* U(I,J+1) + CSS*
     *U(I,J-1) + DPDX * VP(I,J)) / SGMABU
   74 CONTINUE
C
C     **** U, K AND E BOUNDARY CONDITIONS ****
C
C     **** NEAR THE WALL ****
C
      DO 27 I=1,M11
      ZDPLS =UFW(I)*ABS(Z(M2-2)-Z(M2))/ANU
      IF(ZDPLS .EQ. 0.0) ZDPLS=ZPLUS
      UPLS4 = A * ALOG(ZDPLS) + E
      UFW(I) = U(I,M2-2) / UPLS4
      TOWW(I)=ROW*UFW(I)*UFW(I)
   27 CONTINUE
      DO 82 J=1,M22
      ZDPLS=UFWW(J)*ABS(Y(M1-2)-Y(M1))/ANU
      IF(ZDPLS.EQ.0.0) ZDPLS=ZPLUS
      UPLS4=A*ALOG(ZDPLS)+E
      UFWW(J)=U(M1-2,J)/UPLS4
      TOWWW(J)=ROW*UFWW(J)*UFWW(J)
   82 CONTINUE
C
C     **** CALCULATE AVERAGE WALL SHEAR STRESSES ****
C
      SUMW = 0.0
      DO 28 I=2,M1
      TOWM = (TOWW(I) + TOWW(I-1)) / 2.0
      SUMW = SUMW + TOWM * (Y(I) - Y(I-1))
   28 CONTINUE
      TAV1=SUMW/S1
      SUMM=0.0
      DO 72 J=2,M2
      TOWM=(TOWWW(J)+TOWWW(J-1))/2.0
      SUMM=SUMM+TOWM*(Z(J)-Z(J-1))
   72 CONTINUE
      TAV2=SUMM/S2
      TOWAVW =(TAV1+TAV2)/2.0
      UFAVW = SQRT(ABS(TOWAVW/ROW))
      DPDX = 4.0 * TOWAVW / DEQ
C
      DO 29 I=1,M11
      IF(UFW(I).EQ.0.0) UFW(I)=UFAVW
      TKEP(I) = UFW(I) * UFW(I) / SQRT(CMU)
      TEDP(I) = UFW(I) * UFW(I) * UFW(I) / (CAPA * (Z(M2)-Z(M22)))
      ZPLUSP = UFW(I) * (Z(M2)-Z(M22)) / ANU
      YYY(I)=TOWW(I)/TOWAVW
      WZ(I)=ZPLUSP
      UP(I) = UFW(I) * (A * ALOG(ZPLUSP) + E)
```

```
      DO 92 J=1,M22
      IF(UFWW(J).EQ.0.0) UFWW(J)=UFAVW
      TKEPP(J)=UFWW(J)*UFWW(J)/SQRT(CMU)
      TEDPP(J)=UFWW(J)*UFWW(J)*UFWW(J)/(CAPA*(Y(M1)-Y(M11)))
      ZPLUSQ=UFWW(J)*(Y(M1)-Y(M11))/ANU
      ZW(J)=ZPLUSQ
      ZZZ(J)=TOWWW(J)/TOWAVW
      UPP(J)=UFWW(J)*(A*ALOG(ZPLUSQ)+E)
   92 CONTINUE
      DO 931 I=2,M11
      TKE(I,M22)=TKEP(I)
      TED(I,M22)=TEDP(I)
  931 U(I,M22)=UP(I)
      DO 932 J=2,M22
      TKE(M11,J)=TKEPP(J)
      TED(M11,J)=TEDPP(J)
  932 U(M11,J)=UPP(J)
      YRA = ((Y(2) - Y(1))**2 - (Y(3) - Y(1))**2)
      YRB = ((Y(2) - Y(1))**2) / YRA
      YRC = ((Y(3) - Y(1))**2) / YRA
      ZRA=((Z(2)-Z(1))**2-(Z(3)-Z(1))**2)
      ZRB=((Z(2)-Z(1))**2)/ZRA
      ZRC=((Z(3)-Z(1))**2)/ZRA
      DO 77 J=1,M2
      TKE(1,J) = YRB * TKE(3,J) - YRC * TKE(2,J)
      TED(1,J) = YRB * TED(3,J) - YRC * TED(2,J)
      U(1,J) = YRB * U(3,J) - YRC * U(2,J)
      IF(TKE(1,J) .LT. 0.0) TKE(1,J)=0.0
      IF(TED(1,J) .LT. 0.0) TED(1,J)=0.0
      IF(U(1,J) .LT. 0.0) U(1,J)=0.0
   77 CONTINUE
      DO 78 I=1,M1
      TKE(I,1)=ZRB*TKE(I,3)-ZRC*TKE(I,2)
      TED(I,1)=ZRB*TED(I,3)-ZRC*TED(I,2)
      U(I,1)=ZRB*U(I,3)-ZRC*U(I,2)
      IF(TKE(I,1).LT.0.0) TKE(I,1)=0.0
      IF(TED(I,1).LT.0.0) TED(I,1)=0.0
      IF(U(I,1).LT.0.0) U(I,1)=0.0
   78 CONTINUE
C
C
      DO 347 I=2,M1
      TKE(I,M2)=0.0
      TED(I,M2)=0.0
  347 U(I,M2)=0.0
      DO 348 J=2,M2
      TKE(M1,J)=0.0
      TED(M1,J)=0.0
  348 U(M1,J)=0.0
C
C
C     **** AVERAGE BULK VELOCITY CALCULATION ****
C
      SUM = 0.0
      DO 83 J=2,M2
      DO 83 I=2,M1
      UAV = (U(I,J) + U(I-1,J) + U(I-1,J-1) + U(I,J-1)) / 4.0
      DV = UAV * DA(I,J)
      SUM = SUM + DV
   83 CONTINUE
C
C
      UB = SUM*4.0/AREA



C     **** CORRCTN OF U EVERYWHERE IN ORDER TO SATISFY CONT EQ ****
C
      DO 84 J=1,M22
      DO 84 I=1,M11
      U(I,J) = U(I,J) * UBAV / UB
   84 CONTINUE
      DO 500 J=1,M22
      DO 500 I=1,M11
      IF(ICOUNT .EQ. 1) GO TO 300
      RSU=0.0
      XR(I,J)=0.0
      IF(UOLD(I,J).GT.U(I,J)) GOTO 9871
      IF(U(I,J).LT.0.00001) GOTO 186
      RSU=1-UOLD(I,J)/U(I,J)
      GOTO 9872
 9871 IF(UOLD(I,J).LT.0.00001) GOTO 186
      RSU=1-U(I,J)/UOLD(I,J)
 9872 XR(I,J)=RSU
      IF(ABS(RSU) .GT. ABS(RSUM)) RSUM=RSU
  186 U(I,J) = ALFAU * U(I,J) + (1.0 - ALFAU) * UOLD(I,J)
  300 UOLD(I,J)=U(I,J)
  500 CONTINUE
      RRR=UB*ROW*DEQ/AMU
C
      IFREQ = ICOUNT / IRPRNT
      IFREQ = IFREQ * IRPRNT
      IF(ICOUNT.EQ.1) GOTO 3246
      IF(ICOUNT .NE. IFREQ) GO TO 91
  369 PRINT 421, ICOUNT
      PRINT 422, RSWM,RSEPM,RSKM,RSEM,RSUM
      WRITE(6,*) TTT,DPDX,RRR,UFAVW
C
   91 IF(ABS(RSWM) .LE. ALMDW .AND. ABS(RSEPM) .LE. ALMD .AND. ABS(RSK
     *M) .LE. ALMD .AND. ABS(RSEM) .LE. ALMD .AND. ABS(RSUM) .LE. ALMD)
     *GO TO 101
 3246 CONTINUE
      IFREQ = ICOUNT / IPRINT
      IFREQ = IFREQ * IPRINT
      IF(ICOUNT .NE. IFREQ) GO TO 100
C
      CALL PP(OMEG,M1,M2,1,1.00)
      CALL PP(EPS,M1,M2,2,10000.0)
      CALL PP(TKE,M1,M2,3,10.0)
      CALL PP(TED,M1,M2,4,0.100)
      CALL PP(U,M1,M2,5,1.0)
      CALL PP(VORSOR,M1,M2,10,0.100)
      CALL PP(RSWF,M1,M2,21,1000.0)
      CALL PP(RSEPF,M1,M2,22,1000.0)
      CALL PP(YRAT,M1,M2,23,1000.0)
      CALL PP(ZRAT,M1,M2,24,1000.0)
      CALL PP(XR,M1,M2,25,1000.0)
      WRITE(6,*) TOWW,TOWWW,UFW,UFWW
      WRITE(6,*) UB,TOWAVW,UFAVW,DPDX
C     **** SECONDARY VELOCITIES ****
C
C     **** CLEAR LOCATION DUY AND DUZ ****
C
      DO 208 I=1,M1
      DO 208 J=1,M2
      DUY(I,J) = 0.0
      DUZ(I,J) = 0.0
  208 CONTINUE
C
      DO 177 J=1,M22
```

```
      DUY(I,J)=((EPS(I+1,J)-EPS(I,J))*YY(I,J)+(EPS(I,J)-EPS(I-1,J))/
     *YY(I,J))/(Y(I+1)-Y(I-1))
  177 CONTINUE
C
      DO 278 J=2,M22
      DO 278 I=1,M11
      DUZ(I,J)=((EPS(I,J+1)-EPS(I,J))*ZZ(I,J)+(EPS(I,J)-EPS(I,J-1))/
     *ZZ(I,J))/(Z(J+1)-Z(J-1))
  278 CONTINUE
C
C     **** BOUNDARY VALUES ****
C     **** AT THE WALL ****
C
      DO 88 I=2,M11
      DUZ(I,M2)=-EPS(I,M22)/(Z(M2)- Z(M22))
   88 CONTINUE
      DO 86 J=2,M22
      DUY(M1,J)=-EPS(M11,J)/(Y(M1)-Y(M11))
   86 CONTINUE
      DO 2222 J=2,M22
      DUY(1,J) = (EPS(2,J) - EPS(1,J)) / (Y(2) - Y(1))
 2222 CONTINUE
      DO 1111 I=2,M11
      DUZ(I,1)=(EPS(I,2)-EPS(I,1))/(Z(2)-Z(1))
 1111 CONTINUE
C
      DO 4444 J=1,M2
      DO 4444 I=1,M1
      V(I,J) = (1.0 / ROW) * DUZ(I,J)
      W(I,J) = -(1.0 / ROW) * DUY(I,J)
 4444 CONTINUE
C
      SS1=100.0/UB
      CALL PP(V,M1,M2,1,SS1)
      CALL PP(W,M1,M2,2,SS1)
      WRITE(6,*) YYY,ZZZ
  100 IF(ICOUNT .LT. IMAX) GO TO 900
      WWW=1.1111
      WRITE(6,*) WWW
C
  101 CONTINUE
      WRITE(6,*) ICOUNT,RSWM,RSEPM,RSKM,RSEM,RSUM
C     **** SECONDARY VELOCITIES ****
C
C     **** CLEAR LOCATION DUY AND DUZ ****
C
      DO 2708 I=1,M1
      DO 2708 J=1,M2
      DUY(I,J) = 0.0
      DUZ(I,J) = 0.0
 2708 CONTINUE
C
      DO 1777 J=1,M22
      DO 1777 I=2,M11
      DUY(I,J) =  (EPS(I+1,J) - EPS(I-1,J))/(Y(I+1)-Y(I-1))
 1777 CONTINUE
C
      DO 2778 J=2,M22
      DO 2778 I=1,M11
      DUZ(I,J) =  (EPS(I,J+1) - EPS(I,J-1))/(Z(J+1)-Z(J-1))
 2778 CONTINUE
C
C     **** BOUNDARY VALUES ****
C     **** AT THE WALL ****
C
      DO 7788 I=2,M11
      DUZ(I,M2)=-EPS(I,M22)/(Z(M2)- Z(M22))
 7788 CONTINUE
      DO 7786 J=2,M22
      DUY(M1,J)=-EPS(M11,J)/(Y(M1)-Y(M11))
 7786 CONTINUE
      DO 2722 J=2,M22
      DUY(1,J) = (EPS(2,J) - EPS(1,J)) / (Y(2) - Y(1))
 2722 CONTINUE
      DO 1711 I=2,M11
      DUZ(I,1)=(EPS(I,2)-EPS(I,1))/(Z(2)-Z(1))
 1711 CONTINUE
C
      DO 4744 J=1,M2
      DO 4744 I=1,M1
      V(I,J) = (1.0 / ROW) * DUZ(I,J)
      W(I,J) = -(1.0 / ROW) * DUY(I,J)
 4744 CONTINUE
C
C
C     **** FRICTION FACTOR CALCULATION ****
C
      FF = 8.0 * TOWAVW / (ROW * UBAV**2)
C
      PRINT 428, FF,UB
      CALL PP(OMEG,M1,M2,1,1.00)
      CALL PP(EPS,M1,M2,2,1000.0)
      CALL PP(EPS,M1,M2,22,4000.0)
      CALL PP(TKE,M1,M2,3,10.0)
      CALL PP(TED,M1,M2,4,0.100)
      CALL PP(U,M1,M2,5,1.0)
      CALL PP(V,M1,M2,41,100.0)
      CALL PP(W,M1,M2,42,100.0)
      CALL PP(VORSOR,M1,M2,10,1.0)
      WRITE(6,*) UFW,UFWW,TOWW,TOWWW
      SS1=100.0/UB
      S11=100.0/U(1,1)
      SS2=1.0/UFAVW
      S3=1.0/U(1,1)
      S4=1.0/UB
      S5=1.0/(UFAVW*UFAVW)
      S6=S5*S1*S2
      S7=1000.0/(ROW*U(1,1)*Y(M1))
      S8=Y(M1)/U(1,1)
      CALL PP(EPS,M1,M2,111,S7)
      WRITE(6,*) TAV1,TAV2,TOWAVW
      WRITE(6,*) SS1,SS2,S3,S4,S5,S6
      DO 1051 I=1,M1
      TKEP(I)=TOWW(I)/TOWAVW
 1051 TEDP(I)=TOWW(I)/TOWW(1)
      DO 1052 J=1,M2
      TKEPP(J)=TOWWW(J)/TOWAVW
 1052 TEDPP(J)=TOWWW(J)/TOWWW(1)
      DO 1053 I=1,M1
      DO 1053 J=1,M2
 1053 F4(I,J)=SQRT(V(I,J)**2+W(I,J)**2)
      CALL PP(F4,M1,M2,44,SS1)
      CALL PP(F4,M1,M2,444,S11)
      CALL PP(V,M1,M2,45,SS2)
      CALL PP(W,M1,M2,455,SS2)
      CALL PP(V,M1,M2,81,S11)
      CALL PP(W,M1,M2,82,S11)
```

```
      CALL PP(U,M1,M2,52,S4)
      CALL PP(TKE,M1,M2,66,S5)
      CALL PP(OMEG,M1,M2,77,S8)
      CALL PP(ZZL,M1,M2,88,1.0)
      CALL PP(WZC,M1,M2,11,1.0)
      WRITE(6,*) TKEP,TKEPP,TEDP,TEDPP
      CALL PP(V,M1,M2,81,SS1)
      CALL PP(W,M1,M2,82,SS1)
      CALL PP(VORSOR,M1,M2,99,S6)
C
C     TEMPERATURE SUBCYCLE
C
      AK=0.0263
      CP=1007.0
      PR=0.6957105
      PRT=0.9
      OAV=2.0
      TW=300.0
      TBAV=250.0
      DO 6691 I=1,M1
      DO 6691 J=1,M2
      T(I,J)=TBAV
 6691 CONTINUE
      FLUX=ROW*CLWTPR/(CP*ROW*UBAV*AREA)
      PF=9.24*((PR/PRT)**0.75-1.0)
      ALFAT=1.0
      IPNTR=20
      IPNTC=100
      ALMT=0.001
      IIM=2000
      ITER=0
 6680 ITER=ITER+1
      RSTM=0.0
      DO 6601 J=2,KJ
      DO 6601 I=2,KI
      RST=0.0
      ZT(I,J)=0.0
      CE=BEF(I,J)*(2.0*AMU/PR+(AMUT(I,J)+AMUT(I+1,J))/PRT)
      CW=BWF(I,J)*(2.0*AMU/PR+(AMUT(I,J)+AMUT(I-1,J))/PRT)
      CN=BNF(I,J)*(2.0*AMU/PR+(AMUT(I,J)+AMUT(I,J+1))/PRT)
      CS=BSF(I,J)*(2.0*AMU/PR+(AMUT(I,J)+AMUT(I,J-1))/PRT)
      SGMTT=CE+CW+CN+CS+ABS(AE(I,J))+ABS(AW(I,J))+ABS(AN(I,J))
     &+ABS(AS(I,J))
      CEE=CE-AE(I,J)+ABS(AE(I,J))
      CWW=CW+AW(I,J)+ABS(AW(I,J))
      CNN=CN+AN(I,J)+ABS(AN(I,J))
      CSS=CS-AS(I,J)+ABS(AS(I,J))
      TEMP=(CEE*T(I+1,J)+CWW*T(I-1,J)+CNN*T(I,J+1)+CSS*T(I,J-1))/
     &(SGMTT+OAV*VP(I,J)*U(I,J)*FLUX/T(I,J))
      IF(T(I,J).GT.TEMP) GOTO 6603
      IF(TEMP.LT.0.0001) GOTO 6602
      RST=1-T(I,J)/TEMP
      GOTO 6604
 6603 IF(T(I,J).LT.0.0001) GOTO 6602
      RST=1-TEMP/T(I,J)
 6604 ZT(I,J)=RST
      IF(ABS(RST).GT.ABS(RSTM)) RSTM=RST
 6602 T(I,J)=ALFAT*TEMP+(1.0-ALFAT)*T(I,J)
 6601 CONTINUE
      DO 6605 J=1,M2
      T(1,J)=YRB*T(3,J)-YRC*T(2,J)
 6605 CONTINUE
      DO 6606 I=1,M1
      T(I,1)=ZRB*T(I,3)-ZRC*T(I,2)
 6606 CONTINUE
      DO 6607 I=2,M1
      T(I,M2)=TW
 6607 CONTINUE
      DO 6608 J=2,M2
      T(M1,J)=TW
 6608 CONTINUE
      DO 6609 I=1,M11
      FX(I)=(TW-T(I,KJ))*ROW*CP*UFW(I)/(PF+U(I,KJ)/UFW(I))
 6609 CONTINUE
      DO 6610 J=1,M22
      FY(J)=(TW-T(KI,J))*ROW*CP*UFWW(J)/(PF+U(KI,J)/UFWW(J))
 6610 CONTINUE
      SUXM=0.0
      DO 6613 I=2,M1
      SUXM=SUXM+(FX(I)+FX(I-1))*(Y(I)-Y(I-1))/2.0
 6613 CONTINUE
      AV1=SUXM/S1
      SUYM=0.0
      DO 6614 J=2,M2
      SUYM=SUYM+(FY(J)+FY(J-1))*(Z(J)-Z(J-1))/2.0
 6614 CONTINUE
      AV2=SUYM/S2
      OAV=(AV1+AV2)/2.0
      DO 6611 I=2,M11
      T(I,M22)=TW-OAV*(U(I,M22)/UFW(I)+PF)/(ROW*CP*UFW(I))
 6611 CONTINUE
      DO 6612 J=2,M22
      T(M11,J)=TW-OAV*(U(M11,J)/UFWW(J)+PF)/(ROW*CP*UFWW(J))
 6612 CONTINUE
      SUM=0.0
      DO 6615 I=1,M1
      DO 6615 J=1,M2
      TAV=T(I,J)+T(I-1,J)+T(I,J-1)+T(I-1,J-1)
      UAV=U(I,J)+U(I-1,J)+U(I,J-1)+U(I-1,J-1)
      SUM=SUM+TAV*DA(I,J)*UAV/16.0
 6615 CONTINUE
      TB=SUM*4.0/(AREA*UB)
      DO 6616 I=1,M1
      DO 6616 J=1,M2
      T(I,J)=T(I,J)*TBAV/TB
 6616 CONTINUE
      IFQ=ITER/IPNTR
      IFQ=IFQ*IPNTR
      IF(ITER.EQ.1) GOTO 6645
      IF(IFQ.NE.ITER) GOTO 6621
      WRITE(6,*) ITER,RSTM
 6621 IF(ABS(RSTM).LE.ALMT) GOTO 6650
      IFQQ=ITER/IPNTC
      IFQQ=IFQQ*IPNTC
      IF(ITER.NE.IFQQ) GOTO 6645
      CALL PP(T,M1,M2,3333,0.01)
      CALL PP(ZT,M1,M2,3322,1000.0)
      WRITE(6,*) OAV,FX,FY
 6645 IF(ITER.LT.IIM) GOTO 6680
 6650 CONTINUE
      WRITE(6,*) ITER,RSTM
      WRITE(6,*) OAV,TB
      WRITE(6,*) FX
      WRITE(6,*) FY
      CALL PP(T,M1,M2,3333,0.01)
      HTOT=OAV/(TW-TB)
      ANUS=HTOT*DEQ/AK
```

```
      DO 6671 I=1,M1
      FX(I)=FX(I)/OAV
 6671 CONTINUE
      DO 6672 J=1,M2
      FY(J)=FY(J)/OAV
 6672 CONTINUE
      WRITE(6,*) FX
      WRITE(6,*) FY
      AAA=1.0/TB
      CALL PP(T,M1,M2,333,AAA)
      DO 6673 I=1,M1
      DO 6673 J=1,M2
      T(I,J)=(TW-T(I,J))/(TW-TB)
 6673 CONTINUE
      CALL PP(T,M1,M2,4444,1.0)
C
  305 FORMAT(//4X,'THE NODAL DISTANCE IN THE Y - DIRN. (METER) :'/)
  306 FORMAT(//4X,'THE NODAL DISTANCE IN THE Z - DIRN. (METER) :'/)
  400 FORMAT('1',40X,'**** INPUT VALUES ****'///4X,'M1 =',I4/4X,'M2 =
     *',I4/4X,'DEQ  =',F9.6,2X,'(METER)'/4X,'RE  =',F10.2
     */4X,'UBAV  =',E12.5,2X,'(M/SEC)'/4X,'ROW  =',F8.5,2X,'(KG/CU. M)'/
     *4X,'AMU  =',E12.5,2X,'(KG/M SEC)'/4X,'GRSPG1 =',F9.6,2X,'(METER)'
     */4X,'GRSPG2 =',F9.6,2X,'(METER)')
  401 FORMAT(//4X,'CONSTANT VALUES :'/4X,'CMU  =',F7.3/4X,'CE1  =',
     *F7.3/4X,'CE2  =',F7.3/4X,'SIGMK  =',F7.3/4X,'SIGME  =',F7.3/4X,
     *'CAPA  =',F8.4/4X,'CPRIME  =',F7.4/)
  399 FORMAT(///10X,'?? FLAG : WRONG SIDE, GRSPG ?? XXX'///)
  402 FORMAT( 4X,'UNDER RELAXATION FACTORS :'/4X,'ALFAW  =',F7.4/4X,
     *'ALFAEP  =',F7.4/4X,'ALFAK  =',F7.4/4X,'ALFAE  =',F7.4/4X,'
     *ALFAU  =',F7.4//4X,'CONVERGENCE VALUES :'/4X,'ALMD  =',F8.5,
     */4X,'ALMDW  =',F8.5/)
  407 FORMAT(//4X,'ASSUMED INITIAL AND BOUNDARY VALUES ARE :'/4X,
     *'UFAVW =',E12.5/4X,'TOWAVW =',E12.5/4X,'DPDX  =',
     *E12.5/4X,'TKEI  =',E12.5/4X,'TEDI  =',E12.5/)
  418 FORMAT(//4X,'ASSUMED DISSIPTN. I.V. (TED(I,2)) :'/)
  421 FORMAT(///51X,'ICOUNT  =',2X,I5//)
  422 FORMAT(  4X,'RSWM=',E13.6,9X,'RSEPM=',E13.6,9X,'RSKM=',
     *E13.6,9X,'RSEM=',E13.6,9X,'RSUM=',E13.6)
  428 FORMAT( /4X,'F.F.  =',E14.6)
  432 FORMAT( 1X,'     I=',3X,'1',10X,'2',10X,'3',10X,'4',10X,'5',10X,'
     *6',10X,'7',10X,'8',10X,'9',10X,'10',10X,'11'/)
  433 FORMAT(5X,11E11.4/5X,10E11.4)
  434 FORMAT( 1X,'     J=',3X,'1',10X,'2',10X,'3',10X,'4',10X,'5',10X,'
     *6',10X,'7',10X,'8',10X,'9',10X,'10',10X,'11'/)
  439 FORMAT(/4X,'SIGMU  =',F7.3//)
  455 FORMAT(/4X,'DUCT CROSS SECTN. AREA :',E14.6,2X,'(SQ. M)',/4X,
     *'CELL CROSS SECTN. AREA :',E14.6,2X,'(SQ. M)')
  484 FORMAT(//4X,'THE DIMNSNLESS NORMAL DISTANCE FROM THE WALL :',5X,
     *E12.5//)
  485 FORMAT(/4X,'LAW OF THE WALL CONSTANTS :'/4X,'A  =',F10.4/4X,
     *'E  =',F10.4/)
      GO TO 1112
 9999 CONTINUE
      WRITE(6,399)
 1112 STOP
      END
C
C
      SUBROUTINE PP(PHY,M1,M2,N,ST)
      DIMENSION PHY(41,41)
      DO 7933 I=1,M1
      DO 7933 J=1,M2
 7933 PHY(I,J)=PHY(I,J)*ST

      DO 7911 J=1,M1,2
      K=M2-J+1
      WRITE(6,7954) (PHY(I,K),I=1,M1,2)
 7954 FORMAT(/1X,17F7.3)
 7911 CONTINUE
C     WRITE(6,*) PHY
      DO 8911 I=1,M1
      DO 8911 J=1,M2
 8911 PHY(I,J)=PHY(I,J)/ST
      WRITE(6,*) N,ST
      RETURN
      END
```

```
      DO 126 I=1,M1
      DO 126 J=1,M2
      DUY(I,J) = 0.0
      DUZ(I,J) = 0.0
  126 CONTINUE
      DO 499 I=1,16
      YYY(I)=S2
  499 CONTINUE
      DO 2099 I=17,M1
      YYY(I)=S2-Z(I-16)
 2099 CONTINUE
      DO 2098 J=1,M2
      ZZZ(J)=S2-Z(J)
 2098 CONTINUE
      IF(ICOUNT.EQ.2) WRITE(6,*) YYY,ZZZ
      YMAX=S2
      ZMAX = S2
C
      CA = 0.000300
      CM = 2.4
      CK = 1.0
      CW = 4.0
C
C
      DO 551 I=2,M11
      DO 551 J=2,M22
      IF(I.GT.(J+16)) GOTO 2145
      FACTOR=CM*8.0*CA*ROW*UFAVW *UFAVW /(S2*S2)
      BB=S2-Z(J)
      ZP=1.0-(YYY(I)/YMAX)
      ZL=1.0-(BB/YMAX)
      ZM=CK*(1.0-CM*ZP*ZP)
      ZN=(2.0+ZM+(CW-ZM)*ZL*ZL)-((1.0-ZL*ZL)*(CW-ZM))
      DTDY=-((YYY(I+1)-YYY(I))*YY(I,J)+(YYY(I)-YYY(I-1))/YY(I,J))/
     *(Y(I+1)-Y(I-1))
      GOTO 3838
 2145 CC=S1-Y(I)
      FACTOR=CM*8.0*CA*ROW*UFAVW  *UFAVW  /(S2*S2)
      ZP=1.0-(ZZZ(J)/ZMAX)
      ZL=1.0-CC/ZMAX
      ZM=CK*(1.0-ZP*ZP*CM)
      ZN=(2.0+ZM+(CW-ZM)*ZL*ZL)-(1.0-ZL*ZL)*(CW-ZM)
      DTDY= ((ZZZ(J+1)-ZZZ(J))*ZZ(I,J)+(ZZZ(J)-ZZZ(J-1))/
     *ZZ(I,J))/(Z(J+1)-Z(J-1))
      GOTO 3838
 3838 VORSOR(I,J) = FACTOR * ZP*ZL*ZN*DTDY
  551 CONTINUE
```

```
      DO 53 I=1,M11
      DO 53 J=2,M22
      F1(I,J)=((V(I,J+1)-V(I,J))*ZZ(I,J)+(V(I,J)-V(I,J-1))/ZZ(I,J))/
     *(Z(J+1)-Z(J-1))
 53   CONTINUE
      DO 57 J=1,M22
      DO 57 I=2,M11
      F2(I,J)=((W(I+1,J)-W(I,J))*YY(I,J)+(W(I,J)-W(I-1,J))/YY(I,J))/
     *(Y(I+1)-Y(I-1))
  57  CONTINUE
      DO 175 I=1,M11
      F1(I,M2)=-V(I,M22)/(Z(M2)-Z(M22))
  175 CONTINUE
      DO 137 J=1,M22
      F2(M1,J)=-W(M11,J)/(Y(M1)-Y(M11))
  137 CONTINUE
      DO 40 J=1,M22
      DO 40 I=2,M11
      F3(I,J)=((V(I+1,J)-V(I,J))*YY(I,J)+(V(I,J)-V(I-1,J))/YY(I,J))/
     *(Y(I+1)-Y(I-1))
   40 CONTINUE
      DO 171 J=1,M22
      F3(M1,J)=-V(M11,J)/(Y(M1)-Y(M11))
  171 CONTINUE
      DO 51 J=2,M22
      DO 51 I=1,M11
      F4(I,J)=((W(I,J+1)-W(I,J))*ZZ(I,J)+(W(I,J)-W(I,J-1))/ZZ(I,J))/
     *(Z(J+1)-Z(J-1))
   51 CONTINUE
      DO 173 I=1,M11
      F4(I,M2)=-W(I,M22)/(Z(M2)-Z(M22))
  173 CONTINUE
      DO 7771 I=2,M11
      DO 7771 J=2,M22
      IF((I+J).GT.12) FFF(I,J)=1.0
      FFF(I,J)=0.3
 7771 CONTINUE
      DO 178 J=2,M22
      DO 178 I=2,M11
      Q1=0.7636-0.06*FFF(I,J)
      Q2=0.1091+0.06*FFF(I,J)
      Q3=1.5-0.5*FFF(I,J)
      G1=2.0*TKE(I,J)/(Q3*TED(I,J))
      G2=TED(I,J)*(Q1+Q2+Q3-1.0)/3.0
      G3=Q2
      G4=DUY(I,J)
      G5=F3(I,J)
      G6=1.0+G1*(1.0-Q1-Q2)*G5
      G7=DUZ(I,J)
      G8=F4(I,J)
      G9=1.0+G1*(1.0-Q1-Q2)*G8
      G10=F2(I,J)
      G11=F1(I,J)
      TT1=(G1*(G2*ROW-G3*AMUT(I,J)*G4*G4)-2.0*AMUT(I,J)*G5)/G6
      TT2=(G1*(G2*ROW-G3*AMUT(I,J)*G7*G7)-2.0*AMUT(I,J)*G8)/G9
      T1(I,J)=TT1-TT2
      T4(I,J)=-G1*AMUT(I,J)*G3*G4*G7-AMUT(I,J)*(G10+G11)
      IF(ICOUNT.LE.3) GOTO 178
      ZZL(I,J)=T1(I,J)/(ROW*UFAVW*UFAVW)
      WZC(I,J)=T4(I,J)/(ROW*UFAVW*UFAVW)
  178 CONTINUE
```

```
      DO 126 I=1,M1
      DO 126 J=1,M2
      F3(I,J)=0.0
      F2(I,J)=0.0
  126 CONTINUE
      DO 9173 J=1,M2
      DO 9173 I=1,M1
      DUYSQ=DUY(I,J)**2
      DUZSQ=DUZ(I,J)**2
      F2(I,J)=(DUYSQ+DUZSQ)/SIGMU
 9173 CONTINUE
C     **** NOTE: F3 IS A TRANSIENT LOCATION ****
C   F3 AT INTERIOR +MID HOR WALL BISECTOR + VERT WALL
      DO 49 J=2,M22
      DO 49 I=1,M1
      F3(I,J)=((T1(I,J+1)-T1(I,J))*ZZ(I,J)+(T1(I,J)-T1(I,J-1))/ZZ(I,J))
     */(Z(J+1)-Z(J-1))
   49 CONTINUE
      DO 5551 I=1,M1
      DO 5551 J=1,M2
      DUY(I,J)=0.0
      DUZ(I,J)=0.0
      F1(I,J)=0.0
 5551 CONTINUE
      DO 48 J=2,M22
      DO 48 I=2,M11
      DUY(I,J)=((F3(I+1,J)-F3(I,J))*YY(I,J)+(F3(I,J)-F3(I-1,J))/YY(I,J))
     */(Y(I+1)-Y(I-1))
   48 CONTINUE
C     **** CLEAR LOCATION F1 ****
C
      DO 737 I=1,M1
      DO 737 J=1,M2
      F1(I,J) = 0.0
  737 CONTINUE
      DO 99 J=2,M22
      DO 99 I=2,M11
      F1(I,J) = DUY(I,J)
   99 CONTINUE
      DO 55 J=2,M22
      DO 55 I=2,M11
      DUZ(I,J)=0.0
      VORSOR(I,J) = F1(I,J)*0.0005
   55 CONTINUE
```

```
C
      DO 126 I=1,M1
      DO 126 J=1,M2
      DUY(I,J) = 0.0
      DUZ(I,J) = 0.0
  126 CONTINUE
      DO 2234 J=2,M22
      DO 2234 I=1,M11
      DUZ(I,J)=((TKE(I,J+1)-TKE(I,J))*ZZ(I,J)+(TKE(I,J)-TKE(I,J-1))
     */ZZ(I,J))/(Z(J+1)-Z(J-1))
 2234 CONTINUE
C
      DO 2265 J=1,M22
      DO 2265 I=2,M11
      DUY(I,J)=((TKE(I+1,J)-TKE(I,J))*YY(I,J)+(TKE(I,J)-TKE(I-1,J))
     */YY(I,J))/(Y(I+1)-Y(I-1))
 2265 CONTINUE
C
C     **** DV/DY AND DW/DZ BOUNDARY VALUES ****
C     **** AT THE WALL ( NOTE: DUY AND DUZ=O AT THE WALL ****
C
C
      DO 2214 I=1,M11
      DUZ(I,M2) =-TKE(I,M22) / (Z(M2) - Z(M22))
 2214 CONTINUE
C
      DO 2111 J=1,M22
      DUY(M1,J)=-TKE(M11,J)/(Y(M1)-Y(M11))
 2111 CONTINUE
C
C     **** FOR VORTICITY SOURCE TERM CALCULATIONS ****
      DO 2173 J=1,M2
      DO 2173 I=1,M1
      DUYSQ = DUY(I,J)**2
      DUZSQ = DUZ(I,J)**2
      IF(TED(I,J) .EQ. 0.0) GO TO 2178
      FACTOR = CPRIME * AMUT(I,J) / TED(I,J)
      GO TO 2179
 2178 FACTOR = 0.0
 2179 CONTINUE
      F1(I,J) = FACTOR * (DUZSQ - DUYSQ)
      F4(I,J) = FACTOR * DUY(I,J) * DUZ(I,J)
      IF(ICOUNT.LE.2) GOTO 2173
      ZZL(I,J)=F1(I,J)/(ROW*UFAVW*UFAVW)
      WZC(I,J)=F4(I,J)/(ROW*UFAVW*UFAVW)
 2173 CONTINUE
C
      DO 3126 I=1,M1
      DO 3126 J=1,M2
      DUY(I,J) = 0.0
      DUZ(I,J) = 0.0
 3126 CONTINUE
C     **** NOTE: F3 IS A TRANSIENT LOCATION ****
C   F3 AT INTERIOR +MID HOR WALL BISECTOR + VERT WALL
      DO 5549 J=2,M22
      DO 5549 I=1,M1
      F3(I,J)=((F1(I,J+1)-F1(I,J))*ZZ(I,J)+(F1(I,J)-F1(I,J-1))/ZZ(I,J))
     */(Z(J+1)-Z(J-1))
 5549 CONTINUE
      DO 5548 J=2,M22
      DO 5548 I=2,M11
      DUY(I,J)=((F3(I+1,J)-F3(I,J))*YY(I,J)+(F3(I,J)-F3(I-1,J))/YY(I,J))
     */(Y(I+1)-Y(I-1))
 5548 CONTINUE
C     **** CLEAR LOCATION F1 ****
C
      DO 9137 I=1,M1
      DO 9137 J=1,M2
      F1(I,J) = 0.0
 9137 CONTINUE
C
C     **** VORT. SOURCE TERM - NORMAL STRESSES - STORED IN F1 LOCN. ****
C
      DO 8840 J=2,M22
      DO 8840 I=2,M11
      F1(I,J) = DUY(I,J)
 8840 CONTINUE
      DO 6655 J=2,M22
      DO 6655 I=2,M11
      VORSOR(I,J) = F1(I,J)
 6655 CONTINUE
```

```
C
      DO 126 I=1,M1
      DO 126 J=1,M2
      DUY(I,J) = 0.0
      DUZ(I,J) = 0.0
  126 CONTINUE
      DO 2234 J=2,M22
      DO 2234 I=1,M11
      DUZ(I,J)=((TED(I,J+1)-TED(I,J))*ZZ(I,J)+(TED(I,J)-TED(I,J-1))
     */ZZ(I,J))/(Z(J+1)-Z(J-1))
 2234 CONTINUE
C
      DO 2265 J=1,M22
      DO 2265 I=2,M11
      DUY(I,J)=((TED(I+1,J)-TED(I,J))*YY(I,J)+(TED(I,J)-TED(I-1,J))
     */YY(I,J))/(Y(I+1)-Y(I-1))
 2265 CONTINUE
C
C     **** DV/DY AND DW/DZ BOUNDARY VALUES ****
C     **** AT THE WALL ( NOTE: DUY AND DUZ=0 AT THE WALL ****
C
C
      DO 2214 I=1,M11
      DUZ(I,M2) =-TED(I,M22) / (Z(M2) - Z(M22))
 2214 CONTINUE
C
      DO 2111 J=1,M22
      DUY(M1,J)=-TED(M11,J)/(Y(M1)-Y(M11))
 2111 CONTINUE
C
C     **** FOR VORTICITY SOURCE TERM CALCULATIONS ****
      DO 2173 J=1,M2
      DO 2173 I=1,M1
      DUYSQ = DUY(I,J)**2
      DUZSQ = DUZ(I,J)**2
      IF(TED(I,J) .EQ. 0.0) GO TO 2178
      FACTOR = CPRIME * AMUT(I,J) * U(I,J)**2*TKE(I,J)/TED(I,J)**3
      GO TO 2179
 2178 FACTOR = 0.0
 2179 CONTINUE
      F1(I,J) = FACTOR * (DUZSQ - DUYSQ)
      F4(I,J) = FACTOR * DUY(I,J) * DUZ(I,J)
      IF(ICOUNT.LE.2) GOTO 2173
      ZZL(I,J)=F1(I,J)/(ROW*UFAVW*UFAVW)
      WZC(I,J)=F4(I,J)/(ROW*UFAVW*UFAVW)
 2173 CONTINUE
C
      DO 3126 I=1,M1
      DO 3126 J=1,M2
      DUY(I,J) = 0.0
      DUZ(I,J) = 0.0
 3126 CONTINUE
C     **** NOTE: F3 IS A TRANSIENT LOCATION ****
C   F3 AT INTERIOR +MID HOR WALL BISECTOR + VERT WALL
      DO 5549 J=2,M22
      DO 5549 I=1,M1
      F3(I,J)=((F1(I,J+1)-F1(I,J))*ZZ(I,J)+(F1(I,J)-F1(I,J-1))/ZZ(I,J))
     */(Z(J+1)-Z(J-1))
 5549 CONTINUE
      DO 5548 J=2,M22
      DO 5548 I=2,M11
      DUY(I,J)=((F3(I+1,J)-F3(I,J))*YY(I,J)+(F3(I,J)-F3(I-1,J))/YY(I,J))
     */(Y(I+1)-Y(I-1))
 5548 CONTINUE
C     **** CLEAR LOCATION F1 ****
C
      DO 9137 I=1,M1
      DO 9137 J=1,M2
      F1(I,J) = 0.0
 9137 CONTINUE
C
      DO 8840 J=2,M22
      DO 8840 I=2,M11
      F1(I,J) = DUY(I,J)
 8840 CONTINUE
      DO 6655 J=2,M22
      DO 6655 I=2,M11
      VORSOR(I,J) = F1(I,J)
 6655 CONTINUE
```

TABLE 1

SUMMARY OF THE CONSTANTS

Constant	Value	Basis of Choice
C_1	1.44	Computer optimization
C_2	1.92	By reference to decay of turbulence behind a grid
C_μ	0.09	By reference to the properties of the "constant-stress" wall region
σ_ε	1.167	By reference to "Constant-Stress" wall region; $\sigma_\varepsilon = (\kappa^2/\sqrt{C_\mu})/(C_2 - C_1)$
σ_k	1.0	Computer optimization
κ	0.41	Von-Karman Constant
A	2.44	Well-established constant of 'Law of the wall'
B	5.0	Well-established constant of 'Law of the wall'.
Pr_t	0.90	Accepted turbulent Prandtl number based on experiments

TABLE 2

THE FUNCTIONS INVOLVED IN THE GENERAL ELLIPTIC EQUATIONS FOR Rectangular DUCTS

Equation	ϕ	a_ϕ	$b_{\phi,y}$	$b_{\phi,z}$	S_ϕ
	$\bar{U}$	1	$\mu + \mu_t$	$\mu + \mu_t$	$\frac{\partial \bar{P}}{\partial x} = - 4 \bar{\tau} / D_h$
	ω	1	μ	μ	$- \rho \{ [\frac{\partial^2}{\partial y \partial z} (\bar{v}^2 - \bar{w}^2)]$
	$\bar{T}$	1	$\frac{\mu}{Pr} + \frac{\mu_t}{Pr_t}$	$\frac{\mu}{Pr} \frac{\mu_t}{Pr_t}$	$\rho \bar{U} \frac{\partial \bar{T}}{\partial x}$
	Ψ	0	1	1	$- \rho \omega$
	k	1	$\mu + \frac{\mu_t}{\sigma_k}$	$\mu + \frac{\mu_t}{\sigma_k}$	$- \mu_t [(\frac{\partial \bar{U}}{\partial y})^2 + (\frac{\partial \bar{U}}{\partial z})^2] + \rho \varepsilon$
	ε	1	$\mu + \frac{\mu_t}{\sigma_\varepsilon}$	$\mu + \frac{\mu_t}{\sigma_\varepsilon}$	$- C_1 \frac{\mu_t}{k} \varepsilon [(\frac{\partial \bar{U}}{\partial y})^2 + (\frac{\partial \bar{U}}{\partial z})^2] + C_2 \frac{\rho \varepsilon^2}{k}$

TABLE 3. CALCULATION CASES BY LY MODEL

	C_1'	REYNOLDS NO.	ITERATION NO.
1:1	0.0044	34,000	262
		75,000	321
		83,000	371
		100,000	494
		150,000	583
		215,000	732
2:1	0.00045	34,000	1070
		50,000	1486
		100,000	2070
		150,000	2193
2.5:1	0.00010	34,000	1075
		50,000	1161
		100,000	1836
3:1	0.000075	34,000	877
		56,000	901
		60,000	979
		100,000	1080
4:1	0.00005	34,000	911
		50,000	942
		100,000	1194

UNDER-RELAX FACTOR: ω :0.5, ψ :0.5, k:0.5, ε:0.5, $\bar{U}$:1.0

TABLE 4. CALCULATION CASES BY SEALE'S MODEL

	C_2'	REYNOLDS NO.	ITERATION NO.
1:1	0.006	34,000	219
		75,000	211
		83,000	208
		100,000	209
		150,000	350
		215,000	305
2:1	0.0020	34,000	317
		88,000	377
		100,000	403
		150,000	432
2.5:1	0.0012	34,000	365
		50,000	388
		100,000	390
3:1	0.00065	34,000	401
		56,000	443
		60,000	465
		100,000	497
4:1	0.00025	34,000	532
		50,000	543
		100,000	576

UNDER-RELAX FACTOR: ω :0.5, ψ :0.5, K:0.5, ε :0.5, $\bar{U}$:1.0

TABLE 5. CALCULATION CASES BY NR MODEL

	C_3'	REYNOLDS NO.	ITERATION NO.
1:1	0.01	34,000	250
		75,000	249
		83,000	243
		100,000	315
		150,000	602
		215,000	1427
2:1	0.0025	34,000	914
		50,000	1369
		100,000	1558
		150,000	1703
2.5:1	0.0012	34,000	800
		50,000	839
		100,000	902
3:1	0.0009	34,000	1401
		56,000	954
		60,000	892
		100,000	1438
4:1	0.00075	34,000	899
		50,000	966
		100,000	1441

UNDER-RELAX FACTOR: ω :0.75, ψ :0.75, k:1.0, ε :1.0, $\bar{U}$:1.0

TABLE 6. CALCULATION CASES BY k MODEL

	C_4'	REYNOLDS NO.	ITERATION NO.
1:1	0.030	34,000	286
		75,000	258
		83,000	262
		100,000	260
		150,000	397
		215,000	437
2:1	0.0085	34,000	962
		88,000	1273
		100,000	1380
		150,000	1644
2.5:1	0.0055	34,000	1001
		50,000	837
		100,000	1486
3:1	0.004	34,000	1041
		56,000	813
		60,000	886
		100,000	984
4:1	0.0015	34,000	1286
		50,000	969
		100,000	998
		150,000	1209

UNDER-RELAX FACTOR: ω :0.5, Ψ :0.5, k:0.5, ε :0.5, $\bar{U}$:1.0

TABLE 7. CALCULATION CASES BY ε MODEL

	C_5'	REYNOLDS NO.	ITERATION NO.
1:1	0.00004	34,000	428
		75,000	273
		83,000	252
		100,000	363
		150,000	327
		215,000	529
2:1	0.00001	34,000	1016
		88,000	1629
		100,000	2012
		150,000	2402
2.5:1	0.0000075	34,000	1139
		50,000	1182
		100,000	1428
3:1	0.000005	34,000	1214
		56,000	1239
		60,000	1245
		100,000	1262
4:1	0.0000045	34,000	1007
		50,000	1054
		100,000	1087

UNDER-RELAX FACTOR: ω :0.3, ψ :0.3, k:0.5, ε :0.5, $\bar{U}$:1.0

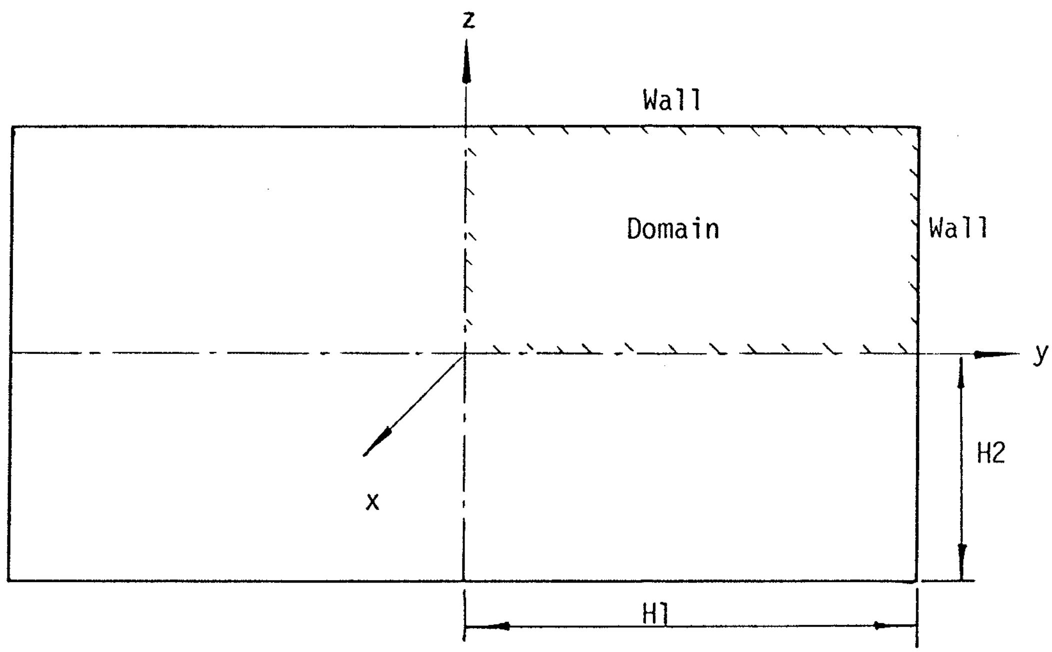

Fig.1 The domain and coordinate system considered for the analytical five models

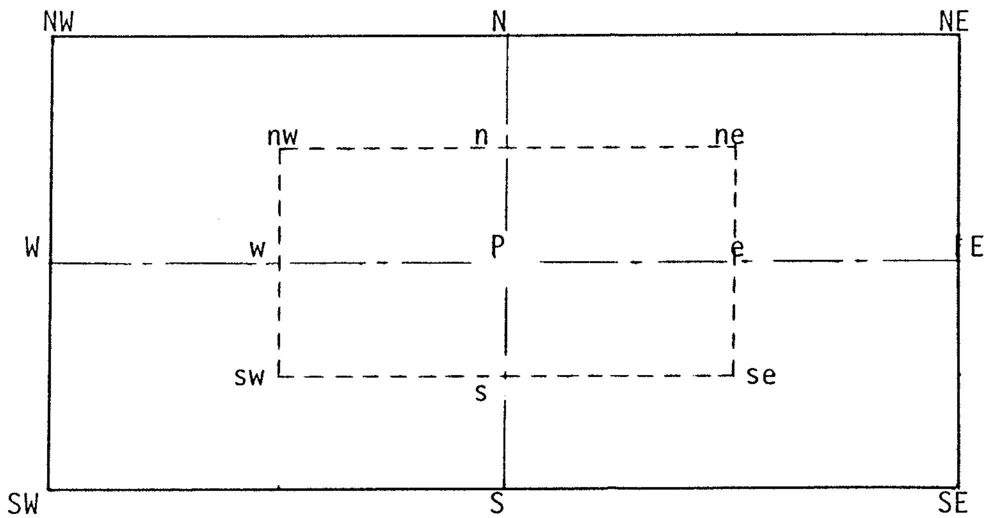

Fig.2 Portion of the finite difference Cartesian grid and the area of integration

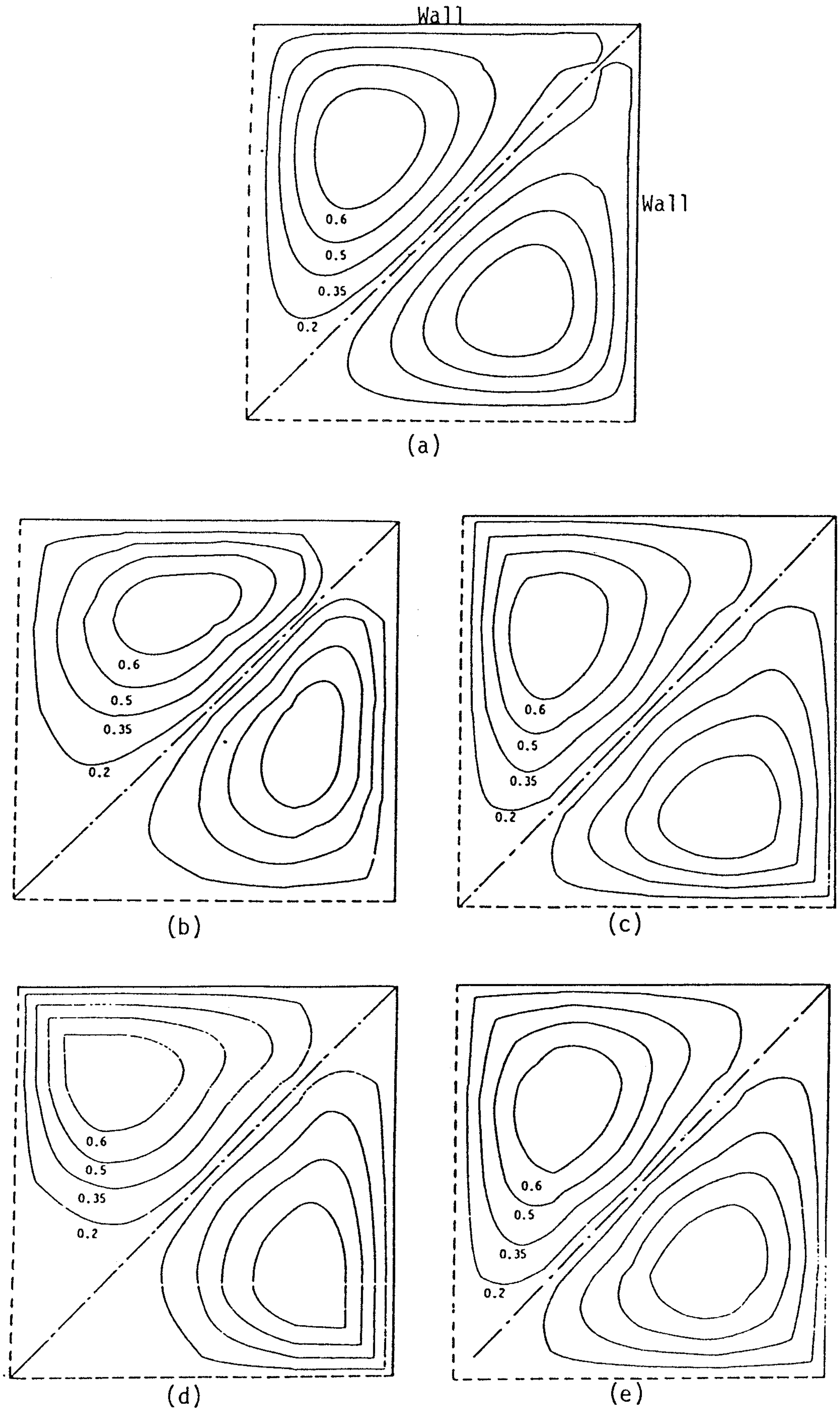

Fig.3 Predicted secondary flow streamlines $(\Psi/\rho \bar{U}_c D_h)*1000$ in square duct; Re=150,000 (a) LY (b) Seale's (c) NR (d) k (e) ε

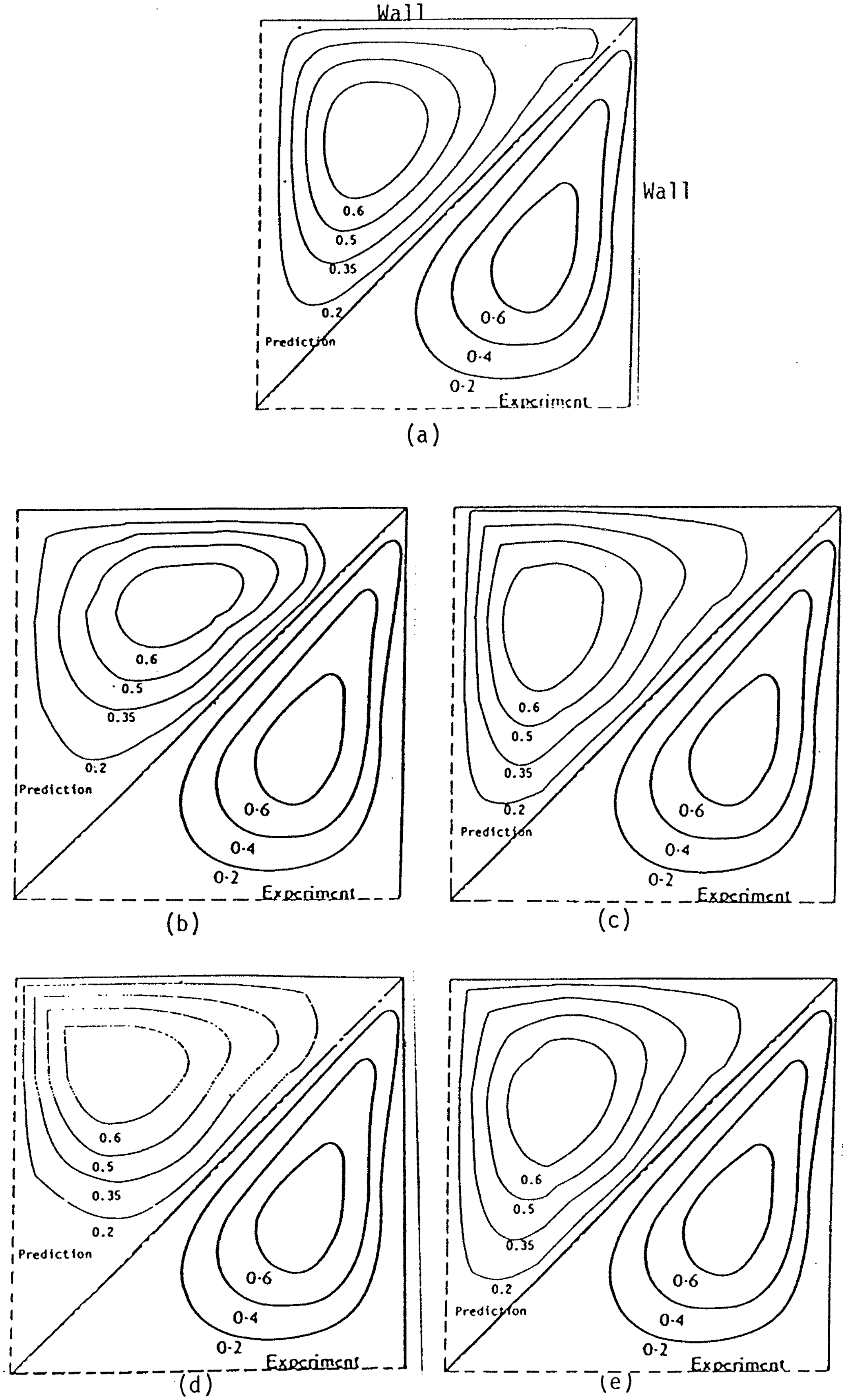

Fig.4 Comparison of the secondary flow streamlines $(\Psi/\bar{U}_c D_h \rho)$*1000 in square duct;

Re=150,000 Lower triangle: Experiment(Gessner & Jones[8])
Upper triangle: Prediction (a)LY (b)Seale's (c)NR (d)k (e) ϵ

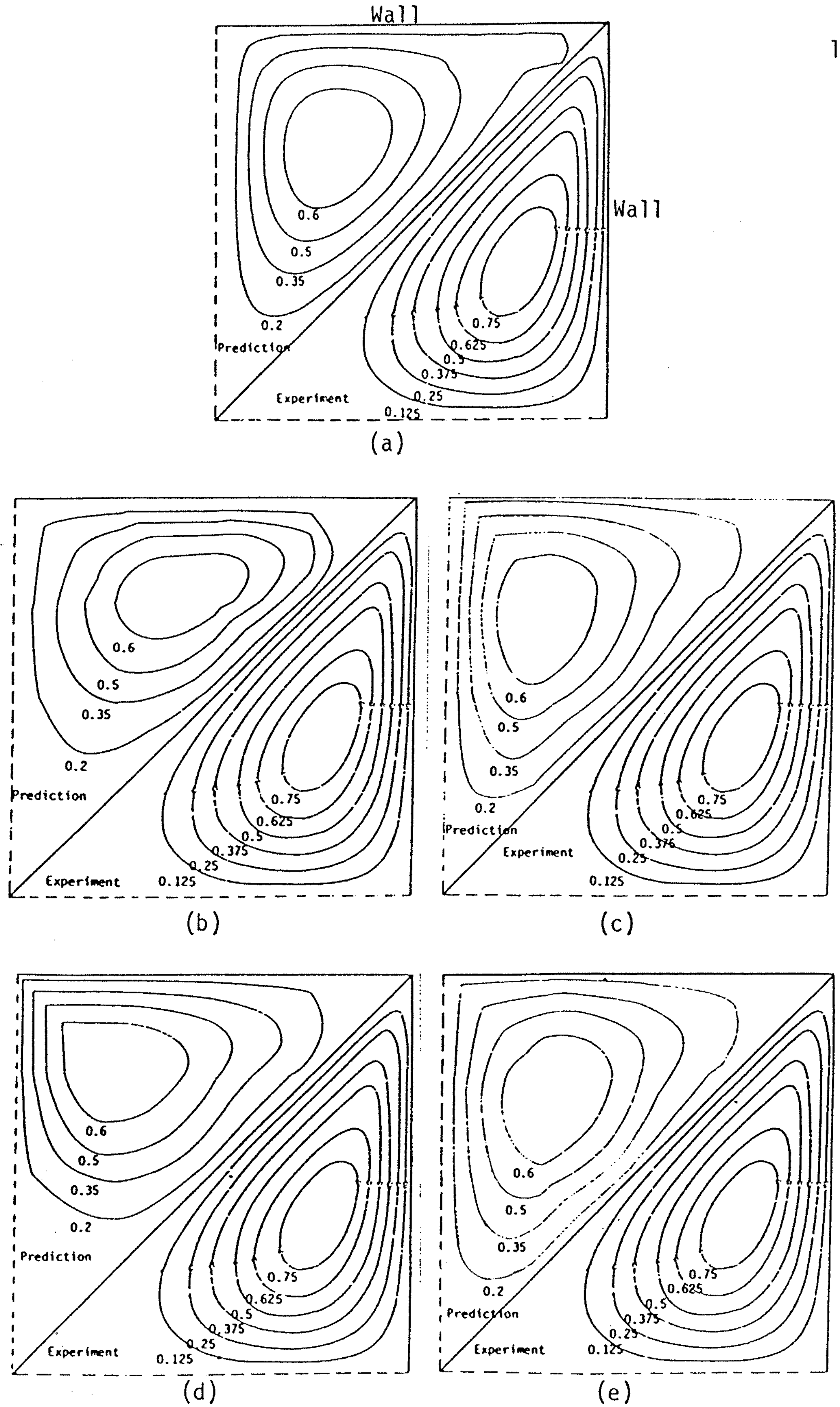

Fig.5 Comparison of the secondary flow streamlines $(\Psi/\bar{U}_c D_h \rho)*1000$ in square duct;
Re=150,000 Lower triangle: Experiment(Hoagland[5])
Upper triangle: Prediction (a)LY (b)Seale's (c)NR (d)k (e) ε

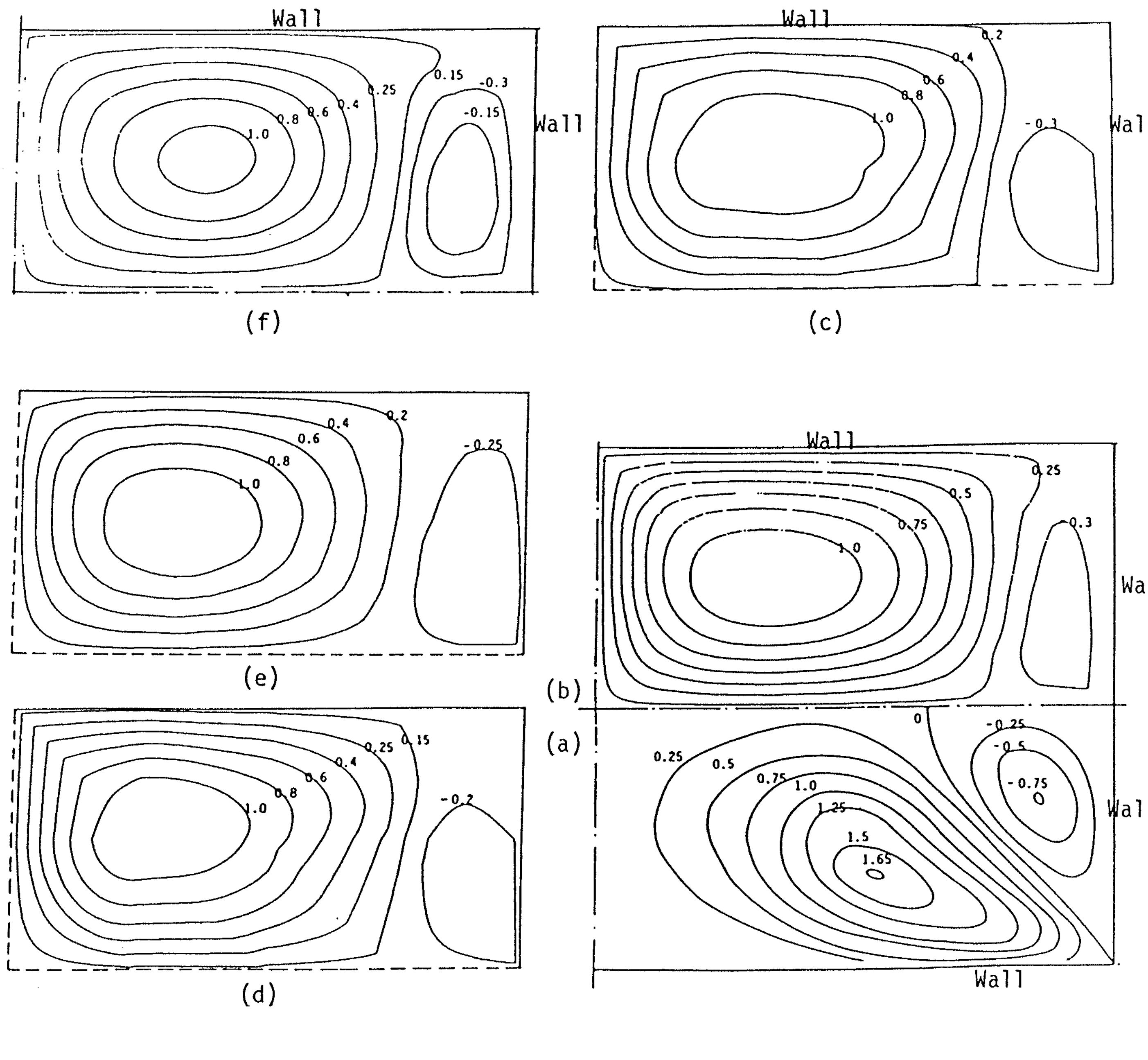

Fig.6 Comparison of secondary flow streamlines $(\Psi/\rho\bar{U}_c D_h)*1000$ in 2:1 duct;

Re=34,000 Experiment: (a) Hoagland[5]
Prediction: (b)LY (c)Seale's (d)NR (e)k (f) ϵ

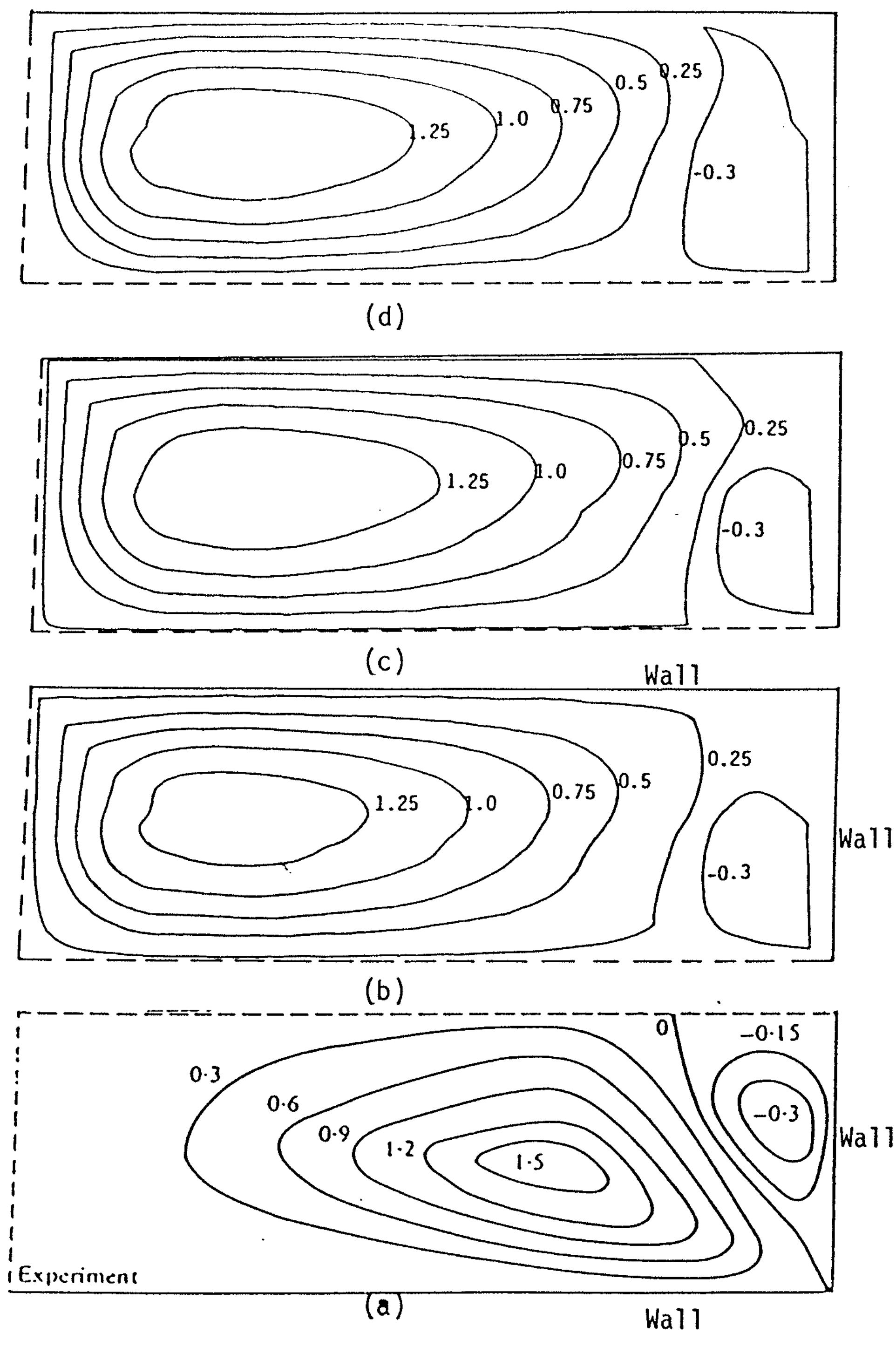

Fig.7 Comparison of secondary flow streamlines $(\Psi/\rho\bar{U}_c D_h)*1000$ in 3:1 duct;
Re=60,000 Experiment: (a) Hoagland[5]
Prediction: (b)LY (c)Seale's (d)NR

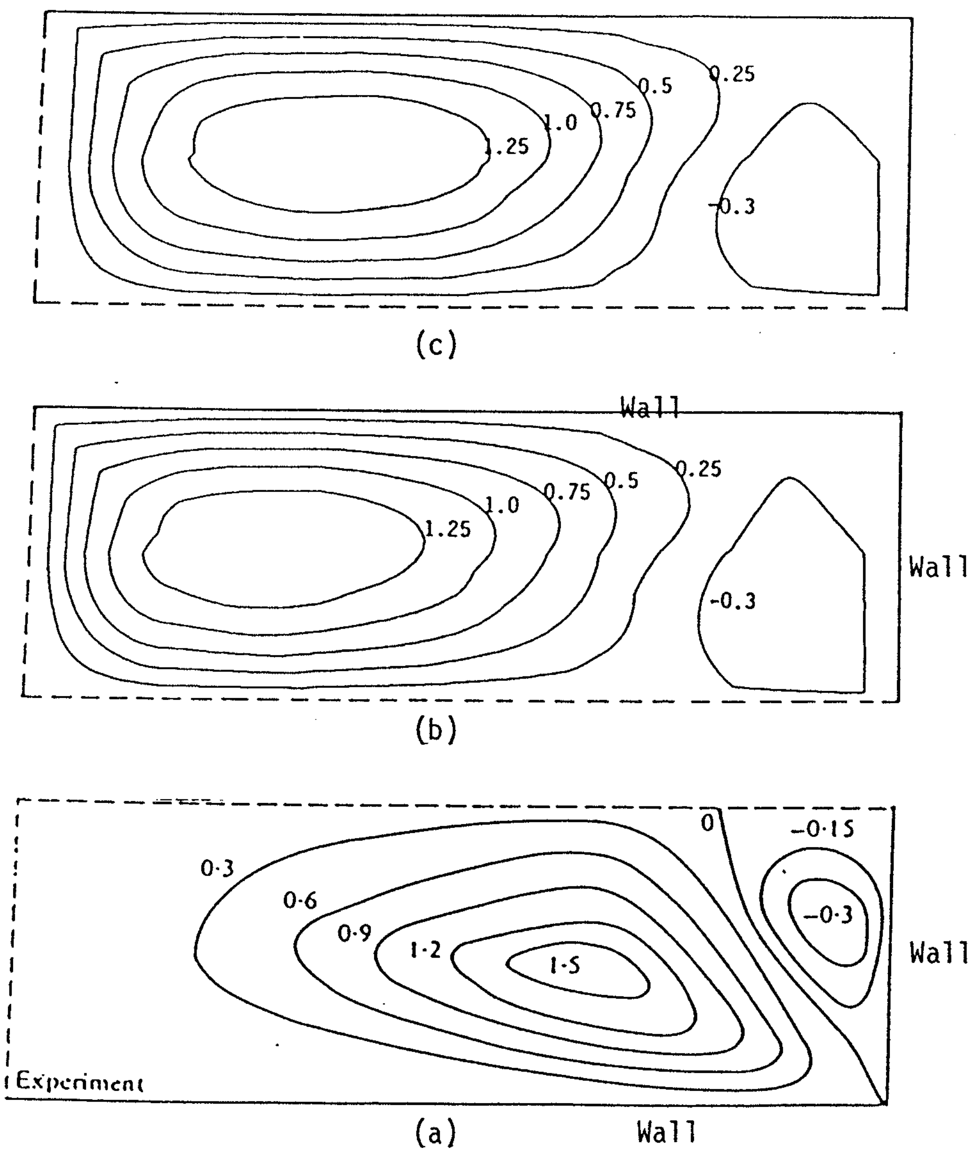

Fig.8 Comparison of secondary flow streamlines $(\Psi/\rho \bar{U}_c D_h)$*1000 in 3:1 duct;
Re=60,000 Experiment: (a) Hoagland[5]
Prediction: (b) k (c) ε

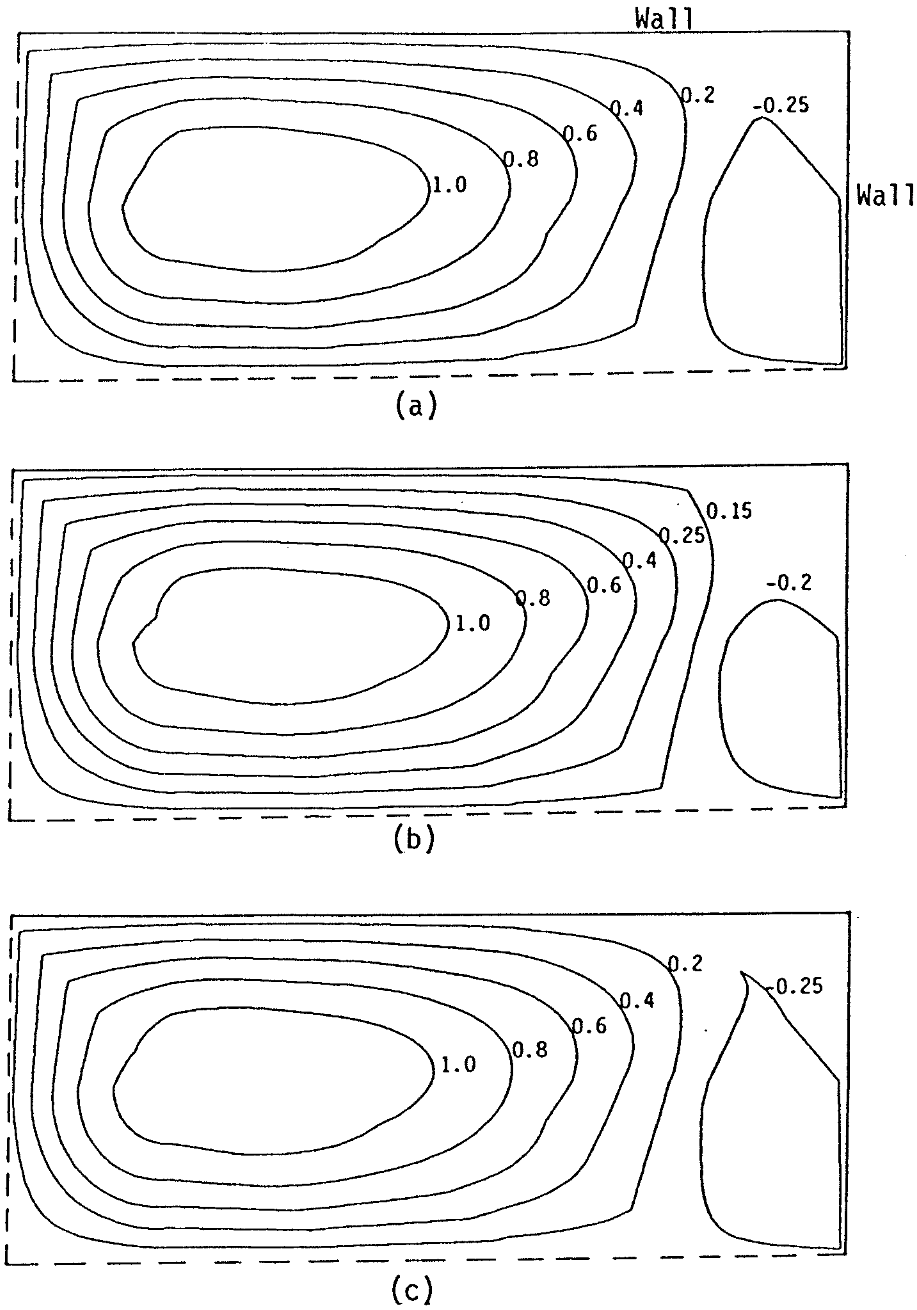

Fig.9 Predicted secondary flow streamlines $(\Psi/\rho\bar{U}_c D_h)$*1000 in 2.5:1 duct; Re=50,000 (a) LY (b) Seale's (c) NR

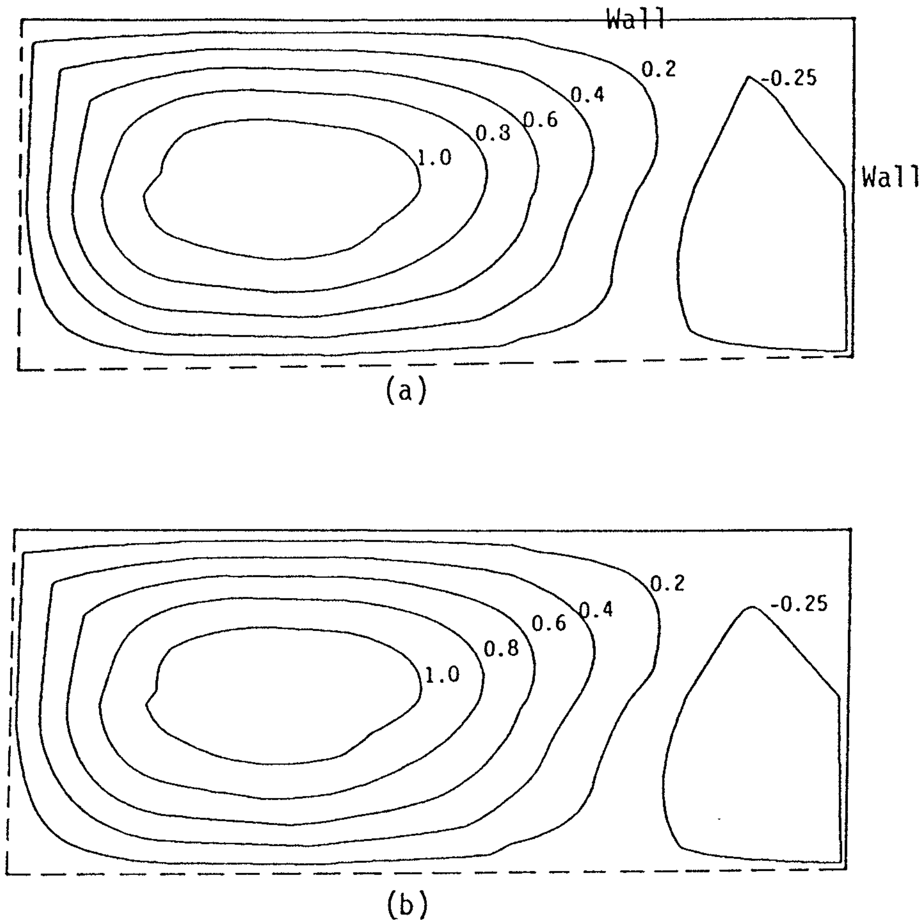

Fig.10 Predicted secondary flow streamlines $(\Psi/\rho\bar{U}_c D_h)$*1000 in 2.5:1 duct; Re=50,000 (a) k (b) ε

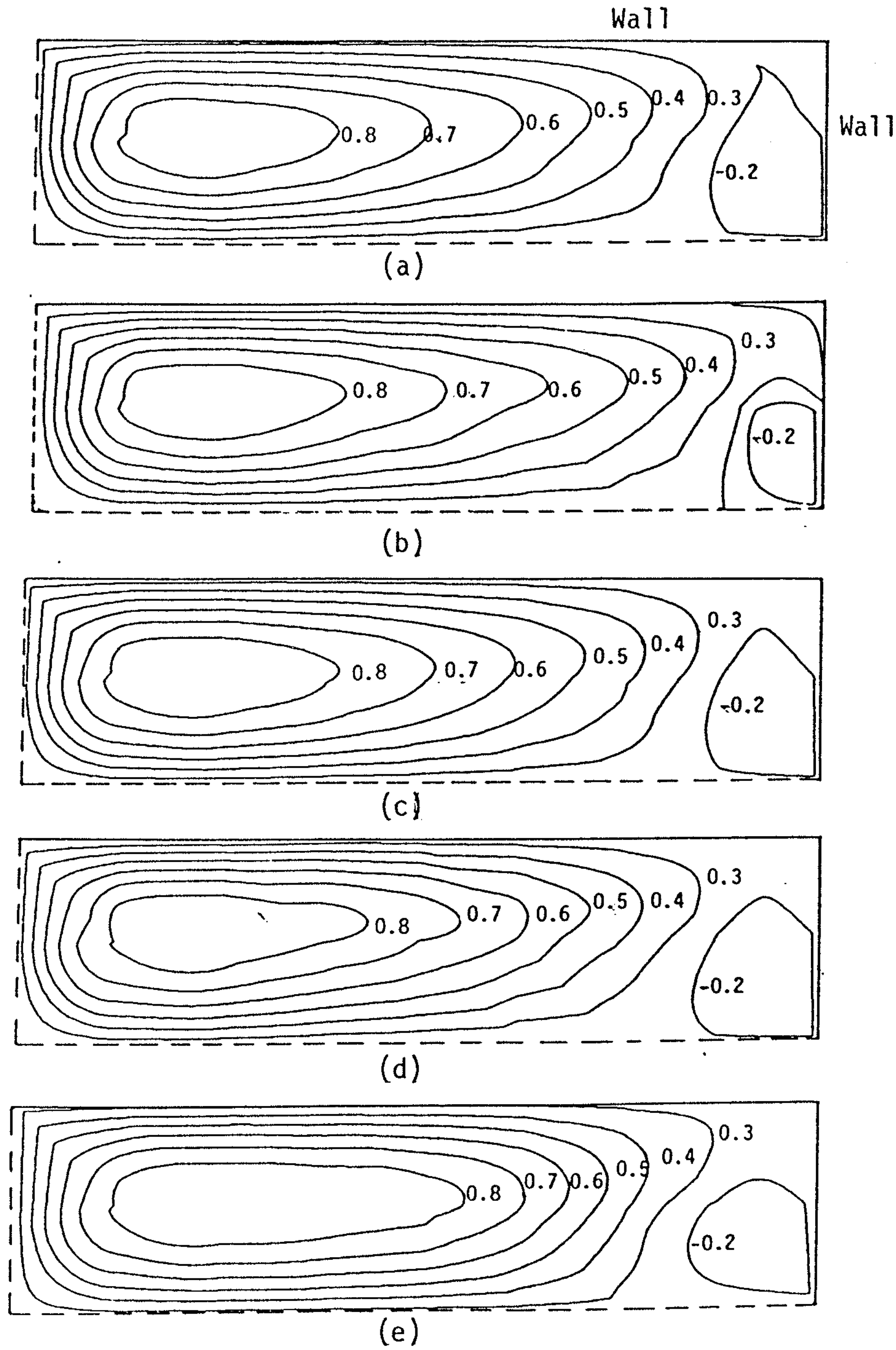

Fig.11 Predicted secondary flow streamlines $(\Psi/\rho \bar{U}_c D_h)*1000$ in 4:1 duct,
Re=50,000 (a)LY (b)Seale's (c)NR (d)k (e) ε

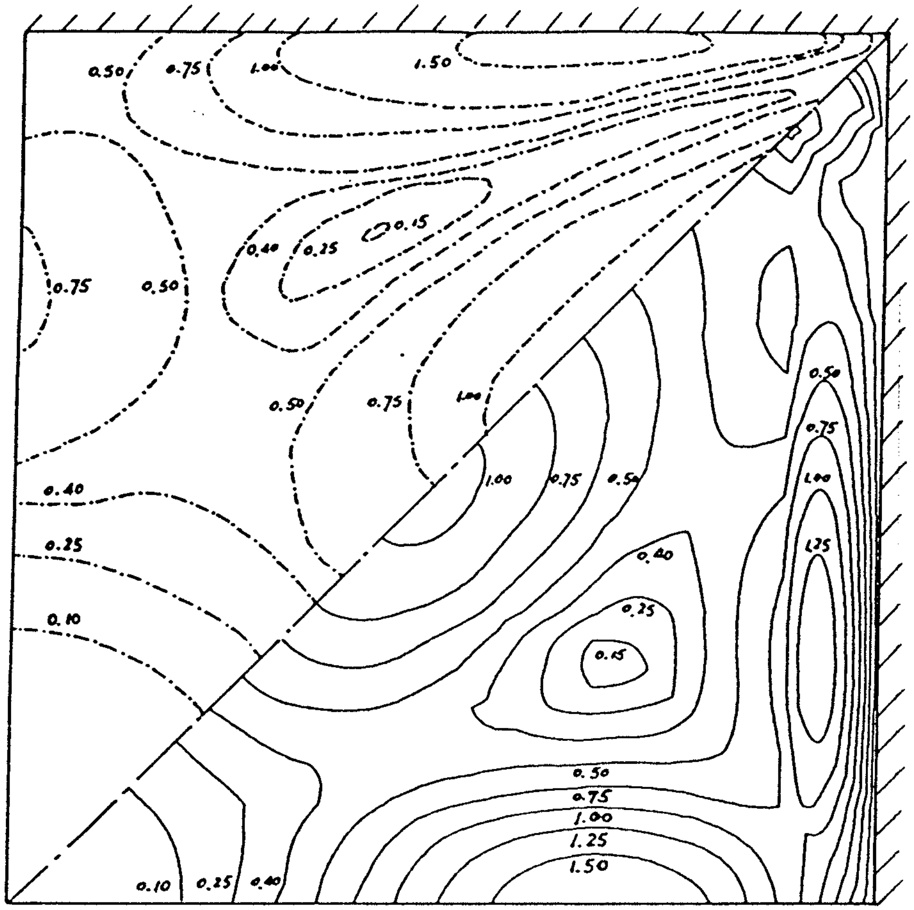

Fig.12 Comparison of resultant secondary velocity $\overline{V}sec/\overline{U}_b$ *100 in square duct:

Re=75,000. Upper triangle: Experiment(Hoagland[5])
Lower triangle: Prediction(LY)

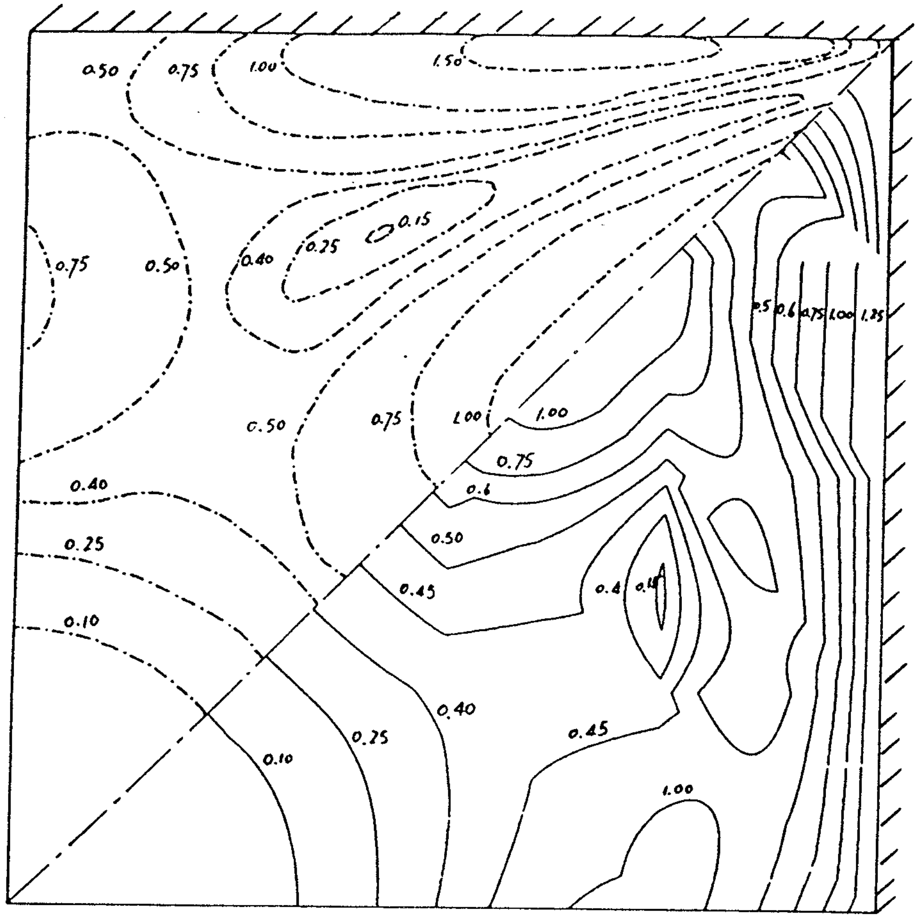

Fig.13 Comparison of resultant secondary velocity $\overline{V}sec/\overline{U}_b*100$ in square duct;
Re=75,000, Upper triangle: Experiment(Hoagland[5])
Lower triangle: Prediction(Seale's)

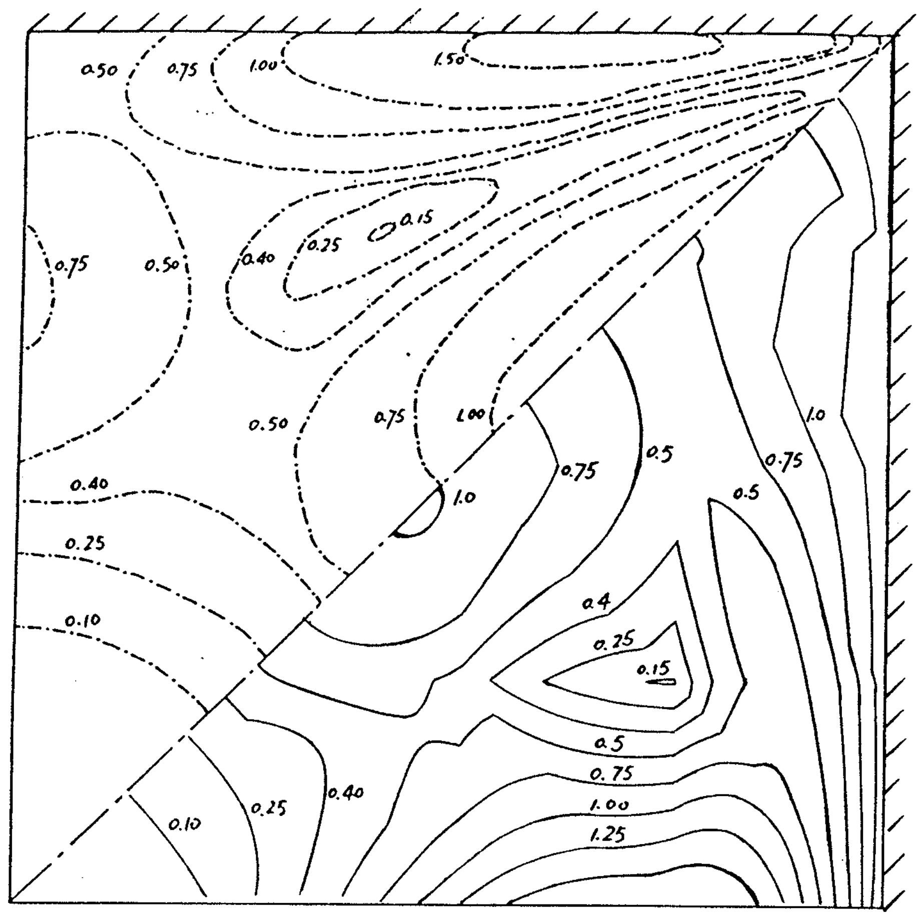

Fig.14 Comparison of resultant secondary velocity $\overline{V}sec/\overline{U}_b$*100 in square duct;
Re=75,000. Upper triangle: Experiment(Hoagland[5])
Lower triangle: Prediction(NR)

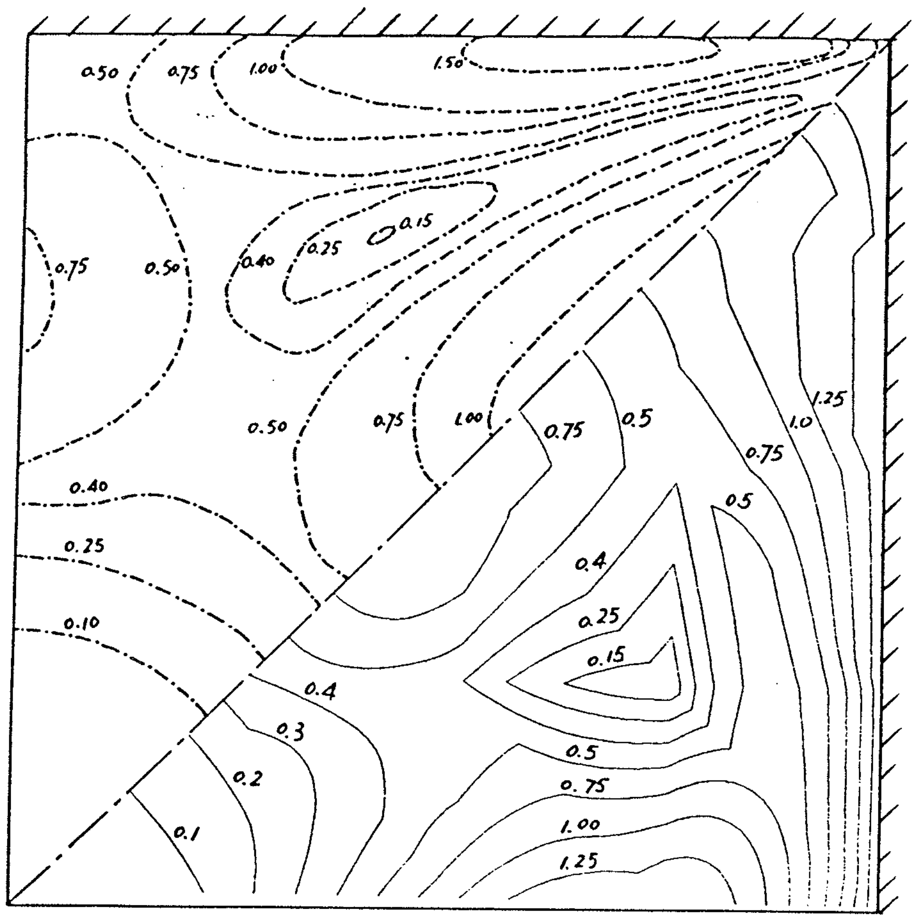

Fig.15 Comparison of resultant secondary velocity $\overline{V}sec/\overline{U}_b*100$ in square duct;

Re=75,000. Upper triangle: Experiment(Hoagland[5])
Lower triangle: Prediction(k)

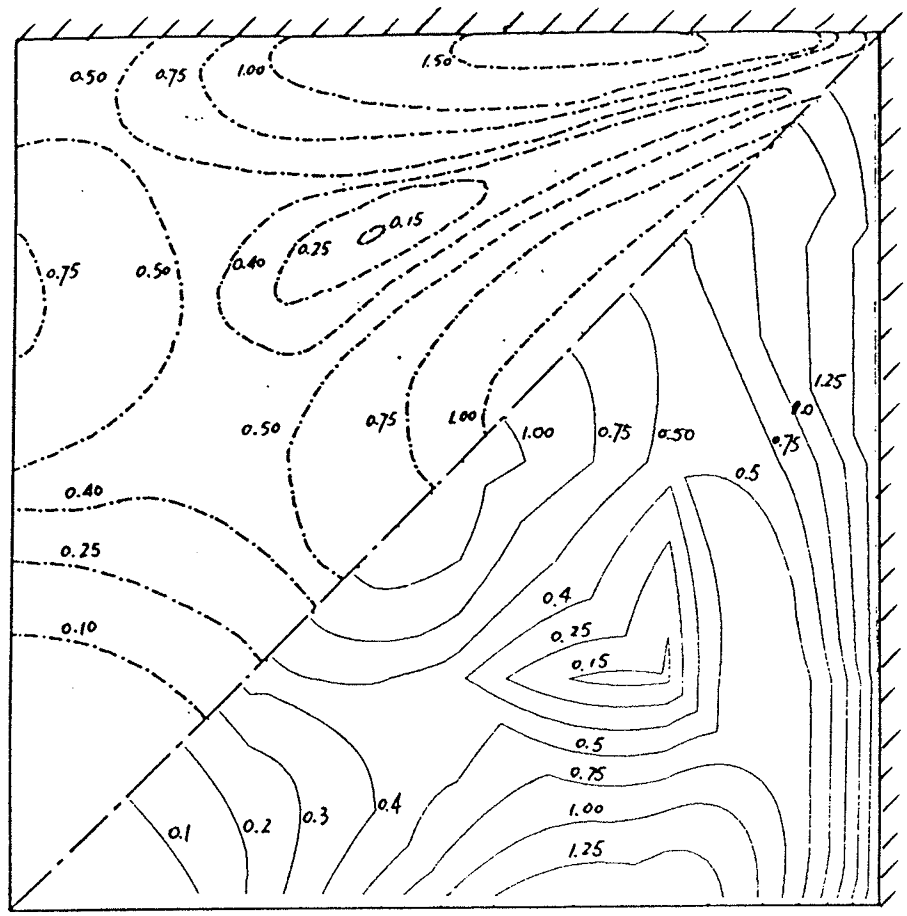

Fig.16 Comparison of resultant secondary velocity $\overline{V}sec/\overline{U}_b*100$ in square duct, Re=75,000. Upper triangle: Experiment(Hoagland[5])
Lower triangle: Prediction(ε)

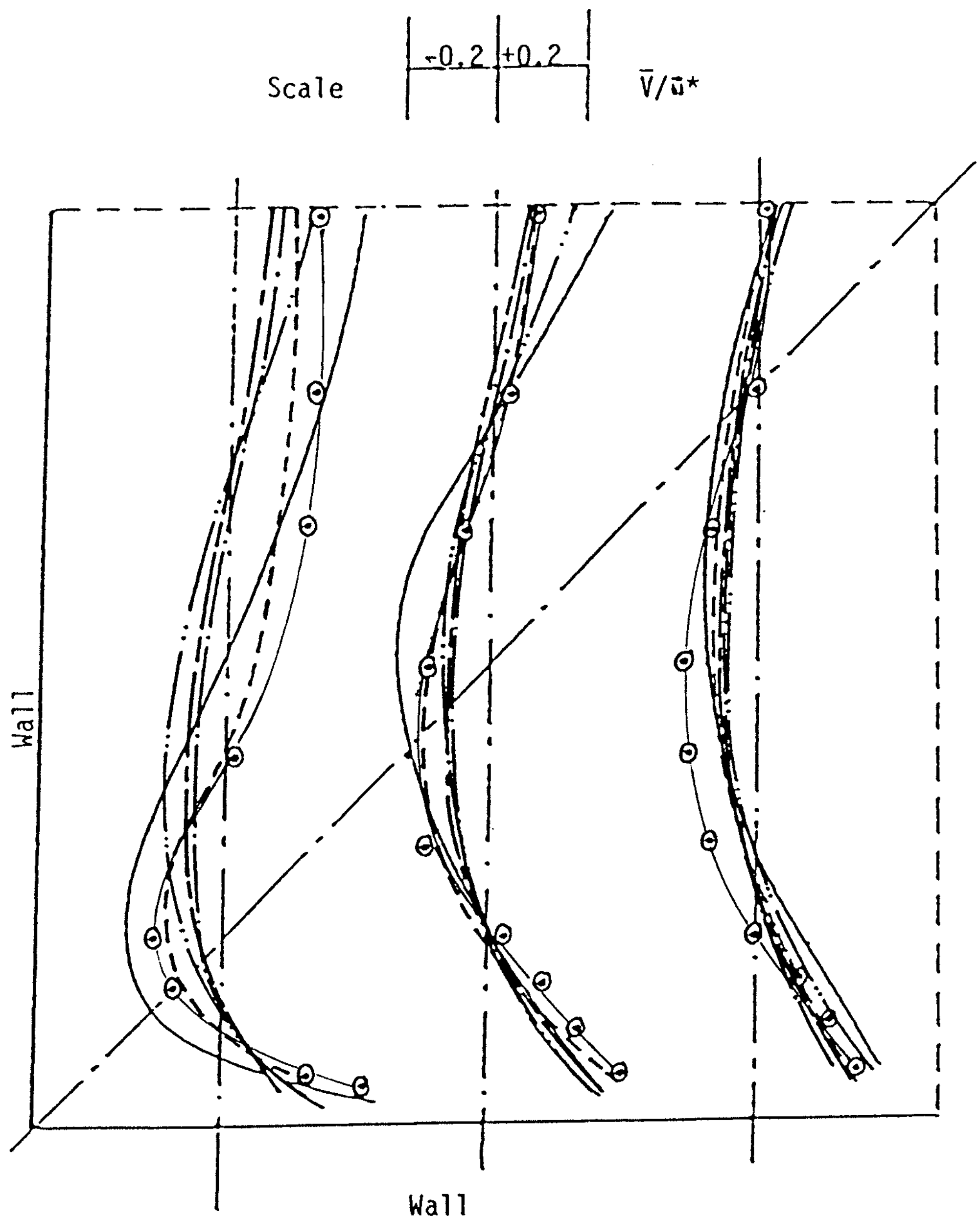

Fig.17 Comparison of secondary velocity profiles $\overline{V}/\bar{u}^*$ in square duct;

Re=215,000. Experiment: —o— by Launder & Ying[9]

Prediction: ——LY, ---- Seale's, —··— NR, —·— k, ——— ε

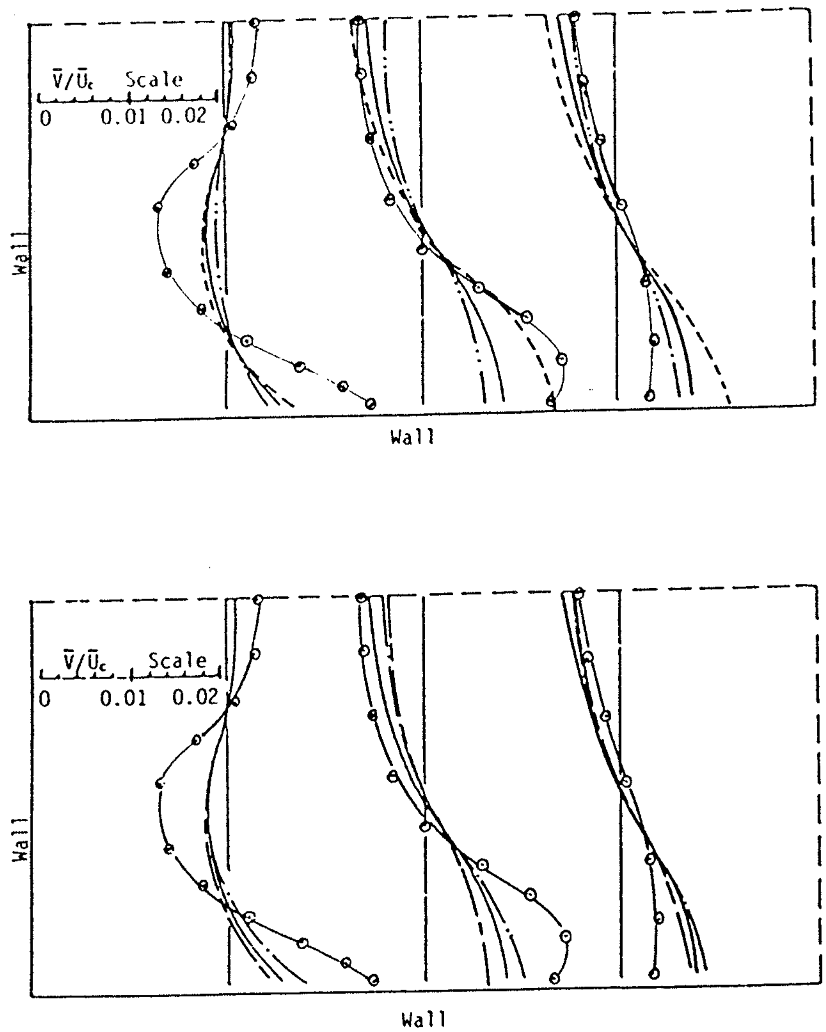

Fig.18 Comparison of secondary velocity profiles $\bar{V}/\bar{U}_c$ in 2:1 duct;
Re=300,000 Experiment: —⊙— by Gessner & Jones[8]
Re=150,000 Prediction: —— LY, - - - - Seale's, —·— NR, —··— k, ——-—— ε

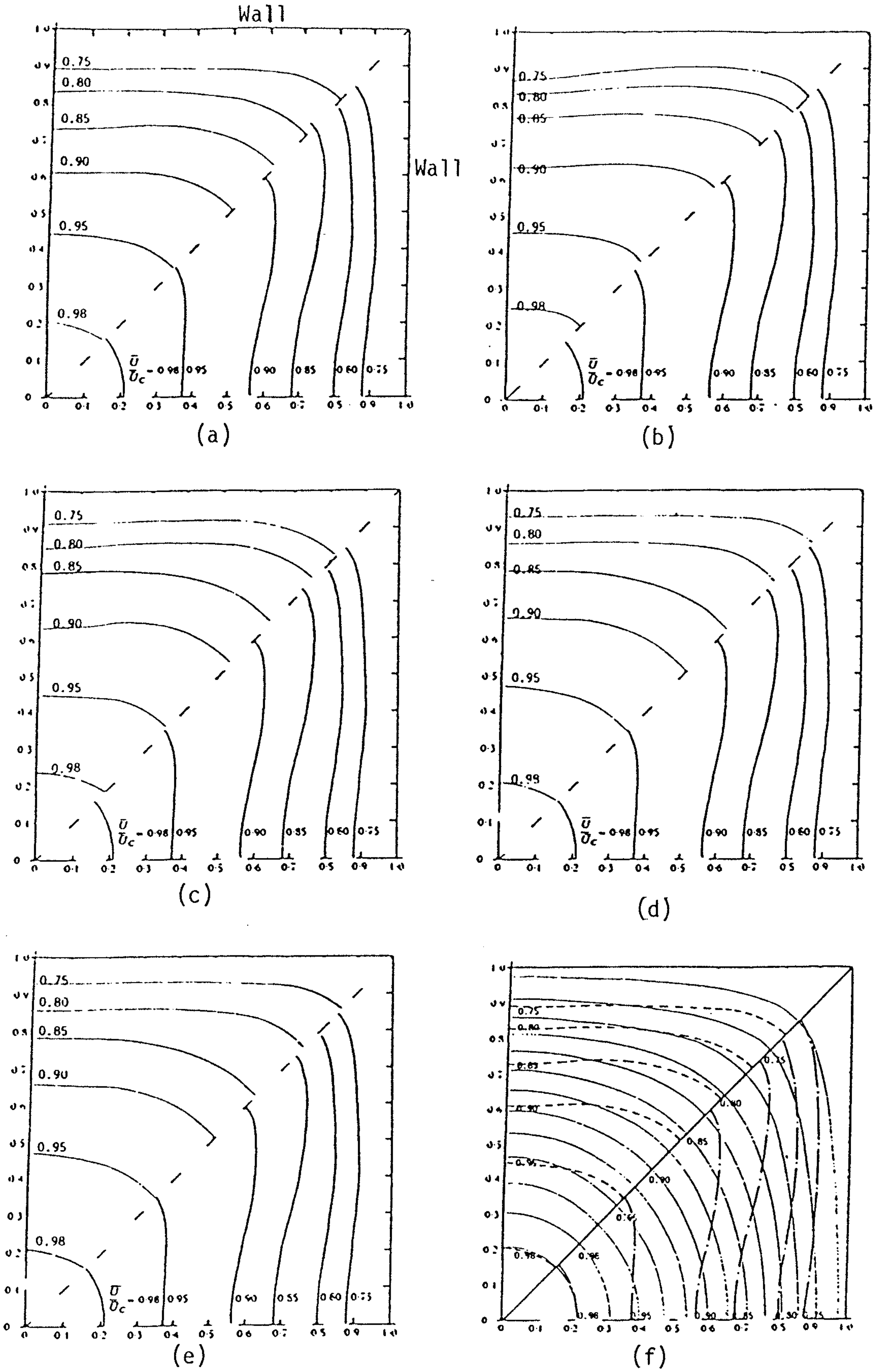

Fig.19 Comparison of isovels $\overline{U}/\overline{U}_c$ in square duct;

Re=34,000 Lower triangle: Experiment(Leutheusser[10])
Upper triangle: Prediction (a)LY,(b)Seale's,(c)NR,(d)k,(e)ε
(f)LY & $\overline{U}/\overline{U}_c$ (Vsec=0)

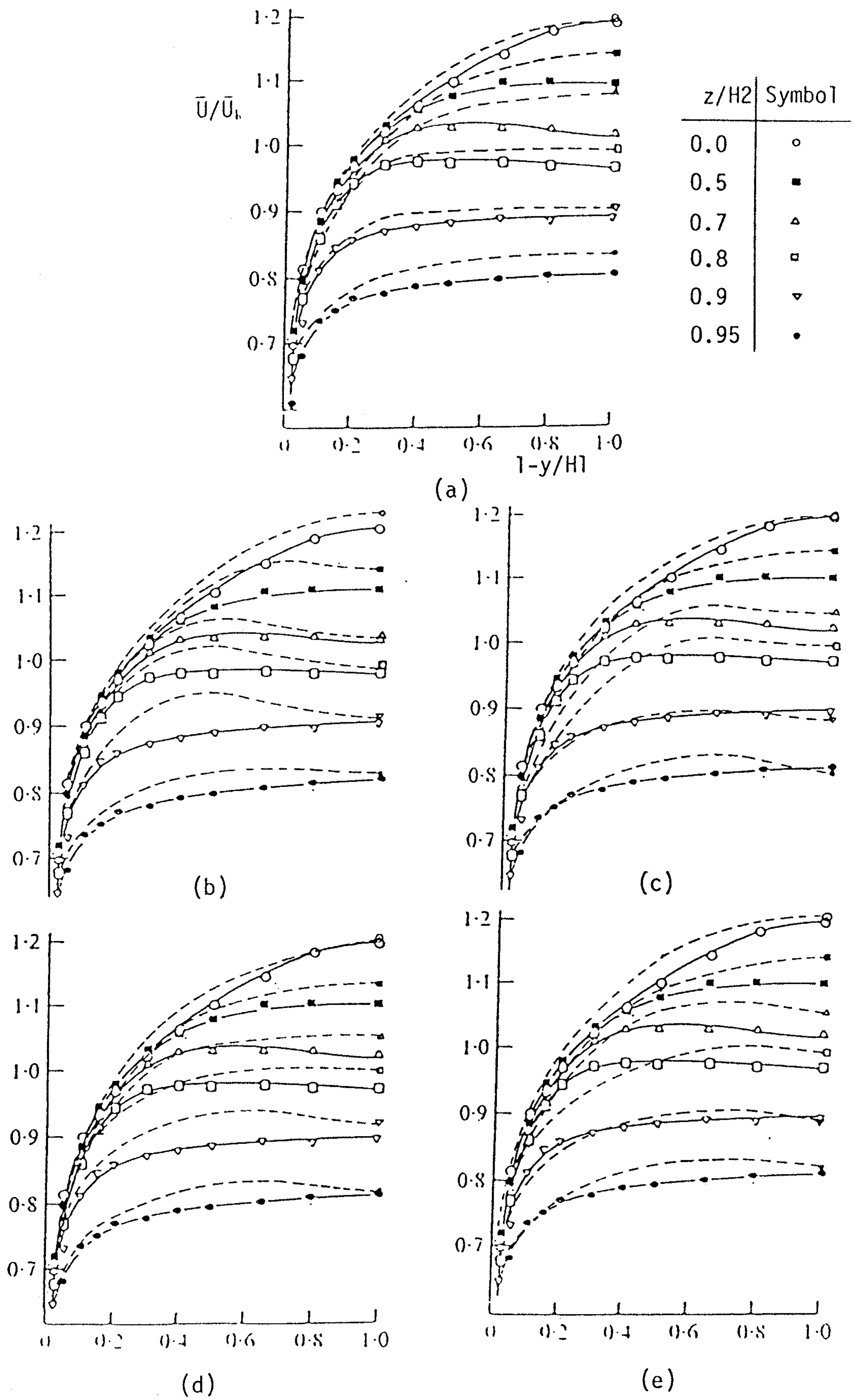

Fig.20 Comparison of axial velocity profiles $\bar{U}/\bar{U}_b$ in square duct;

Re=215,000 Experiment: ——— by Launder & Ying[9]
Prediction: - - - - (a)LY,(b)Seale's,(c)NR,(d)k,(e)ε

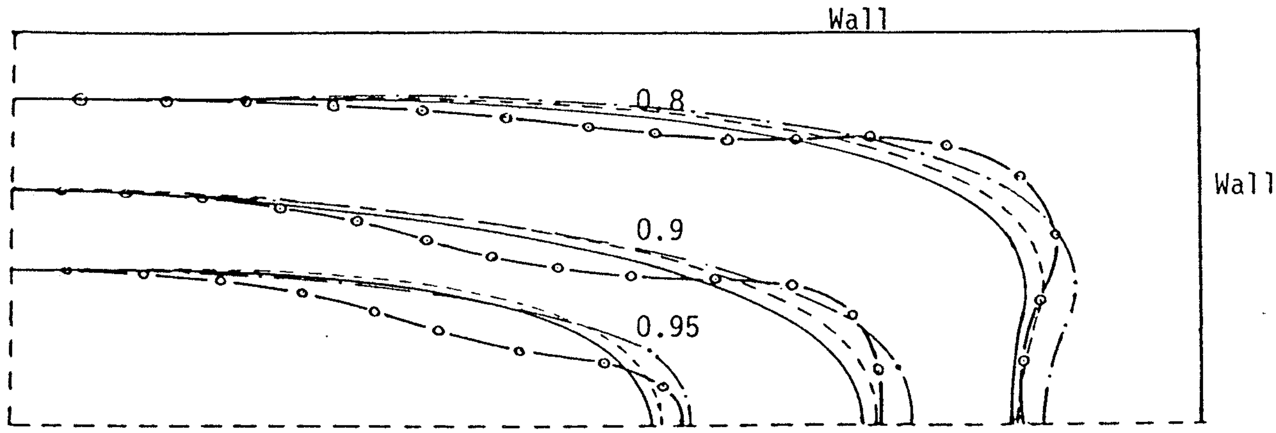

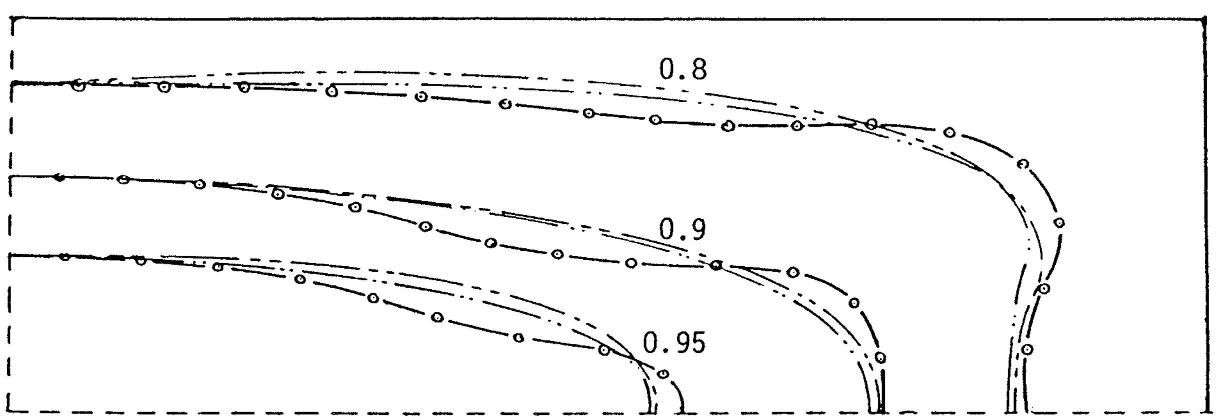

Fig.21 Comparison of axial velocity isovels $\overline{U}/\overline{U}_c$ in 3:1 duct;

Re=**56**,000. Experiment: —o— by Leutheusser[10]
Prediction: —— LY, ----Seale's, —·—NR, ——---k, ——··—— ε

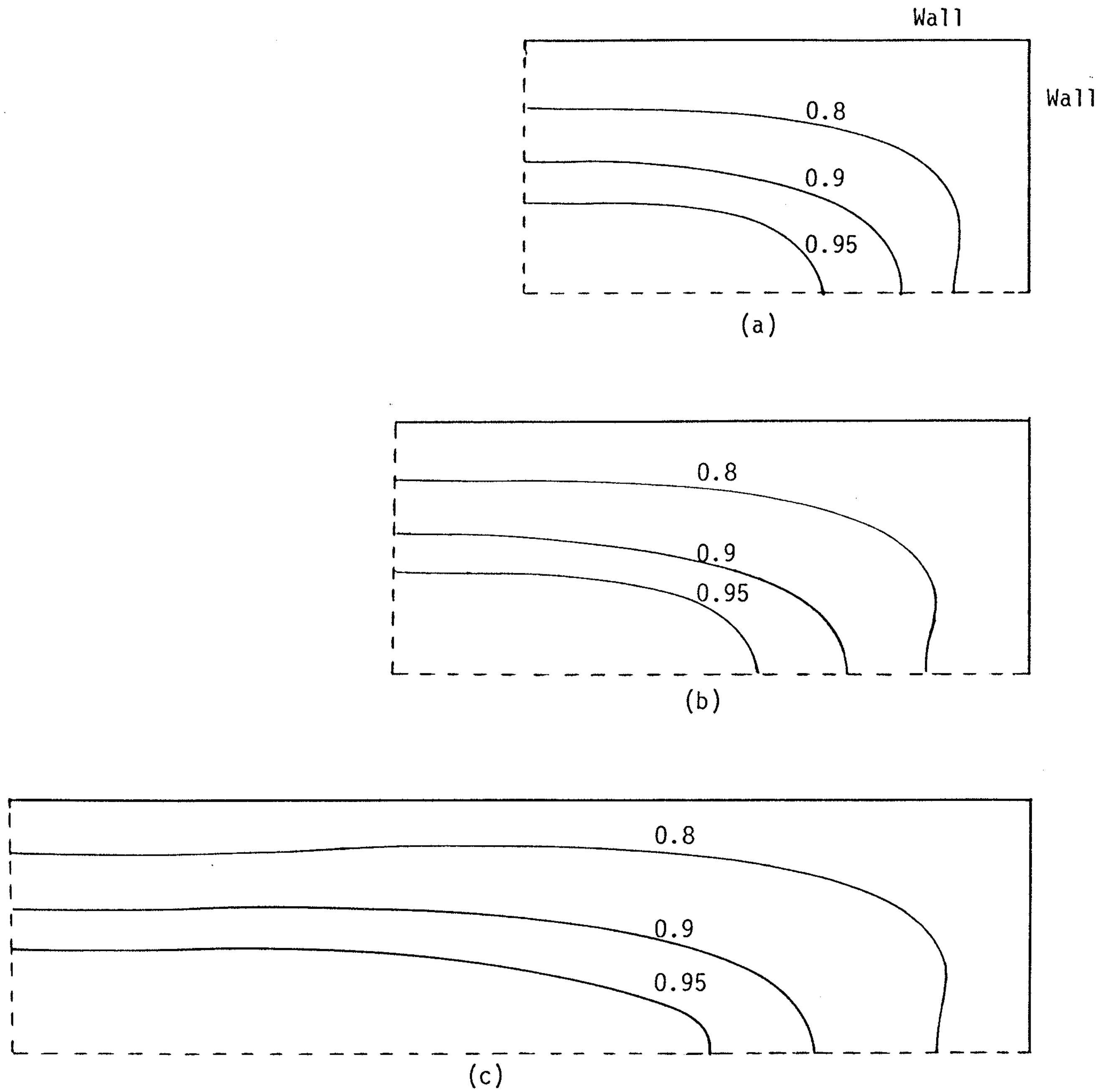

Fig.21-A Predicted axial velocity isovels $\bar{U}/\bar{U}_c$ by LY; Re=100,000. (a) 2:1, (b) 2.5:1, (c) 4:1

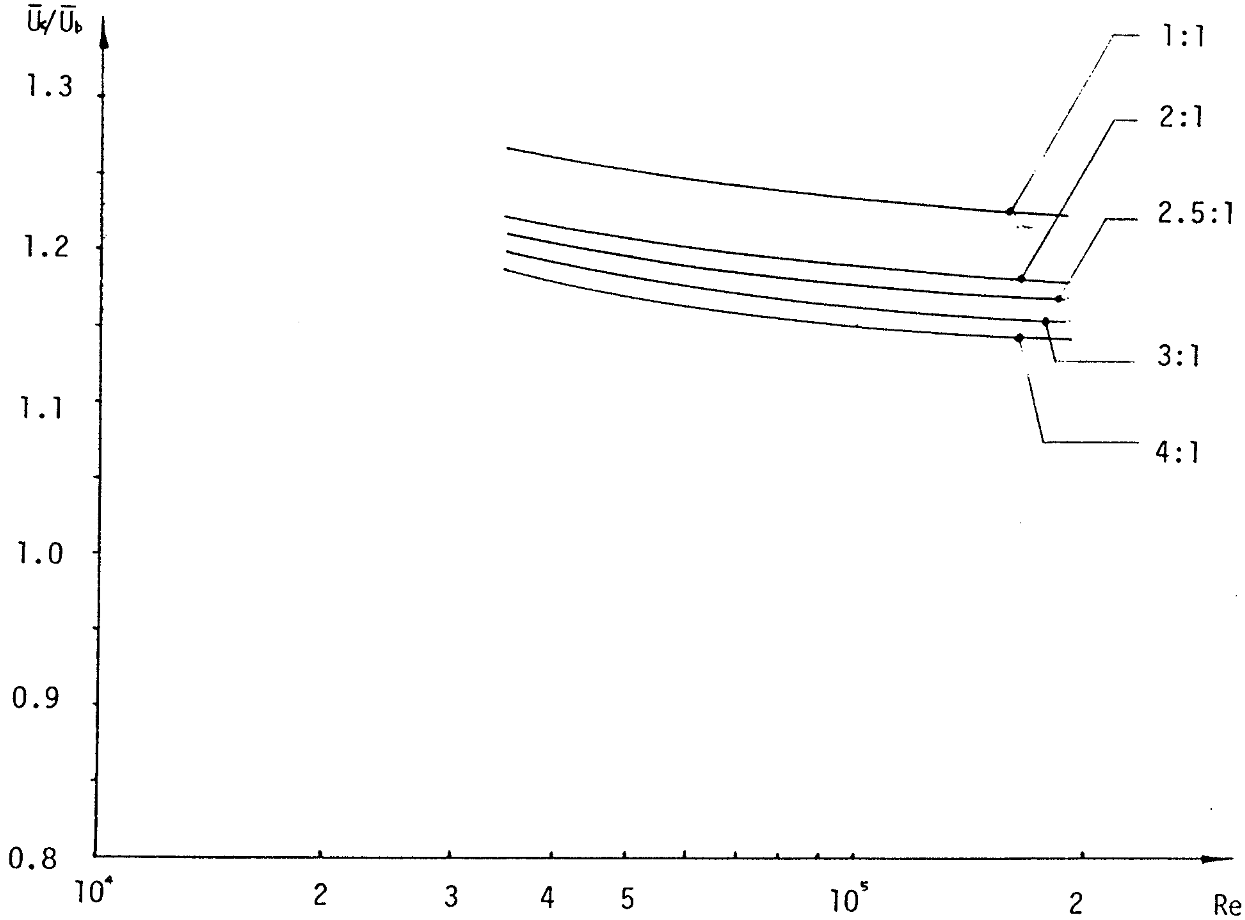

Fig. 21-B Predicted axial velocity $\bar{U}_c/\bar{U}_b$ by LY

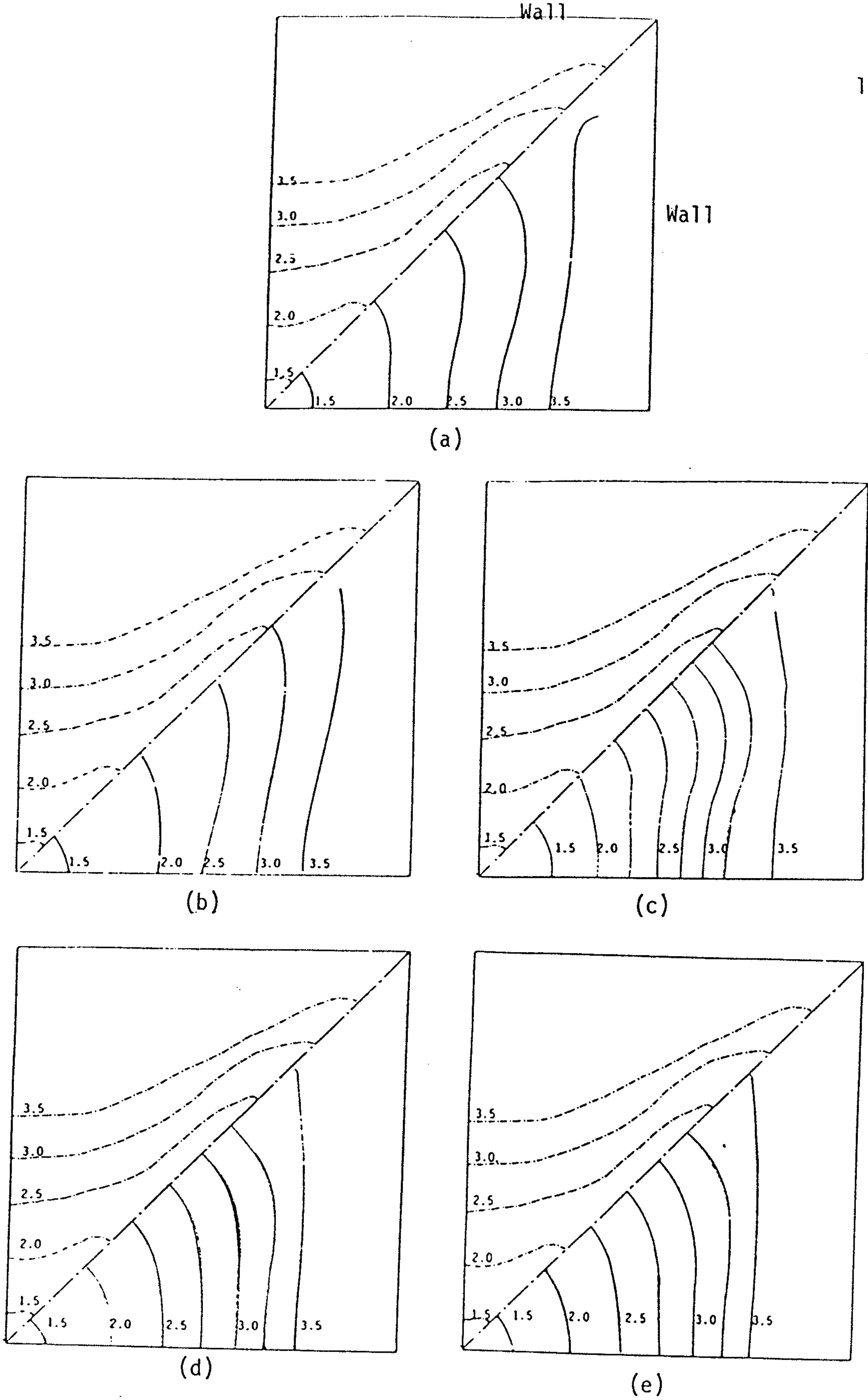

Fig.22 Comparison of k^+ contours in square duct;

Re=83,000. Upper triangle: Experiment(Brundrett & Baines[6])

Lower triangle: Prediction (a)LY,(b)Seale's,(c)NR,(d)k,(e)ε

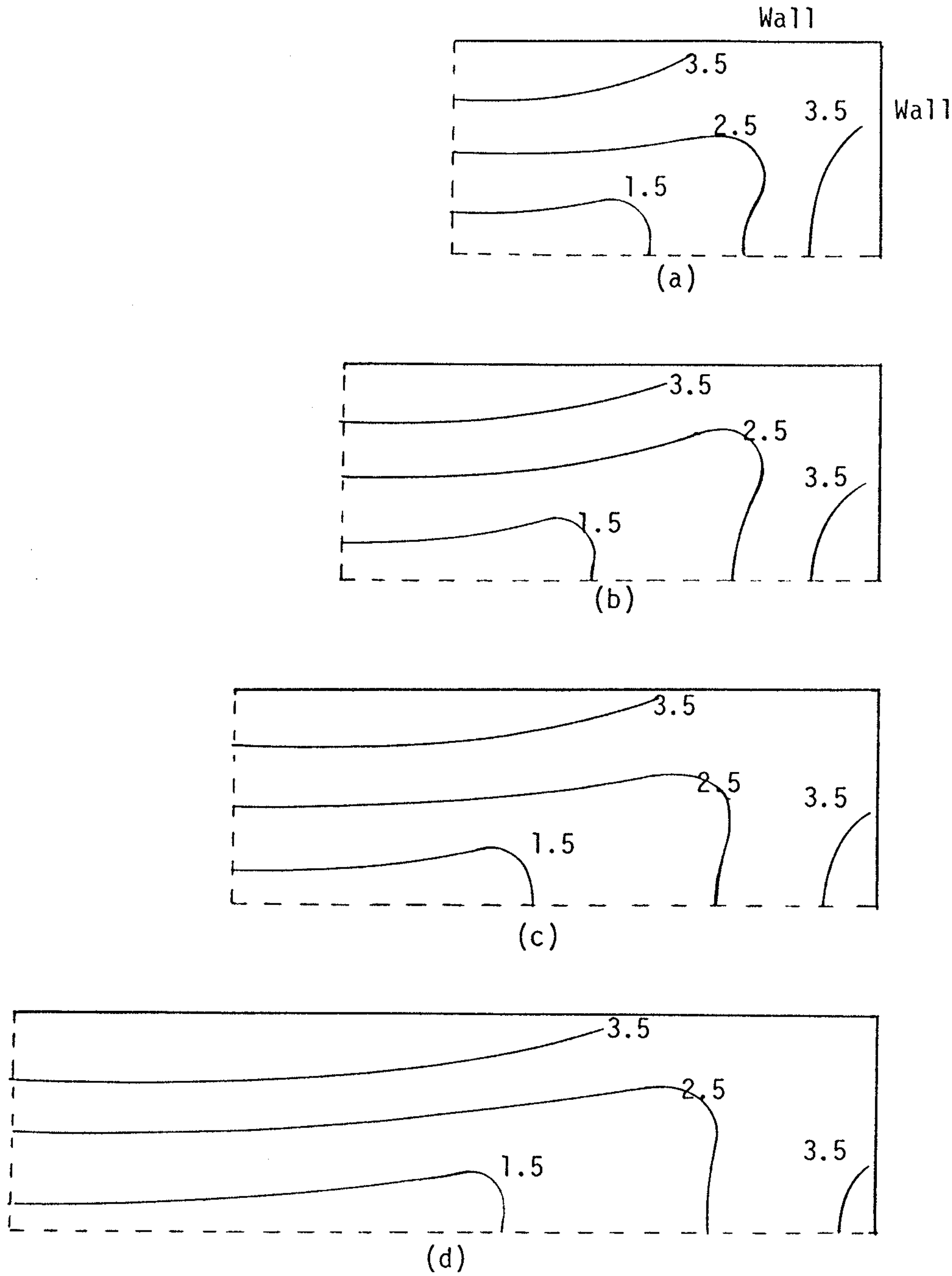

Fig. 22-A Predicted k^+ contours by LY;
Re=100,000 (a) 2:1, (b) 2.5:1, (c) 3:1, (d) 4:1

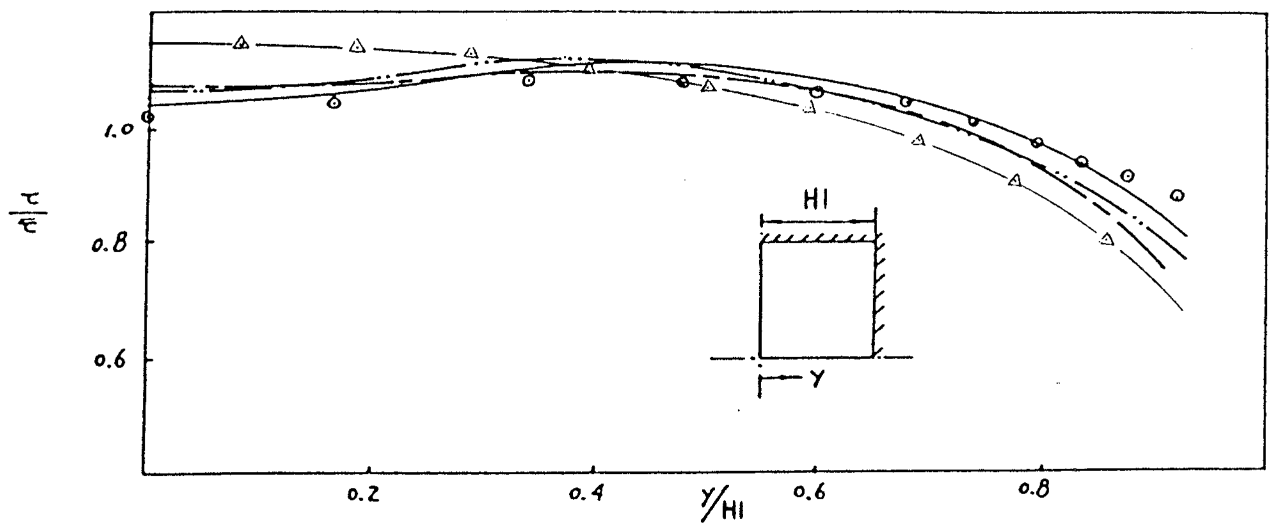

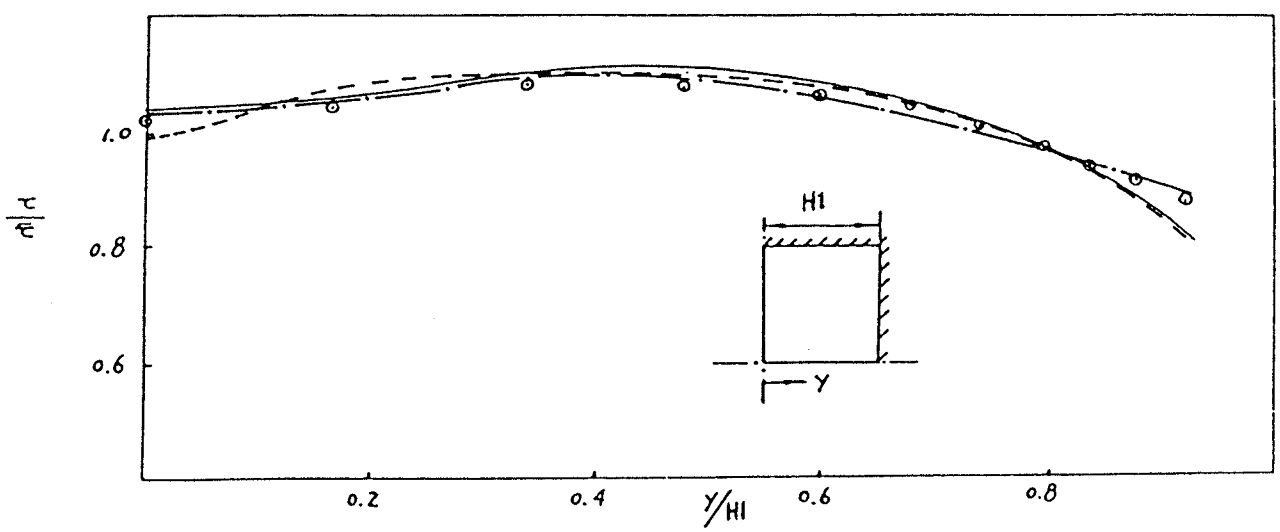

Fig.23 Comparison of wall shear stress distribution $\frac{\tau}{\bar{\tau}}$ in square duct;

Re=34,000. Experiment: ⊙ by Leutheusser[10]
Prediction: —— LY, ---- Seale's, —·—NR, —··— k, —— — —— ε

—△— Wall shear stress without secondary flow

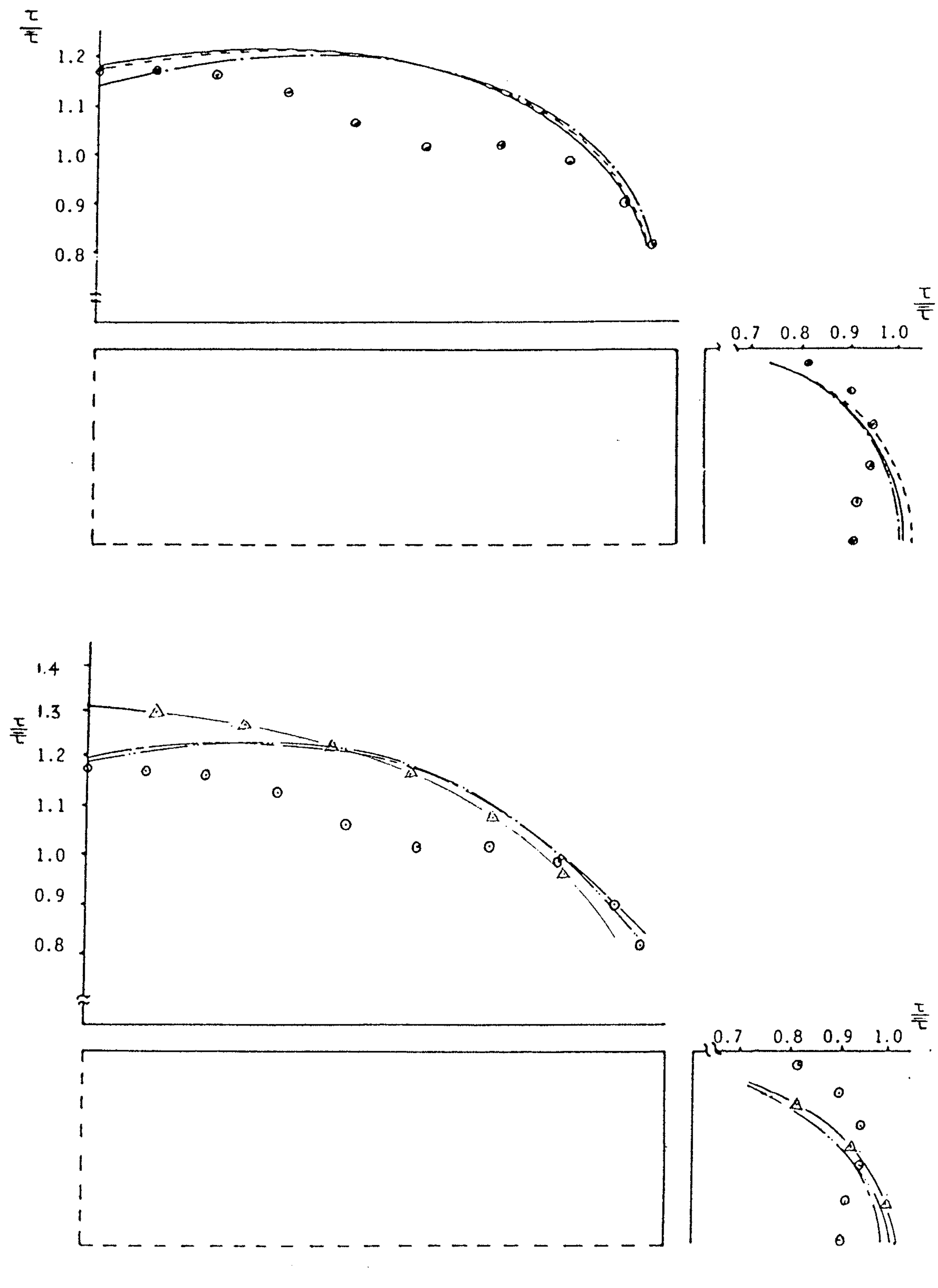

Fig.24 Comparison of wall shear stress distribution $\frac{\tau}{\bar{\tau}}$ in 3:1 duct;

Re=56,000. Experiment: ⊙ by Leutheusser[10]

Prediction: —— LY, ---- Seale's, —·—NR, —··—k, ——-—— ε

—△— Wall shear stress without secondary flow

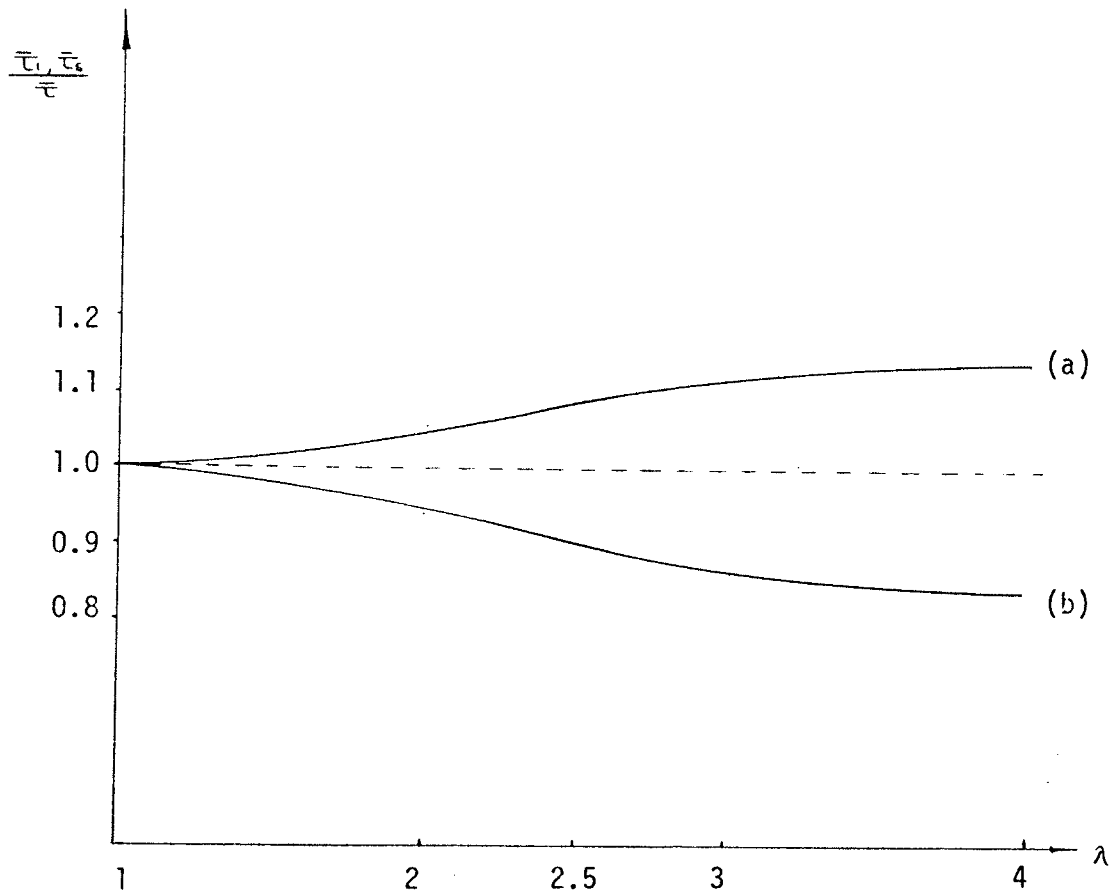

Fig.24-A Predicted average wall shear stress ratio by LY;
(a) $\bar{\tau}_l/\bar{\tau}$, (b) $\bar{\tau}_s/\bar{\tau}$

$\bar{\tau}_l$:Average wall shear stress of long wall
$\bar{\tau}_s$:Average wall shear stress of short wall

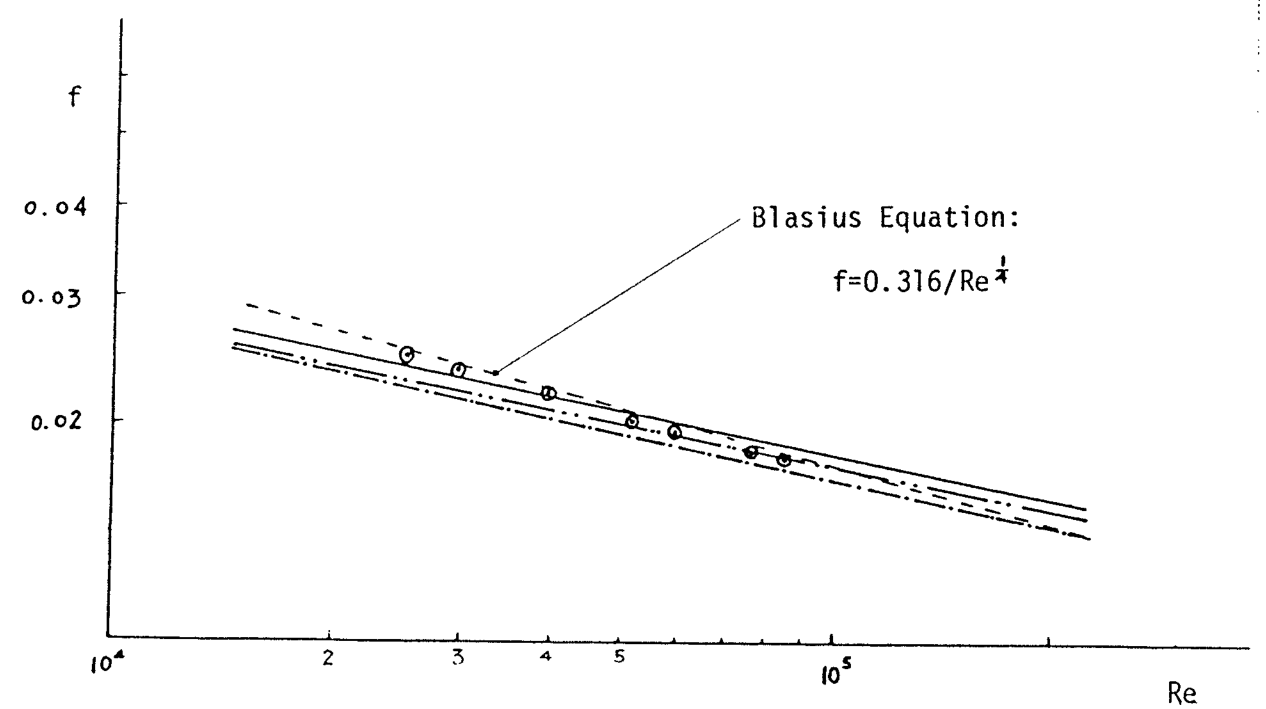

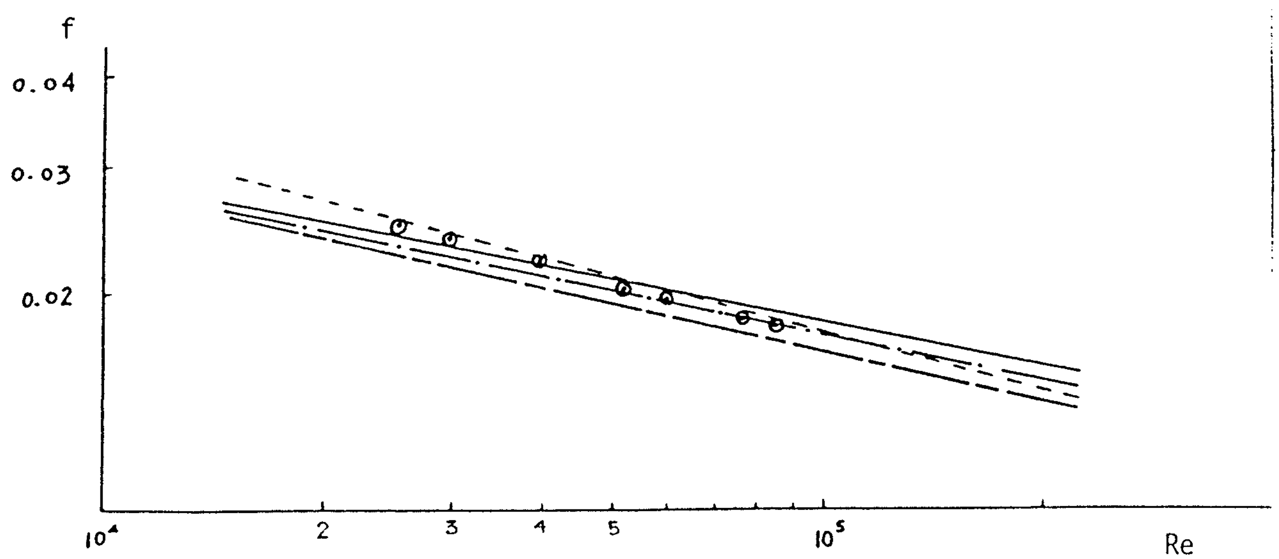

Fig.25 Comparison of friction factor f for square duct;

Experiment: ⊙ by Leutheusser[10], ---- Blasius Equation
Prediction: —— LY, —·— Seale's, —··— NR, ---- k, -·-·-· ε

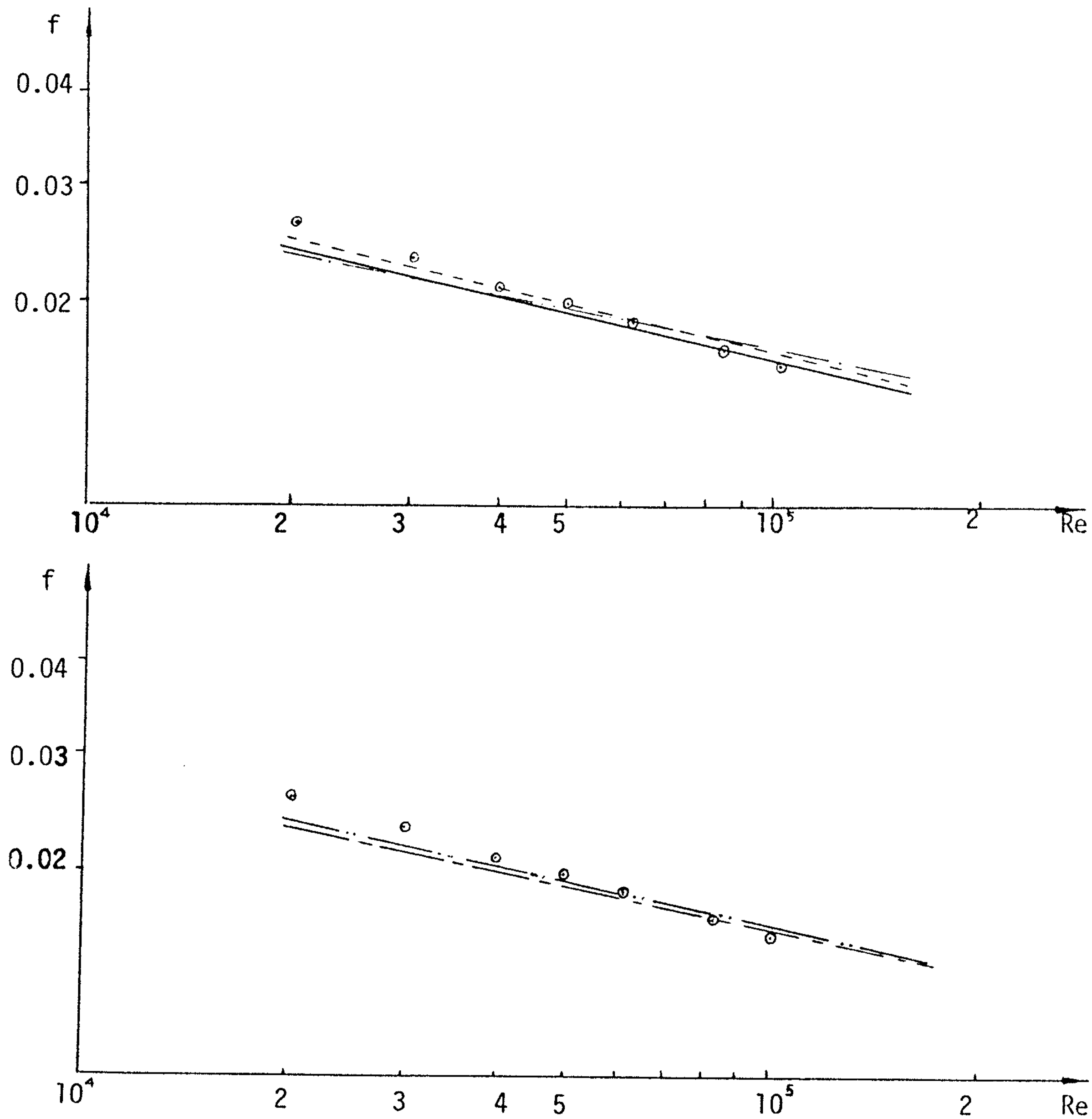

Fig.26 Comparison of friction factor f for 3:1 duct;

Experiment: ⊙ by Leutheusser[10]

Prediction: ——— LY, - - - - Seale's, — —— NR, —— · —k, ——— - —— ε

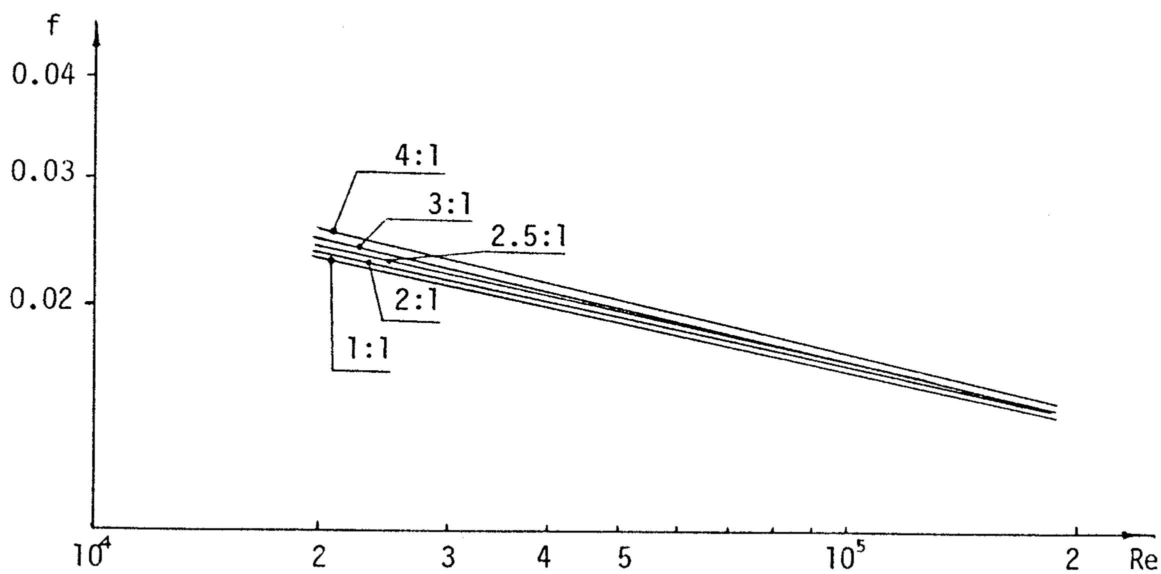

Fig.26-A Predicted friction factor by Seale's model

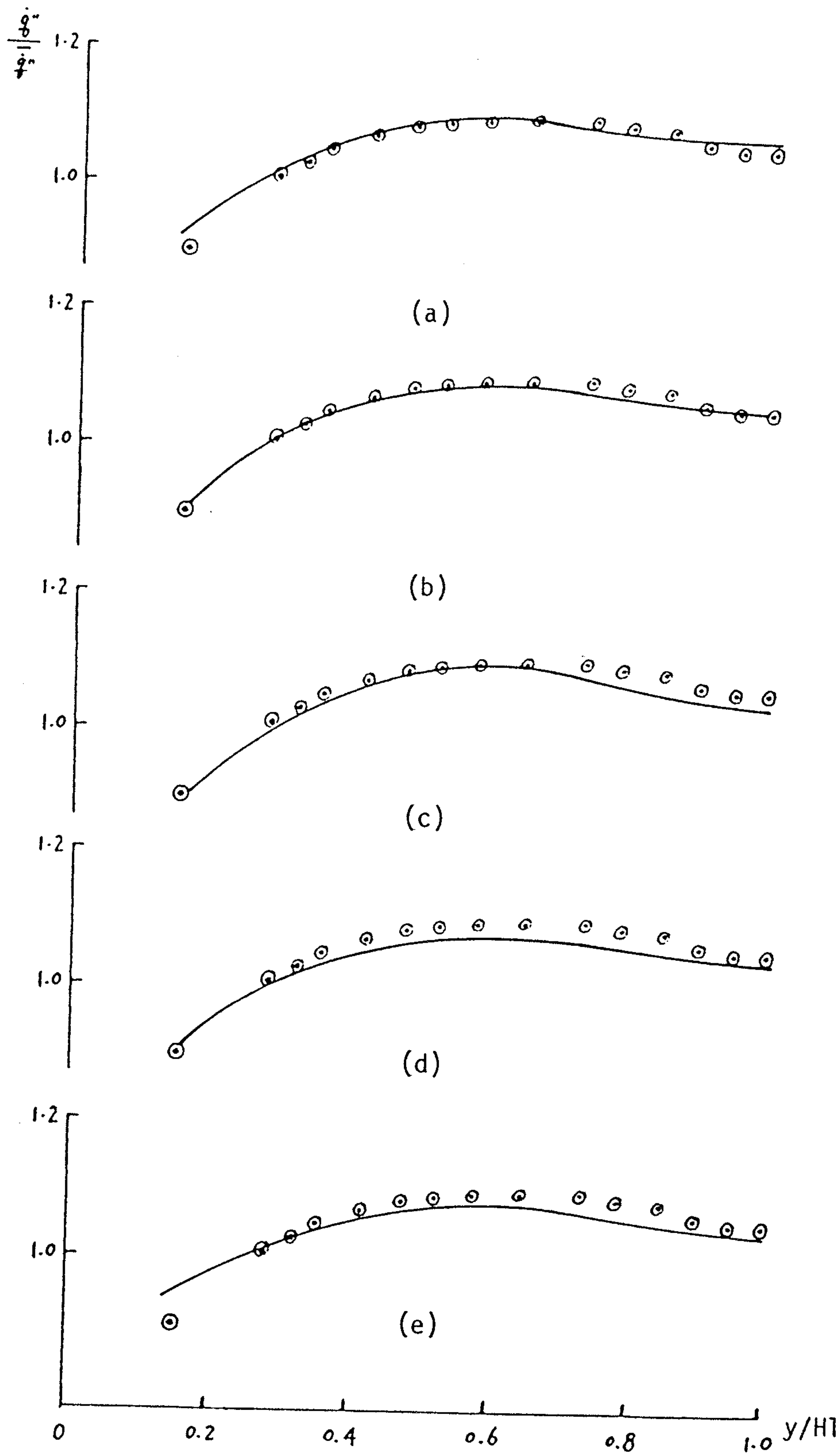

Fig.27 Comparison of wall heat flux $\frac{\dot{q}''}{\bar{\dot{q}}''}$ distribution in square duct;
Re=83,000 Experiment: ⊙ by Brundrett & Burroughs[65]
Prediction: —— (a)LY,(b)Seale's,(c)NR,(d)k,(e)ϵ

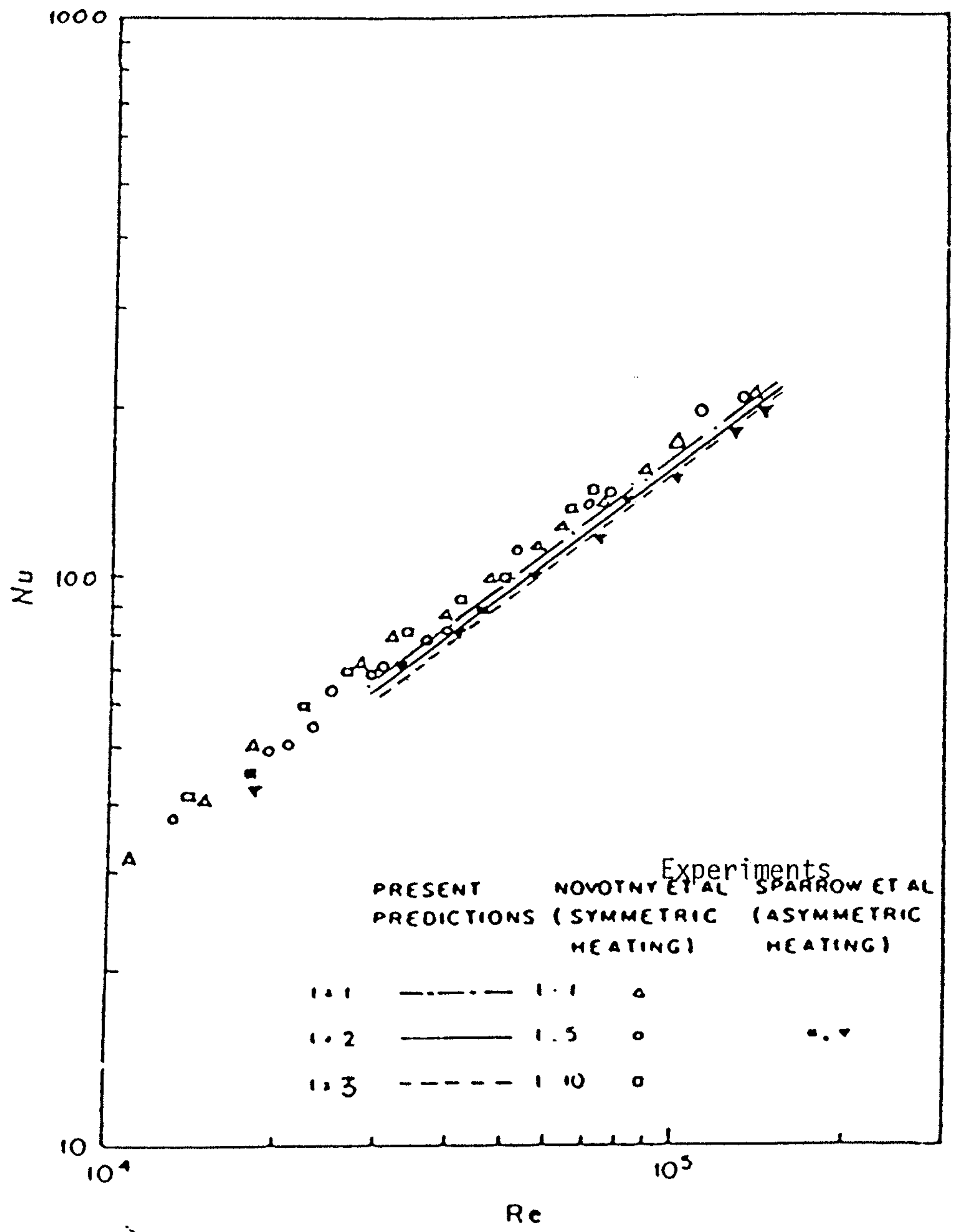

Fig.28 Comparison of Nusselt number for rectangular duct of 1:1,2:1 and 3:1 by LY model

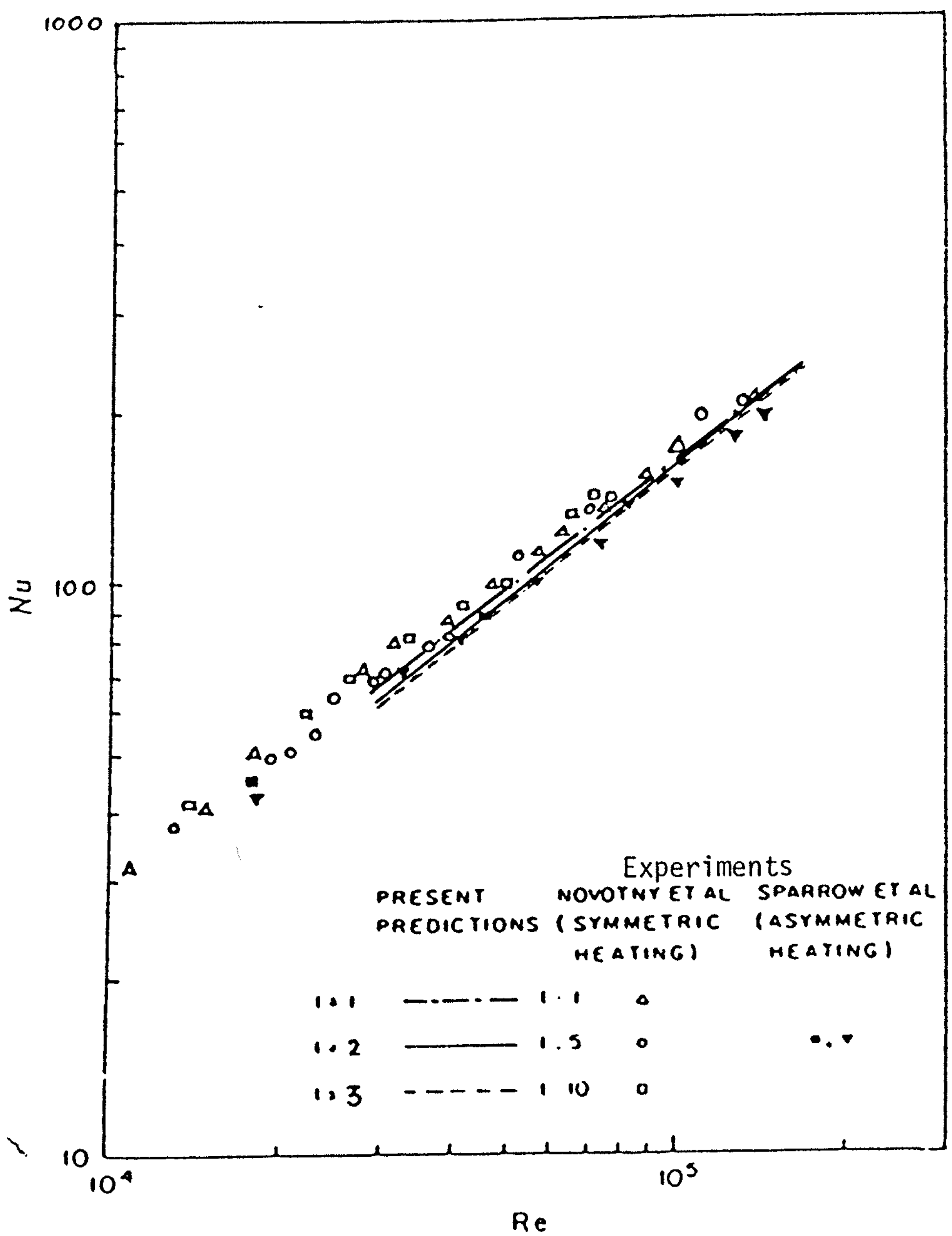

Fig.29 Comparison of Nusselt number for rectangular duct of 1:1, 2:1 and 3:1 by Seale's model

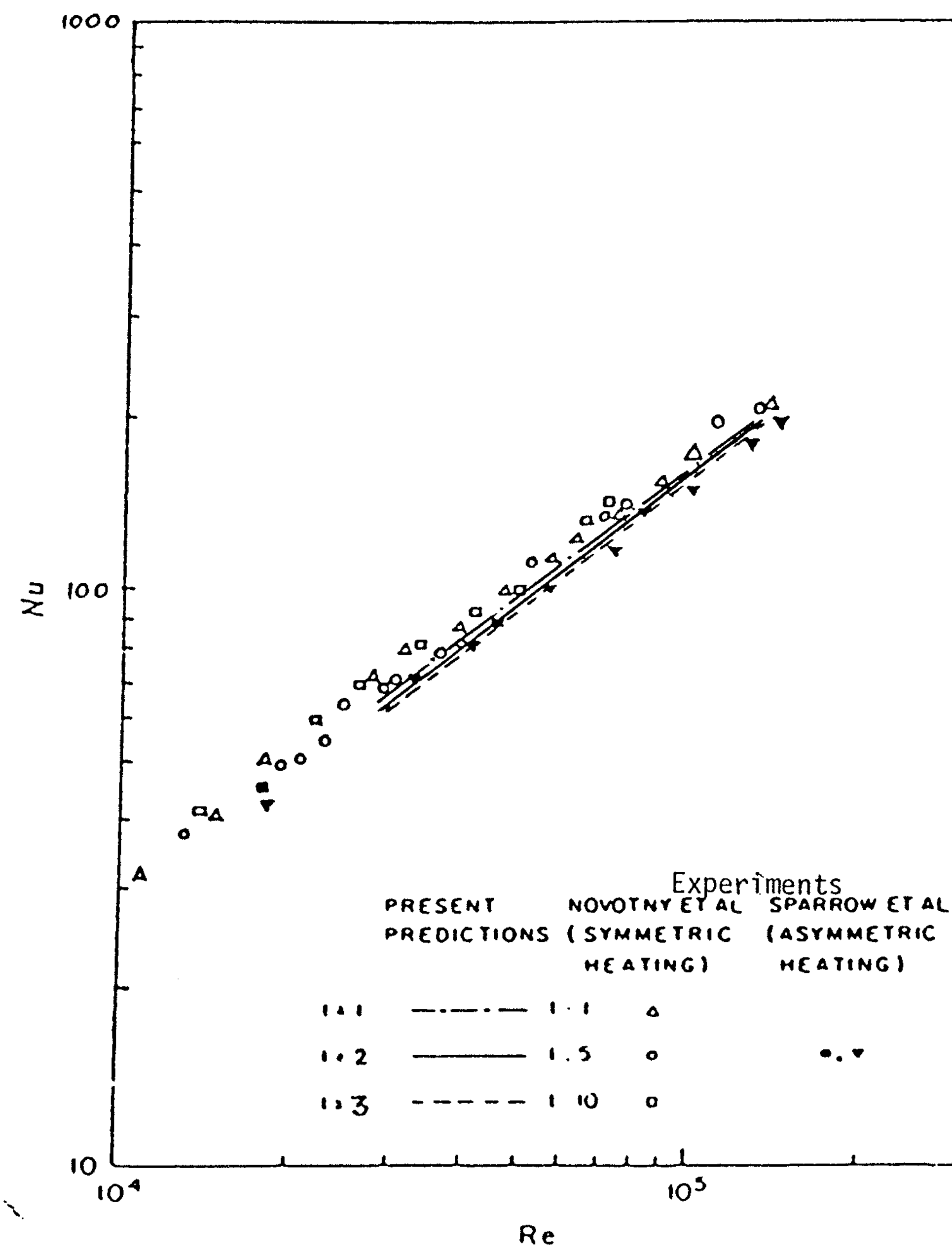

Fig.30 Comparison of Nusselt number for rectangular duct of 1:1, 2:1 and 3:1 by NR model

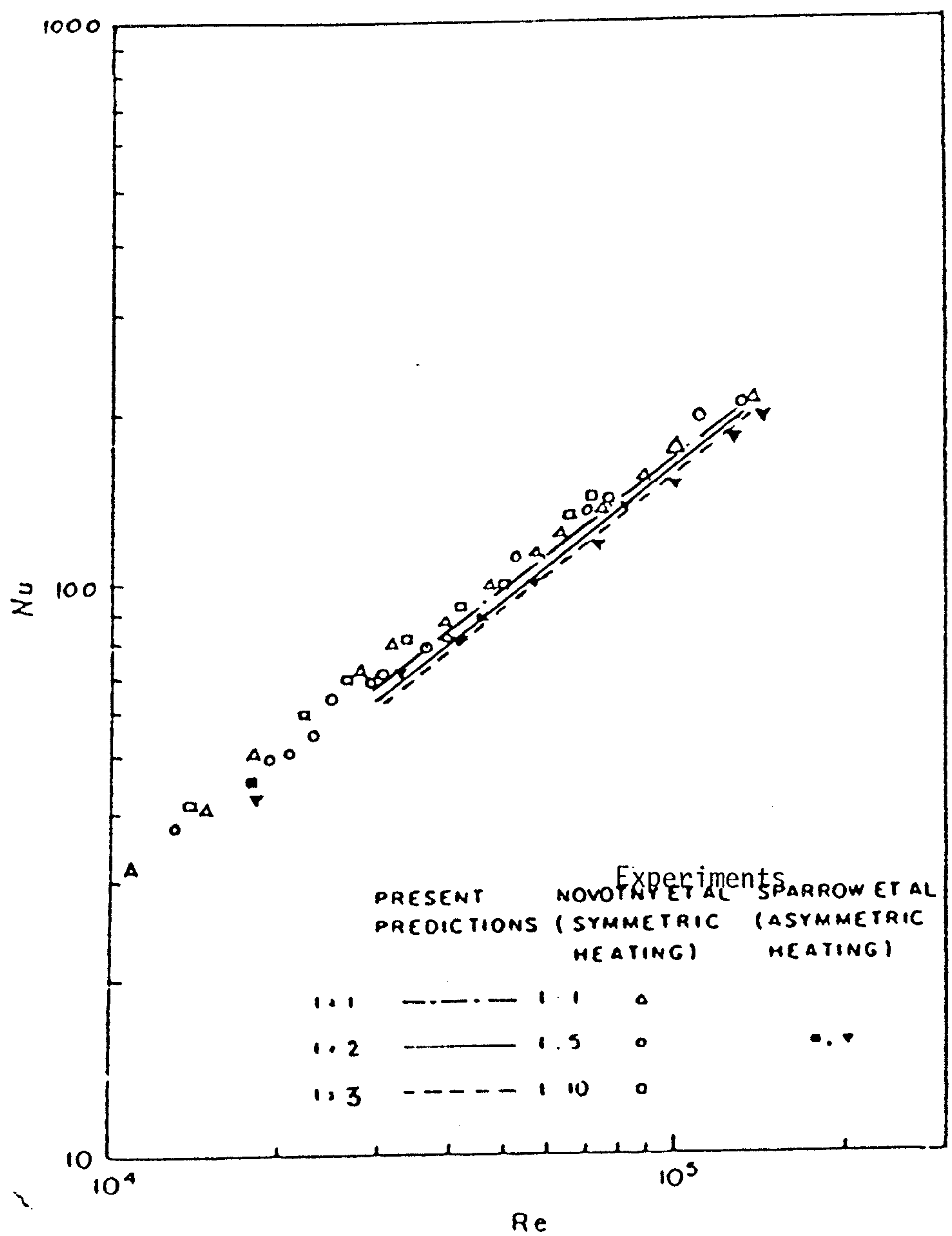

Fig.31 Comparison of Nusselt number for rectangular duct of 1:1, 2:1 and 3:1 by k model

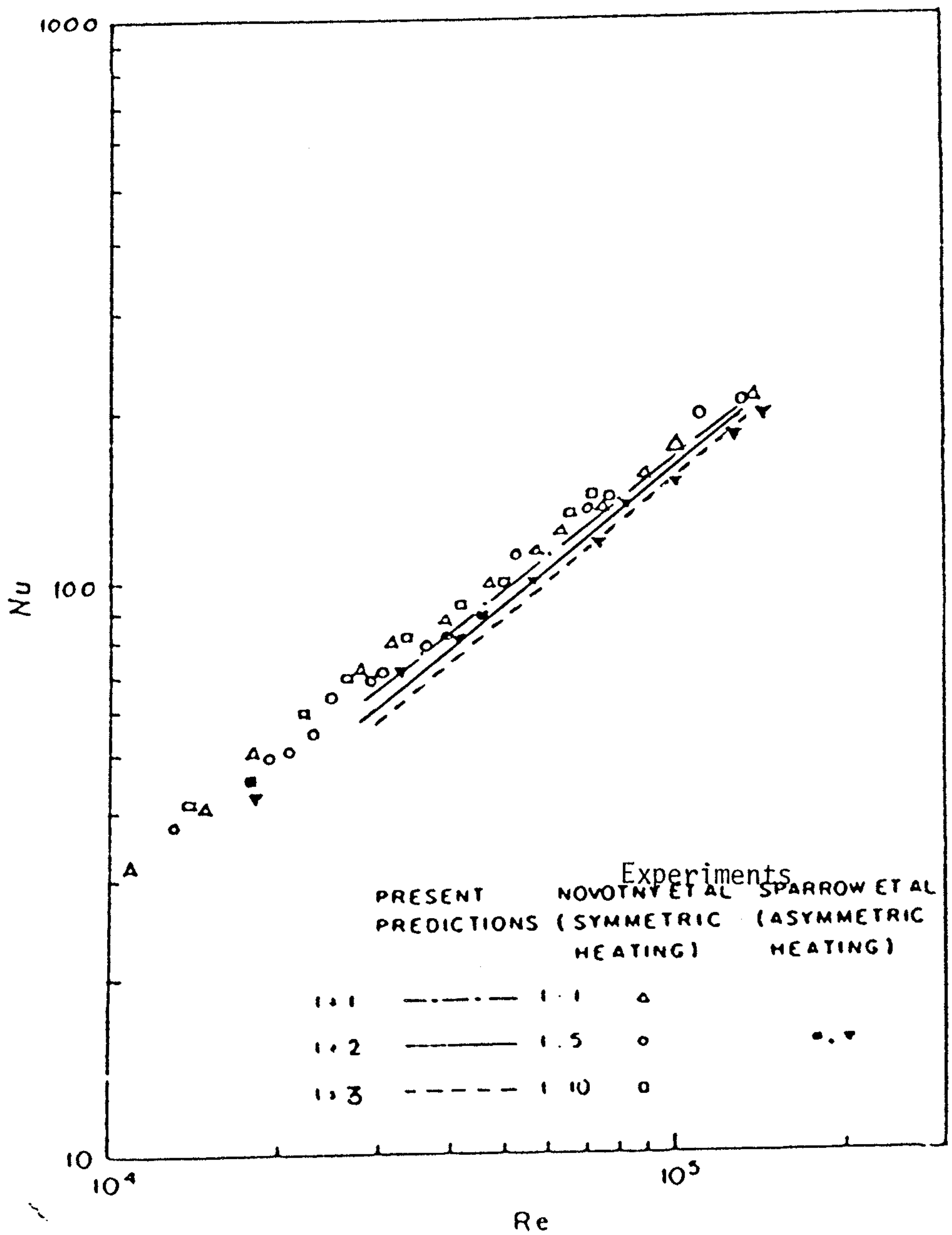

Fig.32 Comparison of Nusselt number for rectangular duct of 1:1, 2:1 and 3:1 by ϵ model

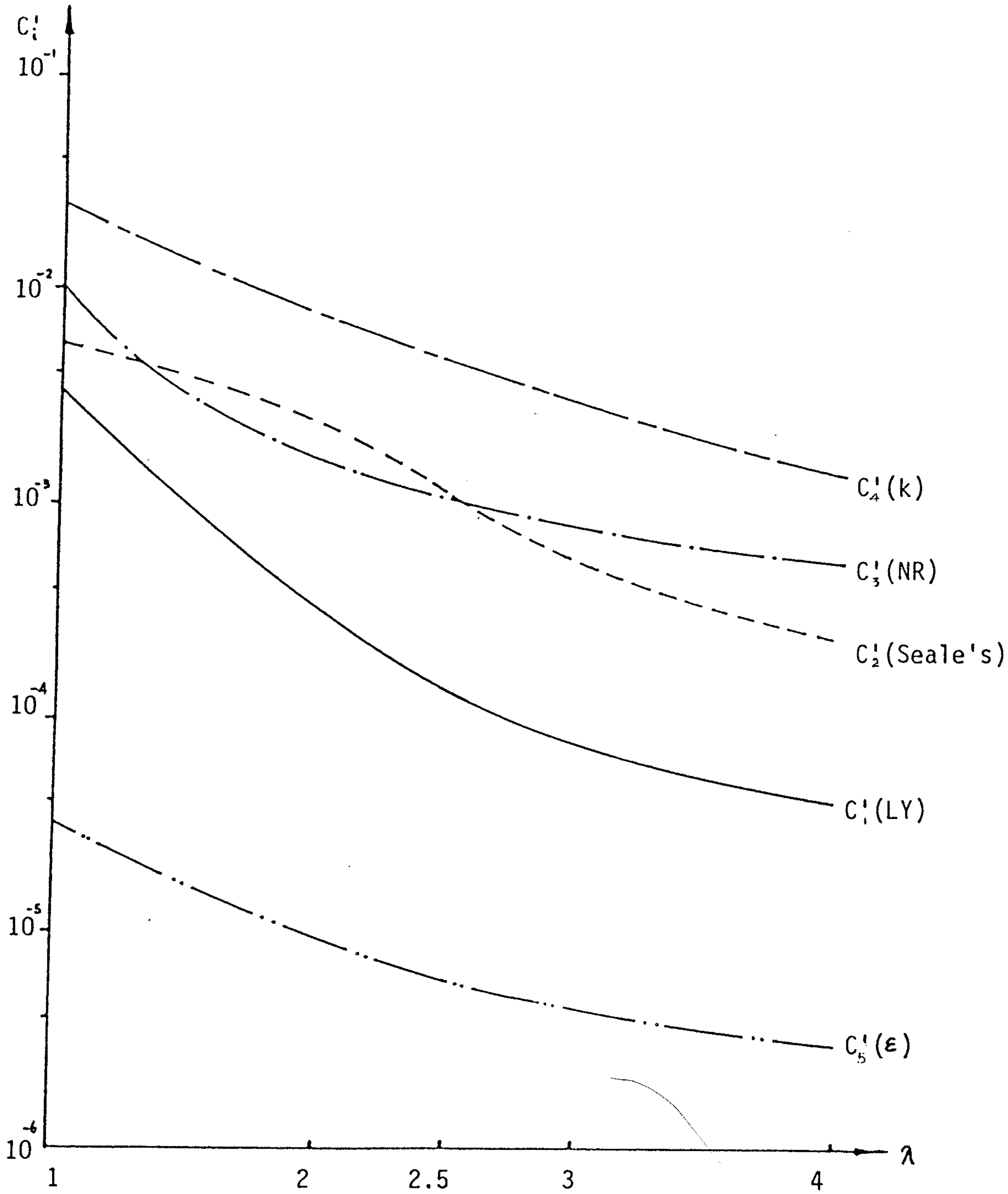

Fig.33 Vorticity source model constants

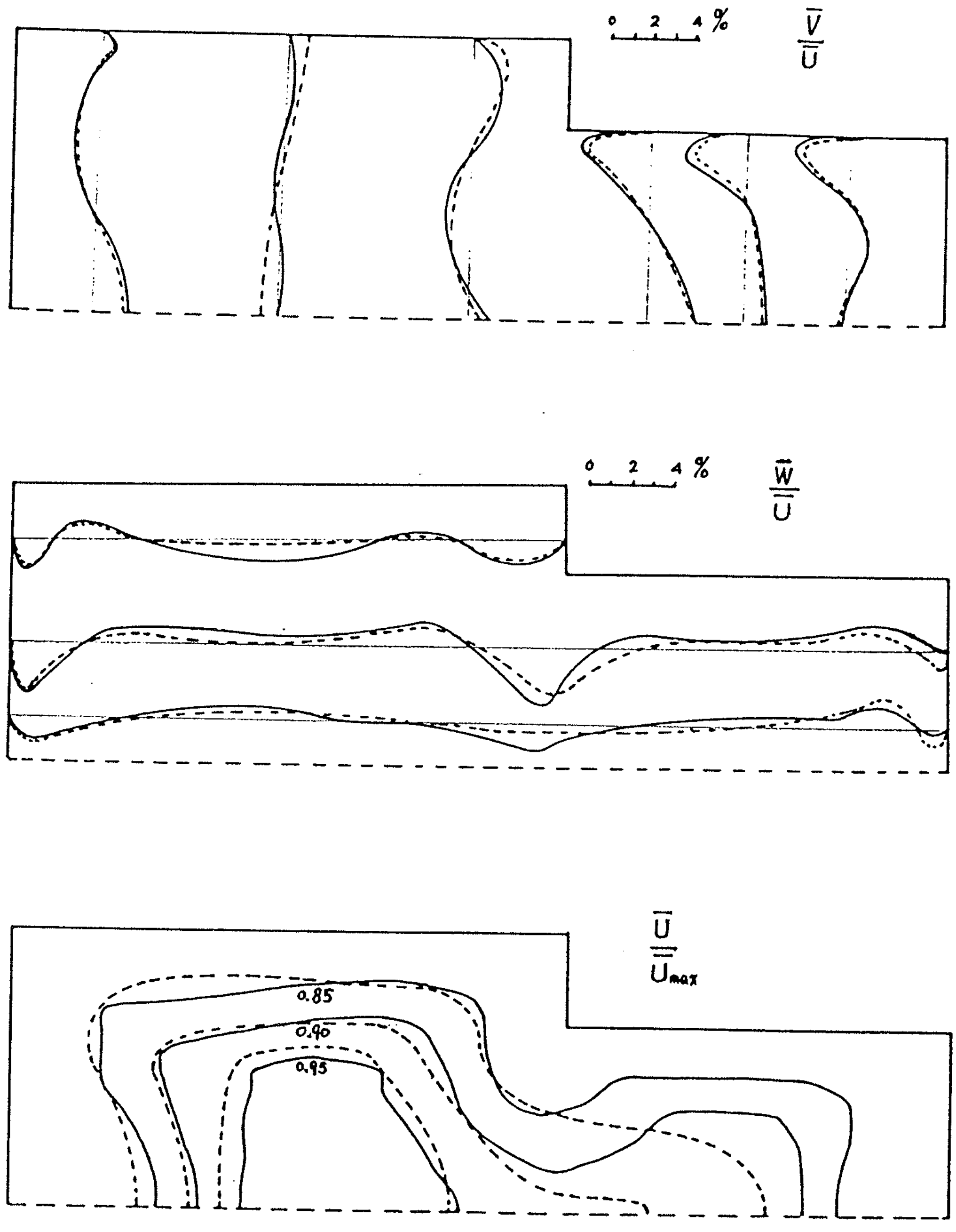

Fig.34 Lyall's duct results ——— Experiments by Lyall[12]
- - - - - Predictions by Seale's model

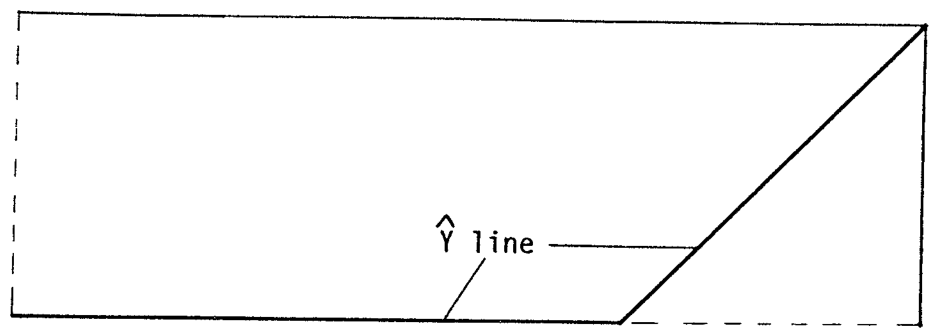

Rectangular duct

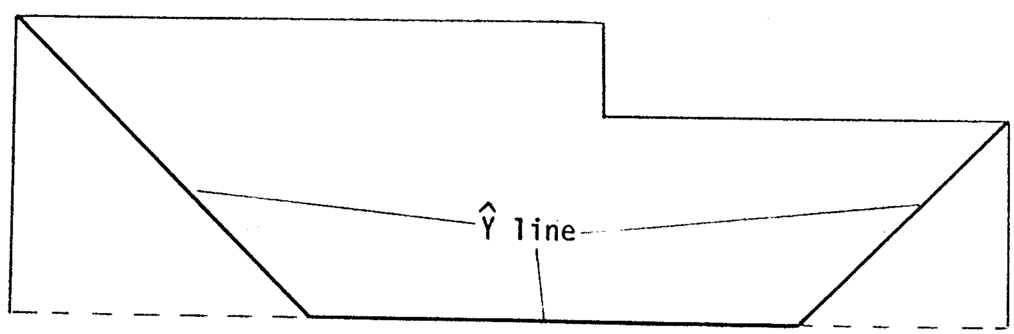

Lyall's duct

Fig.35 The $\hat{Y}$ lines of rectangular duct and Lyall's duct